

AD-A126 919

AN EXPERIMENTAL STUDY INTO THE SCALING OF AN
UNSWEEP-SHARP-FIN-GENERATED... (U) AIR FORCE INST OF TECH
WRIGHT-PATTERSON AFB OH W B MCCLURE JAN 83

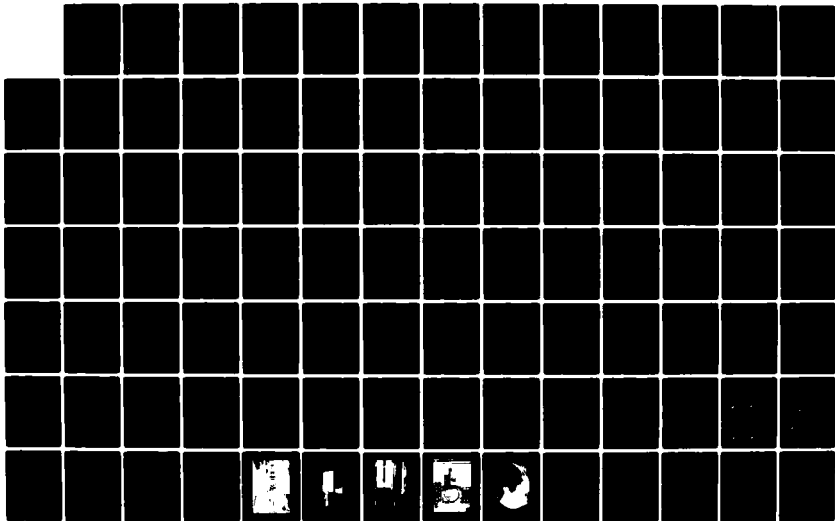
1/2

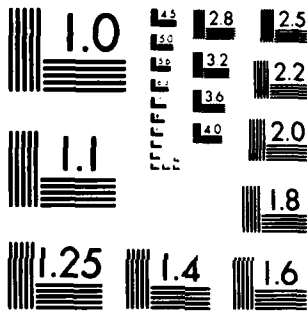
UNCLASSIFIED

AFIT/CI/NR-83-6T

F/G 20/4

NL





MICROCOPY RESOLUTION TEST CHART
NATIONAL BUREAU OF STANDARDS-1963-A

UNCLASS

SECURITY CLASSIFICATION OF THIS PAGE (When Data Entered)

REPORT DOCUMENTATION PAGE		READ INSTRUCTIONS BEFORE COMPLETING FORM
1. REPORT NUMBER AFIT/CI/NR 83-6T	2. GOVT ACCESSION NO. A126 919	3. RECIPIENT'S CATALOG NUMBER
4. TITLE (and Subtitle) An Experimental Study Into The Scaling Of An Unswep-Sharp-Fin-Generated Shock/Turbulent Boundary Layer Interaction	5. TYPE OF REPORT & PERIOD COVERED THESIS/DISSERTATION	
	6. PERFORMING ORG. REPORT NUMBER	
7. AUTHOR(s) William B. McClure	8. CONTRACT OR GRANT NUMBER(s)	
9. PERFORMING ORGANIZATION NAME AND ADDRESS AFIT STUDENT AT: Princeton University	10. PROGRAM ELEMENT, PROJECT, TASK AREA & WORK UNIT NUMBERS	
11. CONTROLLING OFFICE NAME AND ADDRESS AFIT/NR WPAFB OH 45433	12. REPORT DATE Jan 83	
	13. NUMBER OF PAGES 63	
14. MONITORING AGENCY NAME & ADDRESS (if different from Controlling Office)	15. SECURITY CLASS. (of this report) UNCLASS	
	15a. DECLASSIFICATION DOWNGRADING SCHEDULE	
16. DISTRIBUTION STATEMENT (of this Report) APPROVED FOR PUBLIC RELEASE; DISTRIBUTION UNLIMITED		
17. DISTRIBUTION STATEMENT (of the abstract entered in Block 20, if different from Report)		
18. SUPPLEMENTARY NOTES APPROVED FOR PUBLIC RELEASE: IAW AFR 190-17 <i>13 April 83</i>		
19. KEY WORDS (Continue on reverse side if necessary and identify by block number)		
20. ABSTRACT (Continue on reverse side if necessary and identify by block number) ATTACHED		

1

ADA 126919

Lynn E. Wolaver
 LYNN E. WOLAVER
 Dean for Research and
 Professional Development
 AFIT, Wright-Patterson AFB OH

DTIC
ELECTE
 APR 19 1983
S **D**
E

DTIC FILE COPY

DD FORM 1473 1 JAN 73 EDITION OF 1 NOV 65 IS OBSOLETE

UNCLASS

SECURITY CLASSIFICATION OF THIS PAGE (When Data Entered)

83 04 - 19 003

ABSTRACT

The scaling of the three dimensional flow-field generated by a planar shock wave impinging upon a turbulent boundary layer has been investigated. The shock wave was generated by a sharp fin with an unswept leading edge placed at a 10 degree angle-of-attack to the incoming flow. Two fully developed, equilibrium turbulent boundary layers, with incoming thicknesses of 1.29 cm. and .45 cm., were generated on a test surface upon which the fin was mounted. The incoming freestream had a nominal Mach number of 2.95 and a Reynolds number of 6.3×10^7 /meter. All surfaces were near adiabatic wall temperature.

The objectives of the study were to learn more about the basic structure of this type of interaction, to examine the scaling of the resulting flow-field, and to obtain a detailed data set with which to compare numerical predictions. Toward these ends, flow-field yaw angles and pitot pressures, in a single streamwise plane normal to the test surface, were obtained by means of a computer controlled 'self-nulling' cobra probe. The location of each plane (one for the interaction with each boundary layer) was chosen such that it intersected the calculated shock at the same non-dimensional spanwise distance from the fin leading edge. As measured along the shock, the intersections occurred at 26.9 cm. for the interaction with the thicker boundary layer and 13.6 cm. for the thinner one.

The results of this investigation indicate that the scale of the interaction is a function of both local boundary layer thickness and freestream Reynolds number. Further, the height of the interaction above the test surface is greater than previously believed.

PRIMARY SOURCES

1. Oskam, B. "Three Dimensional Flowfields Generated by the Interaction of a Swept Shock with a Turbulent Boundary Layer". Princeton University, Gas Dynamics Laboratory Report 1313, December 1976.
2. Peake, D.J. "The Three-Dimensional Interaction of a Swept Shock Wave with a Turbulent Boundary Layer and the Effects of Air Injection on Separation." Ph.D. Thesis, Carleton University, Ottawa, Canada, March 1975.
3. Dolling, D.S. and Bogdonoff, S.M. "Upstream Influence Scaling of Sharp Fin-Induced Shock wave Turbulent Boundary Layer Interactions." AIAA Paper 81-336, January 1981.
4. Settles, G.S., Perkins, J.J. and Bogdonoff, S.M. "Upstream Influence Scaling of 2D and 3D Shock/Turbulent Boundary Layer Interactions at Compression Corners." AIAA Paper 81-334, January 1981.
5. Kubota, H. "Investigations of Three-Dimensional Shock Wave Boundary Layer Interactions." AFOSR-76-3006, January 1980.
6. Knight, D.D. "A Hybrid Explicit-Implicit Numerical Algorithm for the Three-Dimensional Compressible Navier-Stokes Equations." AIAA Paper 83-223, January 1983.

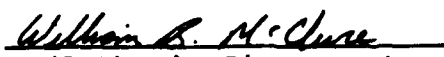
AN EXPERIMENTAL STUDY INTO
THE SCALING OF AN UNSWEPT-SHARP-FIN-GENERATED SHOCK/
TURBULENT BOUNDARY LAYER INTERACTION

by

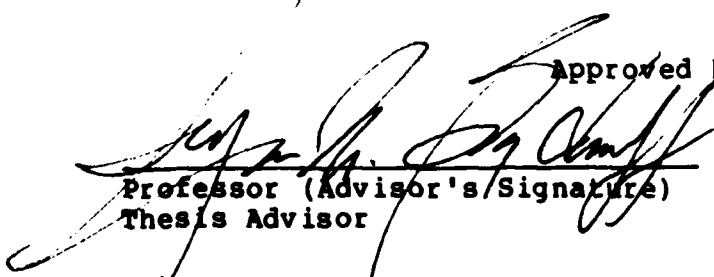
William B. McClure

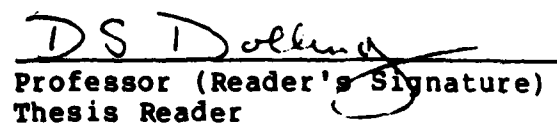
A thesis
presented to Princeton University
in partial fulfillment of the
requirements for the degree of
Master of Science in Engineering
in
Department of Mechanical and Aerospace Engineering

Prepared by:


(Author's Signature)

Approved by:


Professor (Advisor's Signature)
Thesis Advisor


Professor (Reader's Signature)
Thesis Reader

January, 1983

ABSTRACT

An experimental study ~~has been~~ carried out of the three-dimensional shock wave/turbulent boundary layer flow-field generated by a sharp fin with an unswept leading edge at a 10 degree angle-of-attack to the incoming flow. The model was mounted on and normal to either the tunnel floor or a horizontal flat plate. Both test surfaces generated a fully developed, equilibrium turbulent boundary layer, with incoming thicknesses of 1.29 cm. and .45 cm., respectively. The incoming freestream was at a nominal Mach number of 2.95 and a Reynolds number of 6.3×10^7 /meter. ^{to the 7th power} All surfaces were near adiabatic wall temperature.

The three objectives of this study were to learn more about the structure of this type of interaction, to examine the scaling of the resulting flow-field, and to obtain a detailed data set with which to compare numerical computations. To accomplish these goals, flow-field surveys were taken with a computer-controlled nulling cobra probe in a streamwise plane normal to the test surface. The positioning of these planes was such that they were at the same normalized distance from the fin leading edge as measured along the shock. The distance along the shock at which these planes intersected the shock were 26.9 cm. for the thicker boundary layer and 13.6 cm. for the thinner one.

cont - The results show that the scaling of this type of interaction is dependent upon both local boundary layer thickness and freestream Reynolds number. Further, the interaction extends farther above the test surface than previously believed.

AKNOWLEDGEMENT

Thanks are extended to the many people who aided me with this study. In particular, the guidance of Dr. D. S. Dolling and my advisor, Professor S. M. Bogdonoff, was greatly appreciated. I am also grateful to Dr. G. S. Settles for his valuable insight and comments. Thanks to the technical staff; W. Stokes, R. Gilbert, and G. Katona. Finally, I would like to thank my wife, Diane, for her continuing support and assistance in drafting this thesis.

This study was funded by the Air Force Office of Scientific Research under contract F49620-81-K-0018.

This thesis carries 1597-T in the records of the Department of Mechanical and Aerospace Engineering.

LIST OF SYMBOLS

L_S	distance along shock wave measured from fin leading edge
L_{SND}	$L_S / \delta_S * Re_\delta^{1/3}$
L_U	streamwise distance from calculated shock to upstream influence
L_{UN}	upstream influence measured normal to the calculated shock
L_{UND}	$L_U / \delta_S * Re_\delta^{1/3}$
M	Mach number
M_N	Mach number normal to the calculated shock
P	surface static pressure
P_P	pitot pressure
P_1	upstream static pressure
$\overline{P/P_1}$	P_P normalized by stilling chamber pressure
Re	freestream Reynolds number
X	streamwise distance downstream of fin leading edge
X_S	streamwise distance downstream of calculated shock
X_S (SCALED)	$X_S / \delta_S * Re_\delta^{1/3} * 1/M_N$
Y	spanwise distance from fin leading edge
Z	distance normal to and measured from test surface
Z (SCALED)	$Z / \delta_S * Re_\delta^{1/3} * 1/M_N$
α	fin angle-of-attack

α_R	2D ramp angle
α_0	surface streak angle
δ_0	incoming boundary layer thickness
δ_1	boundary layer thickness at upstream influence
δ_S	boundary layer thickness at intersection of streamwise line and calculated shock position
δ_W	wedge deflection angle (Peake)
δ^*	boundary layer displacement thickness
ΔY	Y displacement of virtual origin
θ	boundary layer momentum thickness

LIST OF FIGURES

- 1 Experimental geometries generating 3D shock wave/boundary layer interactions
- 2 Unswept sharp fin interaction and coordinate system
- 3 Cobra probe measurements of Peake (4) at Mach 4 for a 16 degree fin
- 4 Cobra probe measurements of Peake (4) at Mach 2 for an 8 degree fin
- 5 'Double viscous layer' model of Kubota (16)
- 6 Experimental configurations for Case 1 and Case 2
- 7 Princeton University 20 cm. x 20 cm. windtunnel
- 8 Test models
- 9 Probe tips
- 10 Probe and drive configuration for Case 2
- 11 Eccentric window with Tip 2
- 12 Yaw angle results varying probe tips
- 13 Normalized pitot pressure results varying probe tips
- 14 Yaw angle results varying fin height
- 15 Normalized pitot pressure results varying fin height
- 16 Surface pressure distributions along a streamwise line varying fin position in Case 1
- 17 Kerosene graphite trace for Case 1
- 18 Kerosene graphite trace for Case 2
- 19 Replicated surface pattern for Case 1 assuming conical symmetry

- 20 Replicated surface pattern for Case 2 assuming conical symmetry
- 21 Streamwise surface pressure distributions of Lu (34) for 15 degree fin interaction collapsed assuming conical symmetry
- 22 Kerosene graphite trace and replicated surface pattern for 15 degree fin interaction
- 23 Surface isobar pattern for Case 1
- 24 Comparison of normalized upstream influence for several investigations
- 25 Surface streak angles through interaction at the same normalized position
- 26 Surface pressures along lines normal to the calculated shock at the same normalized position
- 27 Typical yaw angle and normalized pitot pressure results from a cobra probe survey
- 28 Comparison of Mach numbers derived in Case 1 with the results of Oskam (1)
- 29 Flow-field yaw angles for Case 1
- 30 Flow-field yaw angles for Case 2
- 30a Yaw angle results upstream of the calculated shock for both Cases
- 31 Yaw angle results 20 incoming boundary layer thicknesses downstream of the calculated shock
- 32 Normalized flow-field pitot pressures for Case 1
- 33 Normalized flow-field pitot pressures for Case 2
- 34 Skin friction lines calculated by Knight (29)
- 35 Comparison of yaw angle results with computation of Knight (29)
- 36 Comparison of normalized pitot pressure results with computation of Knight (29)
- 37 Normalized pitot pressures in flow-field with dimensions normalized by boundary layer thickness

- 38 Yaw angles in flow-field with dimensions normalized by boundary layer thickness
- 39 Normalized pitot pressure in flow-field with dimensions normalized by method of Settles et al (6)
- 40 Yaw angles in flow-field with dimensions normalized by method of Settles et al (6)
- 41 First appearance of high-yaw angle anomaly at differing spanwise locations in Case 1
- 42 Schematic of computer-controlled cobra probe

CONTENTS

ABSTRACT	ii
AKNOWLEDGEMENT	iv
LIST OF SYMBOLS	v
LIST OF FIGURES	vii

<u>Chapter</u>	<u>page</u>
I. INTRODUCTION	1
II. LITERATURE REVIEW	5
Experimental Investigations	6
Numerical Investigations	15
Application	18
III. EXPERIMENTAL PROGRAM	22
Objective	22
Incoming Conditions	23
Data Aquisition	24
IV. EQUIPMENT AND INSTRUMENTATION	26
Wind Tunnel Facility	26
Test Sections	27
Shock Generators	28
Data Aquisition Techniques	28
Surface Flow Visualization	29
Temperature	29
Pressure	29
Stilling chamber pressure	29
Surface pressure	30
Probes	30
Pressure transducers	32
Probe placement	32
Computer System	34
Interference and Perturbation Studies	35
V. RESULTS AND DISCUSSION	39
Surface Measurements	39
Kerosene-Lampblack Patterns	39

. Surface Pressure Distributions	42
Scaling of Surface Features	43
Flow-field Surveys	45
Yaw Angle Measurements	47
Pitot Pressure Measurements	50
Comparison with the Computation of Knight (29)	50
Scaling of Survey Results	51
Large Upstream Yaw Angles	53
 VI. CONCLUSIONS	 55
Recommendations for Future Study	57
 REFERENCES	 59
 <u>Appendix</u>	 <u>page</u>
A. EXPLANATION OF PROBE NULLING OPERATION	63

Chapter I
INTRODUCTION

The breaking of the sound barrier by a manned aircraft in 1947 presented many new challenges to the fluid dynamicist. Particularly important among these was the need to understand interactions between boundary layers and shock waves. Phenomena experienced in regions where these interactions occur (e.g. high heat transfer rates, redistributions of wall pressure, boundary layer separation) have made such an understanding imperative in the proper design of high speed aircraft, missiles, and turbomachinery. To this end, a large number of experiments and, more recently, computations involving these interactions have been carried out.

The shock wave/boundary layer interactions most often encountered in practice are those in which the incoming boundary layer is turbulent. The majority of investigations have, therefore, been concentrated in this area. As a starting point, many of these studies have examined those interactions which are two-dimensional in nature, such as that generated by a reflecting oblique shock wave or by a compression corner. The 'removal' of one dimension allows for greater experimental and computational resolution and simplification of the flow-field. From the two-dimensional

studies, a better understanding of many aspects of these interactions has been achieved, yet much remains to be learned. Among the questions to be answered is the effect of the third dimension on this interaction.

Although not as extensively investigated as the two-dimensional interaction, the three-dimensional interaction generated by a swept shock wave impinging on a turbulent boundary layer has also received attention. The added spatial dimension, however, complicates the approaches frequently used in investigating the two-dimensional case. It thus becomes difficult, tedious, and expensive to obtain a complete experimental data set for even one interaction. The amount of work is increased further by the number of combinations of geometries and incoming conditions that must be studied. In the future, these problems may be alleviated by generating the flow-field numerically. This approach, however, requires a complete set of accurate experimental data by which to validate the computational codes. A full understanding of the three-dimensional shock wave/turbulent boundary layer interaction must, therefore, have its roots in experiment.

Of all three-dimensional shock wave/turbulent boundary layer interactions, one of the most frequently investigated has been that generated by a fin with a sharp, unswept leading edge, mounted normally to a turbulent boundary layer-

generating surface and at an angle-of-attack to an oncoming uniform supersonic flow. This choice has been guided by both the simplicity of the geometry and the appearance of the resulting interaction in engineering applications. Experiments using this configuration have been performed over a fairly wide range of Mach numbers, freestream Reynolds numbers, and incoming boundary layer thicknesses, though a systematic variation of any one of these parameters has been rare. In addition, the detail of many investigations has been inadequate, the great majority of data being limited to surface features. Oskam et al (1,2,3) and Peake (4) have made probe surveys above the test surface - but their investigations were limited to only two planes of a few select interactions.

In a more orderly approach to the study of this flow-field, a series of experiments has been performed at the Princeton Gas Dynamics Laboratory by Dolling and Bogdonoff (5) to determine the effect of shock generator angle and incoming conditions on this interaction. Their findings, though limited to observations of the shock's upstream influence on the test surface, show that the length scale follows a semi-empirically derived trend dependent upon the Mach number normal to the calculated shock, the freestream Reynolds number, and the local boundary layer thickness. The question is raised as to whether or not the same scaling can be applied to other characteristic lengths of this interaction.

The current study examines the effect of changes in incoming boundary layer thickness on the fin-generated shock wave/turbulent boundary layer interaction. Flow-field yaw angles and pitot pressures were obtained by computer-controlled nulling cobra probe surveys. This acquisition method resulted in a high-resolution data set from which the objectives of this study could be approached. These objectives were:

1. to examine the scaling of the flow-field above the test surface
2. to learn more about the flow-field structure
3. to obtain a detailed data set with which to compare numerical codes which will calculate this flow-field

Chapter II

LITERATURE REVIEW

Investigations of three-dimensional interactions between shock waves and turbulent boundary layers have been carried out by many investigators with a variety of shock-generating geometries (Fig. 1). These have included fins with blunt leading edges (both swept and unswept); fins with sharp, sweptback leading edges; and compression corners in which the corner line has been sweptback to the oncoming flow. One of the simplest configurations consists of a plate with a sharp, unswept leading edge¹ mounted normal to a flat surface on which a boundary layer develops (as depicted in Fig. 2). When placed at an angle-of-attack to a supersonic flow, this geometry generates a shock wave perpendicular to the boundary layer. Though the configuration is very basic, years of research have not been able to fully explain the resulting interaction. This section will review those studies which have been made of the unswept sharp fin interaction in order to place the current work in perspective.

¹ For future reference, this type of generator will be referred to simply as a 'fin' or 'shock generator'.

2.1 EXPERIMENTAL INVESTIGATIONS

The first major study using this configuration was a series of experiments carried out by Stanbrook (7). Oil-flow patterns and limited surface pressure distributions were taken at various fin angles over a Mach number range from 1.6 to 2.0. The surface flow visualizations indicate that flow on the test surface in the vicinity of the calculated shock² is turned through angles greater than that of the freestream. With increasing shock strength, the incoming streaks eventually merged with those downstream along a line upstream of the calculated shock position. It was felt that this line represented the point at which the incoming boundary layer separated from the surface. A "suction peak" in the surface pressure distribution accompanying the appearance of this feature led to the conjecture that the resulting free shear layer rolls up into a vortex and trails downstream. Because of the difficulty in determining the exact fin angle at which separation first occurred ('incipient separation'), the point at which the surface streaks first paralleled the calculated shock was chosen. This criterion was admitted to be quite arbitrary, but it insured flow opposite in direction to the gradient of increasing pressure for all separated cases. It was found that the appearance of inci-

² The term 'calculated shock' is used here as reference to the shock wave calculated by inviscid, two-dimensional oblique shock theory for the given generator angle and incoming Mach number.

ipient separation could then be correlated over the range of parameters examined with a pressure rise across the shock of 1.5, a value much lower than that found to be required for the onset of two-dimensional shock-induced separation.

A second observation made by Stanbrook was that the effects of the shock were felt farther upstream ('upstream influence') than in two-dimensional shock wave/turbulent boundary layer interactions with an equal pressure rise. The size of the interaction was also noted to increase along the shock over the entire test region. This effect was thought to be the result of disturbance propagation along rearward-facing Mach cones in the boundary layer. Far enough from the fin, this mechanism would reach an equilibrium, and the line denoting upstream influence would become parallel to the calculated shock ('cylindrical symmetry'). The interaction could thus be simplified and treated as though it were quasi-two-dimensional. Stanbrook, however, did not observe such a condition in his experimental data.

³ Among these differences was the fact that Stanbrook used a tripped boundary layer while all later studies have been carried out with untripped layers. Two-dimensional investigations by Hammitt and Hight (10) have indicated that such a difference may substantially affect the interaction length. Although neither McCabe nor Lowrie noted any qualitative difference between Stanbrook's results and their own, this effect might partially explain the disagreement between later work done by Peake and a corresponding numerical computation (discussed later in this chapter).

With slightly different incoming flow conditions,³ McCabe (8) and Lowrie (9) carried out further experimental studies of this flow field. In addition to oil-flow patterns, McCabe acquired more extensive surface pressure distributions. Accepting Stanbrook's definition, McCabe found good agreement between the appearance of incipient separation and a pressure rise across the shock of 1.5 at Mach numbers up to 3. The ensuing vortex was explained as the result of vortex tubes in the boundary layer wrapping themselves around the fin's leading edge. This idea of vorticity conservation was extended through a simple, quasi-two-dimensional, inviscid analytic model. By assuming the vorticity in the boundary layer to be convected downstream at the freestream velocity and allowing slip at the wall, an equation was derived which predicted the maximum surface flow angle for a given Mach number and generator angle-of-attack. The scheme performs well at small angles where relatively weak shock waves are produced, but over-predicts the experimentally found angle at which the surface flow is deflected to an angle equal to that of the calculated shock. Such error is explained by the fact that, at small fin angles, the interaction grows very slowly along the shock and is, thus, very close to being cylindrically symmetric. With the stronger interactions, as McCabe noted, no such symmetry is observed and, hence, the assumption of two-dimensionality no longer holds. It was envisioned that it would take a dis-

tance on the order of 60 boundary layer thicknesses (measured along the shock) for cylindrical symmetry to be reached in these stronger cases.

McCabe also concluded that it may not be possible to make direct comparisons between the three-dimensional and two-dimensional shock wave/turbulent boundary layer interactions. This conclusion was supported by a comparison of his data with that obtained by Gadd (11) for a normal shock wave of comparable strength. Similar support was later found by Os-kam (1) when comparing his three-dimensional data with the results of the normal shock/turbulent boundary layer study performed by Kooi (12)

In contrast to McCabe, Lowrie approached the interaction as a three-dimensional boundary layer problem. This more rigorous analysis centers around a compressible version of Johnston's triangular crossflow model (13), in which the layer is divided into two regions. The upper region is assumed to be inviscid, with crossflow velocities linearly proportional to the streamwise velocity defect. The lower region, on the other hand, is characterized by a balance between the viscous and pressure forces, resulting in a linear relationship between the crossflow and streamwise velocities. A resulting plot in the $u-v$ plane is thus triangular in shape.

Velocity profiles were derived at various locations in the interaction from yawed-pitot pressure surveys and corresponding surface static pressures. It was assumed, as in most boundary layer calculations, that there was no normal static pressure gradient. The results were subsequently presented in u-v plots. Though they seem to support the proposed model, it should be noted that only those surveys which conformed to the triangular shape are presented. Further, it has now been shown that there is, indeed, a normal static pressure gradient resulting from compression waves near the surface. These features greatly complicate any boundary layer approach and, thus, remove many of its advantages.

Peake (4) followed Lowrie with extensive measurements of this interaction at three conditions: just prior to incipient separation, just past incipient separation, and well past incipient separation. Although a boundary layer assumption was invoked here as well to derive velocity profiles, the majority of the conclusions resulting from this study were based on the measurements themselves. From oil-flow patterns taken at progressively increasing generator angles and at Mach numbers of 2 and 4, it was noted that separation appears through a "gradual, progressive, relatively steady,⁴ --process" in which there is no indication

⁴ Work done by Dolling and Bogdonoff (14) and Dolling and Murphy (15) has shown that two-dimensional shock-induced separation can be quite unsteady. Though a direct compar-

of sudden fluid eruption from the surface. This made it difficult to pinpoint the exact generator angle which induced incipient separation. For this reason, Stanbrook's criterion was chosen to delineate the separated from the unseparated cases.

Following the previous hypothesis of Stanbrook and McCabe, Peake attempted to substantiate the presence of a vortex in the separated flow. Supported by the presence of both troughs in the pitot pressure surveys near the surface and unusually high flow angles well away from the surface (Fig. 3), it was inferred that the separated free shear layer rolls up "into a flattened vortex roughly within the depth of the original undisturbed boundary layer". The pressure trough location corresponds to that of the vortex core. As can be seen in Fig. 4, however, the same features are already present in the unseparated case, though smaller in magnitude. This raises the question of whether the separation vortex (if it in fact exists) is responsible for the presence of these features or if they are the result of some other mechanism.

Kubota (16) extended the idea of a vortex dominated flow field with the aid of vapor screen visualizations. These results indicated the importance of the boundary layer on

ison may not be able to be drawn with the three-dimensional case, these results do point out the necessity of investigating the steadiness of the so-called separated region further before such a statement can be made.

the generator itself and led to the development of a 'double viscous layer model'. This model proposes the existence of a small vortex in the corner between the shock generator and the test surface. The vortex is always present in the interaction, regardless of fin angle, and is submerged in the flow which separates from the generator surface and reattaches to the test surface (Fig. 5). Such a feature would account for the high heat transfer rates and the surface pressure peaks associated with the region closest to the fin root. It may also account for the common patterns seen in Peake's separated and unseparated cases.

At low angles-of-attack, the incoming boundary layer on the test surface remains attached, but is turned by the streamwise pressure gradient imposed by the shock and by the flow originating on the fin. As the angle is increased, a point is reached at which this layer separates from the surface, rises up and over the flow coming off the fin, and rolls up into a large vortical shear layer.

In light of the work of Lighthill (17) on 'skin-friction line topology', in conjunction with this model, Kubota came up with a different criterion for the presence of separation from the previously-mentioned investigators. For this study, the flow was said to be separated if the oil-streaks upstream of the interaction coalesced into a single line in

front of the shock,⁵ - not just when the streaks passed from the downstream to the upstream side of the shock. This required a stronger shock to initiate separation than was previously accepted. Further, Kubota found that some flow patterns exhibit this 'complete convergence' through only part of the interaction. In such a case, far enough from the fin, the coalescence line decays into a region of 'incomplete convergence' where the oil streaks do not merge. Interpreting this in terms of the above requirement for separation, the incoming boundary layer would be only partially separated.

The angle of the coalescence line, whenever present, was calculated by a simple method combining the approaches of McCabe and Lowrie, but conserving angular momentum as opposed to vorticity. When Stanbrook's criterion is applied, this method predicts the same generator angle required to induce incipient separation as does McCabe's.

The most complete set of flow field surveys in this interaction (to date) were carried out by Oskam et al (1,2,3) under conditions both prior to and just past Stanbrook's so-called incipient separation point (as defined by Stanbrook). In addition to those values obtained in Peake's

⁵ Subsequent findings by Oskam et al (1,2,3) indicate that this requirement may be as arbitrary as Stanbrook's definition of requirement for separation since, by changing the oil mixture, a coalescence line could be initially generated over a range of generator angles.

surveys, static pressure was measured along lines normal to the test surface. The results of these surveys conclusively disproved the assumption of previous investigators by revealing the presence of a normal pressure gradient. The velocities in a plane parallel to the boundary layer generating surface were then properly derived. By continuity, the third velocity component and pitch angle were obtained.⁶ The resulting picture shows pitch angles of only 5 degrees in the vicinity of the so-called separation (oil-flow coalescence) line, which concurs with Peake's finding of no sudden eruption. Further, the data indicate no presence of a vortical structure, though it should be noted that the techniques used were not capable of showing such if it were sufficiently weak.

As this evidence failed to support the flow-field models embracing a vortex or vortical structure, Oskam proposed that the interaction was dominated by compression and expansion waves. An analytic, inviscid approach was used to determine the shock-on-shock interaction between the compression waves originating on the surface and the shock generated by the fin. Four surface isobars forward of the calculated shock were chosen as initial generatrices of

⁶ To check these values, pitch angles were experimentally measured at several locations in the flow field. Although agreement with the derived values is good, the measurements are open to debate since they were obtained using a stationary 3-hole probe oriented normally to a Mach gradient.

these compression waves. Though the results compare favorably with the experimental data, patching was required to satisfy the tangency conditions of flow direction and static pressure between regions downstream of the calculated shock. This indicates the possibility of a more extensive wave system than the calculation accounts for.

The end result of these experiments is the proposal of two different models for this interaction; one vortex-dominated, the other wave-dominated. Neither, however, has been supported sufficiently by experimental data.

2.2 NUMERICAL INVESTIGATIONS

With the development of larger and faster computers, it has become possible to numerically compute many flow fields utilizing the full, time-dependent Navier-Stokes equations. This approach has been taken for the sharp fin-generated shock wave/turbulent boundary layer interaction by Hung and McCormack (18), Horstman and Hung (19), and Knight (29). The method is simplified in these codes by ignoring bulk viscosity and the specific turbulent energy in the normal stress component. The remaining turbulent stress is modeled with an algebraic eddy-viscosity model (after Escudier (20)). Law's experiment (21) is simulated by the Hung/McCormack study, while the Horstman/Hung study simulates the works of Peake and Oskam. The predictions are very good for

all but Peake's separated cases - a disagreement which might be due to the experimenter's introduction of a vortex generator upstream of the interaction to create a two-dimensional incoming boundary layer (see previous footnote).

Four interesting points can be drawn from the results of these computations:

1. Even with a relatively simple turbulence model, good results are obtained. This is not found to be the case in two-dimensional separated flows where even one- and two-equation models are not adequate for predicting the entire flow.
2. The streamwise grid spacing does not allow for good resolution of the main shock, much less the wave structure postulated by Oskam. Although finer spacing of these points would improve the problem for the former feature, it is doubtful whether the latter features would be strong enough to be seen in the resulting computation. Thus, this approach may not be able to support Oskam's model.
3. Depending on the perspective taken, it is possible to perceive a vortical structure in the results. In the study of Horstman and Hung, transverse velocity vectors in a plane normal to the wedge surface seem to indicate a vortex in the corner region of both the unseparated and the extensively separated cases of Peake. When similar vectors are shown in a plane

normal to the centers of these structures, the features disappear from the unseparated case, but are retained in the separated one. The problem with this last view is that the magnitude of the velocity normal to this plane is lost and, hence, the 'strength' of the structure cannot properly be judged.

4. Even in the extensively separated case, a particle initially .05 boundary layer thicknesses above the test surface upstream of the interaction rises to a height of only .3 boundary layer thicknesses by the time it leaves the computational domain 20 thicknesses downstream. This corresponds to a pitch angle of less than one degree.

Though the numerical calculations, in their present state, are not able to resolve the question of flow field structure, they do have a great immediate potential. Computations of this interaction have, thus far, been limited to comparisons with previous experimental work. But now that they are able to adequately predict some of the results, it would be extremely useful to precede further experimental work with a corresponding computation. In this manner, key features might be located much more efficiently. Further, correct prediction of a previously uninvestigated flow-field would lend greater credibility to the numerical code.

2.3 APPLICATION

While the structure of the fin-generated shock wave/turbulent boundary layer interaction has not yet clearly been determined, the results of previous studies have been useful in developing schemes for applying the data to engineering uses. This approach has the benefit not only of immediate utility, but also that the trends observed during such a process must be accounted for in the final flow-field model.

The simplest of these techniques is the empirical fit. It consists of fitting the data to some mathematical function, whether or not the function itself has any physical relevance. For this particular interaction, features such as peak pressure, maximum heat transfer, and surface flow coalescence locations have been fit by Token (22), Hayes (23), Neumann and Hayes(24), and Scuderi (25). All have been moderately successful in predicting values within the range of the initial data.

Another, but more significant, approach is scaling. This method requires a more substantial basis than curve fitting, such as a dimensional analysis of important physical parameters. The first work of this type for three-dimensional shock wave/turbulent boundary layer interactions was carried out by Settles et al (6) for compression corners. As no previous work had been done in this area, Settles began with a dimensional analysis of the two-dimensional interaction of

a ramp-generated shock with an incoming turbulent boundary layer. The governing parameters chosen for the analysis were those laid out by Green (26). These are:

1. the magnitude of the pressure rise across the shock
2. the nature of the disturbance
3. the incoming boundary layer
4. the incoming Reynolds number
5. some measure of the incoming boundary layer thickness

The particular characteristic chosen for scaling was the distance between the corner of the ramp and the point of upstream influence measured along a streamwise line. Values for this feature are well documented or are easily obtained from either surface pressure distributions or surface flow patterns. The general relationship was found to be:

$$L_U = f(Re, \delta_o, \alpha_R, M)$$

For a constant ramp angle and incoming Mach number, the resulting dependence becomes:

$$(L_U \times Re^{-a}) / \delta_o^{a+1} = \text{Constant}$$

From previous experimental studies, the average value for 'a' was found to be -1/3, though there was some variation with ramp angle. This result points out that, in addition to the accepted practice of scaling interaction distances by the incoming boundary layer thickness, there is a Reynolds number 'residual' that must be accounted for. Analytic ex-

aminations by Lighthill (27) and Inger (28) for the unseparated ramp-generated shock wave/turbulent boundary layer interaction show a similar dependence. It is interesting to note that this trend holds for the separated as well as unseparated case, especially in light of the findings of unsteadiness in the former.

Settles then applied the same approach to the three-dimensional interaction generated by a compression corner with a sweptback leading edge. This required the addition of a term to account for spanwise distance. For constant sweep, ramp angle, and Mach number, the scaling becomes:

$$(L_U \times Re^{-a})/\delta_1^{a+1} = f((Y \times Re^{-b})/\delta_1^{b+1})$$

with reference to Fig. 2 for notation. The boundary layer thickness at the point of upstream influence is used here because of the variation in the incoming value for cases where the sweep angle is large. From a rather extensive data base, it was found that $a=b=-1/3$ gave an overall good fit. These exponents are not universal and may only apply to the range of variables tested. Further, this approach was only applied to upstream influence lengths.

Dolling and Bogdonoff (5) applied the same method to the geometry used by Oskam, Peake, etc., and met with good success. Instead of measuring the upstream influence in a streamwise direction, however, it was measured normal to the

calculated shock in order to enhance the effect of differing generator angles. A method of accounting for the shock strength was found by dividing the non-dimensionalized upstream influence length by the normal Mach number. This allowed the upstream influence lengths obtained at various fin angles to be collapsed onto the same curve. When this method was used to scale the complete surface pressure distribution, though, the results were inconclusive. This was due to the fact that interpolation in a region of severe gradients was required to obtain some of the surface pressures.

As this approach has met with so much success in scaling the upstream influence, the next logical step is to apply it to other features - both on and off the surface. This, then, is the objective of the current study.

Chapter III
EXPERIMENTAL PROGRAM

3.1 OBJECTIVE

This study was undertaken primarily to examine the application of the three-dimensional scaling methods of Settles et al (6) and Dolling and Bogdonoff (5) to the entire three dimensional shock wave/turbulent boundary layer interaction. To accomplish this, an experimental configuration similar to those of Oskam et al (1,2,3) and Dolling and Bogdonoff (Fig. 2) was used. A generator angle of 10 degrees was chosen for two reasons. First, a complete set of surveys of this interaction was obtained by Oskam et al and the resulting flow field computed by Knight (29). As the present incoming conditions were almost identical to those used in these works, it was possible to make direct comparisons. Second, with these incoming conditions, the interaction displayed prominent surface features. It was therefore assumed that the features off the test surface would be significant enough to be examined by the experimental techniques employed. These locations of these features could then be compared when the flow-field was scaled.

3.2 INCOMING CONDITIONS

The variable chosen for this study was boundary layer thickness. Two were used; a 'thick' layer generated on the nozzle surface and floor, and a 'thin' layer generated on a flat plate (Fig. 6). Both surfaces were near adiabatic conditions. These layers have been extensively surveyed, and have been shown to be two-dimensional, fully turbulent, equilibrium⁷ boundary layers (30). The incoming parameters - where 'incoming' is defined at the streamwise location of the fin leading edge - were:

	δ_0 (cm.)	δ^* (cm.)	θ (cm.)	C_f
THICK	1.25	0.34	0.07	0.00119
THIN	0.50	0.16	0.03	0.00136

The boundary layer thicknesses at the points where the calculated shock wave would cross the streamwise cut along which surveys were made were 1.55 cm. on the floor and .59

⁷ As defined by the wall-wake law.

cm. on the plate. The importance of these values will become apparent later in this chapter.

The incoming freestream conditions were nominally the same for both boundary layers. For the thick boundary layer, the Mach number was 2.93 and the freestream Reynolds number was 62×10^6 /m. For the thinner layer, these values were 2.91 and 61×10^6 /m, respectively.

3.3 DATA AQUISITION

Two types of measurements were made during the course of this study. The first were of a global nature, and consisted of surface flow patterns and pressure distributions in the interaction. These were used to insure that the scaling method could be applied as successfully to this study as it was to past studies. The second type of measurements taken were yaw angle and pitot pressure surveys along streamwise cuts through the interaction. The spanwise location of these cuts was chosen such that they, according to the scaling method, were at the same non-dimensional length along the shock (L_{SND}).

It should be noted that a slight difference existed between this work and that upon which the scaling method was based. Settles' and Dolling's nondimensionalizing factor depended on the 'local boundary layer thickness' (i.e. the boundary layer thickness at the point furthest upstream along

a given line where surface data indicates the first effects of the shock wave). As it was difficult to know this location beforehand, the value of the boundary layer thickness at the point where the calculated shock (if it were present) would intersect a streamwise cut was used. Comparisons made at the end of the study showed that this approximation resulted in less than a 2% difference had a comparison been made using the local boundary layer thickness instead.

Chapter IV
EQUIPMENT AND INSTRUMENTATION

4.1 WIND TUNNEL FACILITY

This study was carried out in the Princeton University 20 cm. x 20 cm. supersonic blowdown tunnel (Fig. 7). Pressurized air for this facility is provided by four Worthington four-stage compressors. The air is dried to avoid condensation problems during tunnel operation. It is stored at ambient temperature and pressures up to 20 MPa in four above-ground tanks, with a total volume of 56.6 cubic meters. When needed, it is released into the stilling chamber through a hydraulically controlled 20.32 cm. valve. The throttling process is non-adiabatic and there are no heaters to maintain the stilling chamber temperature. Therefore, there is a variation of several degrees Kelvin in the temperature of the chamber during tunnel operation. The chamber pressure, on the other hand, is regulated at a set value between .45 MPa and 3.45 MPa. From the stilling chamber, the air is expanded through a convergent/divergent nozzle to a nominal Mach number of 3 and passed into the working section of the tunnel. This working section is made up of three interchangeable 90.2 cm. long units.

4.2 TEST SECTIONS

Two different test sections were used during the course of this study, each installed immediately downstream of the nozzle exit. The first was that employed by Oskam et al, and is described in full detail in Reference 3. This section was fitted with two (top and bottom) 30.48 cm. diameter windows, centered 6.35 cm. off the tunnel centerline. These gave the section flexibility in variety and placement of instrumentation. The test arrangement in this section will, henceforth, be referred to as Case 1.

The second section had windows of the same dimensions, but on the sides as opposed to top and bottom. This made room for a 2.54 cm. wide streamwise slot through the ceiling of the section and centered 1.27 cm. off tunnel centerline. All probe movement in this section was along this slot, which allowed for easy streamwise placement, but restricted surveys to only one spanwise location. The section was spanned by a horizontally mounted flat plate with a sharp leading edge. As this arrangement left only 15.24 cm. clearance between the surface of the plate and ceiling, a liner had to be removed from beneath the plate in order to maintain the tunnel's cross-sectional area. The test arrangement in this section will be referred to as Case 2.

4.3 SHOCK GENERATORS

The shock generators manufactured for this study are shown in Fig. 8. The larger generator (29.21 cm. x 13.97 cm.) was used in Case 1 and mounted flush with the section floor, while the smaller one (29.21 cm. x 8.89 cm.) was used in Case 2 and mounted in a similar fashion on the plate. Both fins were 1.27 cm. thick aluminum and machined with unswept leading edges of thickness less than .01 cm.. Each was sting mounted and braced vertically and horizontally. Neither fin spanned the vertical distance between the tunnel ceiling and the test surface.

The accuracy of the generator angle-of-attack for both Cases was estimated to be within .25 degrees of the desired value. In Case 1, the angle was measured with a universal bevel protractor; in Case 2, with a dial caliper. Checks were made to insure that both fins were mounted normal to the test surface.

4.4 DATA ACQUISITION TECHNIQUES

4.4.1 Surface Flow Visualization

A surface flow visualization technique reported by Settles and Teng (31) was chosen over standard oil-flow techniques. A mixture of kerosene and finely ground lampblack powder were mixed to form a flowing paste, which was then

spread on the test surface in a thin band upstream of the interaction. When the tunnel was started, this mixture thinned as it spread over the surface. The kerosene evaporated and left fine streaks of lampblack which, upon complete drying and tunnel shut-down, were impressed on transparent tape and mounted on white paper to create a permanent, full scale, undistorted record of the flow pattern. As the upstream mixture did not flow into the region neighboring the fin, patterns in this area were acquired by spreading a band of the mixture in the corner between the fin and surface.

4.4.2 Temperature

Stilling chamber temperature was measured with a chromel-alumel thermocouple, referenced to an ice-bath. The accompanying amplifier was calibrated against a millivolt source to an accuracy of better than the equivalent of 1 degree Kelvin.

4.4.3 Pressure

4.4.3.1 Stilling chamber pressure

Pressure in the tunnel stilling chamber was monitored by a Pace 500 PSI transducer, referenced to atmospheric pressure. Readings were accurate to .017 MPa.

4.4.3.2 Surface pressure

Surface pressures were obtained with one of two systems. When surface pressure distributions were being taken, measurements were made by two Druck 50 PSI transducers, each installed in a computer-controlled 48-port Model 48J4 Scanivalve and referenced to vacuum. A 250 millisecond delay was allowed between successive readings to permit pressure in the volume between the Scanivalve port and the transducer face to reach equilibrium.

During flow field surveys, surface pressure was measured at a single point upstream of the interaction by a Pace 25 PSI transducer, referenced to vacuum. The Druck transducers were accurate to 100 Pa; the Pace to 860 Pa.

4.4.4 Probes

A conventional nulling 'cobra' probe, so-called because of its appearance and method of operation, was chosen over other survey techniques for several reasons. First, due to Mach number gradients, stationary 3- or 5-hole probes were inadequate. Second, hot-wire and laser techniques were not sufficiently developed at the time to investigate such complex interactions. Finally, previous investigations of the sharp fin-generated interaction with this type of probe by Peake and Oskam had proven successful.

Two probe tips were constructed from stainless steel tubing with outer and inner diameters of .081 cm. and .051 cm., respectively. These tubes were silver soldered, side-by-side, and rolled flat to final frontal dimensions of .064 cm. high and .318 cm. wide. The two side tubes were then cut away at a 45 degree angle relative to the tip centerline, and the face squared off. Both are shown in Fig. 9.

The first probe tip, Tip 1, was designed to make surveys in the region adjacent to the test surface while connected to a shaft running through the section ceiling (as depicted in Fig. 10 for Case 2). To minimize interference problems caused by the presence of this shaft, the tip was bent to place its center port 4.2 cm. below the axis of rotation. In addition, the lowest 5.7 cm. of the shaft had a diamond cross-section to avoid a detached shock wave. This tip was used to survey the interactions of both Case 1 and Case 2.

Tip 2 was designed to make surveys on the surface through which it entered the tunnel. This procedure was used to avoid the interference caused by a shaft extending across the test section, particularly when operating in close proximity to the fin or sidewall. It was mounted in a 5.08 cm. diameter plug, and used in conjunction with the eccentric rotatable window (described later in this chapter) in Case 1. Construction constraints limited the vertical travel of Tip 2 to 5 cm.

4.4.4.1 Pressure transducers

Two pressure transducers were needed for probe operation; one for nulling and one for measuring pitot pressure. The former was an Endevco 8507 15 PSI transducer used in a differential mode and accurate to 259 Pa. Each side of this transducer was connected to a side port of the probe tip. The latter was an Endevco 8507 50 PSI transducer, referenced to vacuum and accurate to 862 Pa. The sensing side of this transducer was connected to the center port of the probe tip. These units were chosen because of their small size, permitting them to be installed inside the probe shaft. This reduced the time necessary for the pressure at the transducer face to reach equilibrium (about 50 milliseconds) and thereby increased the survey speed.

4.4.4.2 Probe placement

Streamwise positioning of the probe was different in each Case. For Case 1, this was accomplished using a rotatable eccentric window (Fig. 11). It consisted of three progressively smaller circular inserts, each centered 5.08 cm. off the center of the next larger one. The largest insert was of the same diameter as the section's window, while the smallest was concentric with the axis of probe rotation. Placement was accomplished by rotating the inserts relative to each other such that the desired probe location was ob-

tained. For Case 2, as was previously mentioned, the streamwise positioning was done by moving the probe in the ceiling slot. For both Cases, accuracy of this placement was within .04 cm. in the X- and Y-direction.

The probe drive (Fig. 10) controlled the probe's vertical and yaw motions. Vertical movement was provided by a stepper motor in conjunction with a precision worm gear. Position in this direction was measured with a linear potentiometer, calibrated against a dial gauge and accurate to .007 cm. Similarly, the yawing motion was provided by a stepper motor through a bevel gear, with angular position read by a multi-turn potentiometer. Calibration for yaw angle measurement was accomplished in a two-step procedure:

1. With the tunnel running and the probe placed in the freestream upstream of the interaction, the probe was manually rotated until the 'nulling' transducer indicated no pressure difference between the outer ports of the probe. This position was then referenced as the 'zero-yaw' position.
2. The remainder of the range was calibrated against a dial indicator, with a resulting accuracy of .2 degrees.

4.4.5 Computer System

At the center of the control and acquisition system was a Hewlett-Packard 1000 minicomputer. Control commands were issued to the stepper motors and Scanivalves via a Hewlett-Packard 2240 Measurement and Control Processor. The data was read into the system by a Preston Scientific GMAD 4 analog-to-digital converter. The GMAD 4 has an input range of +/- 10 volts and an output sequence of 14 bits (plus sign), giving it a resolution of better than 1 millivolt. This voltage was substantially below the equivalent error of any of the transducer systems.

Computer control over the cobra probe increased survey efficiency. Surveys were completed about four times faster than similar work carried out by Oskam manually. A simplified description of the surveying operation is given in Appendix A.

Full calibration of the test apparatus was carried out at least once a day prior to the start of testing. All pressure transducers were calibrated against precision Wallace and Tiernan absolute pressure gauges.

4.5 INTERFERENCE AND PERTURBATION STUDIES

Several tests were carried out to examine the effect of test configuration on the interaction and of the interaction on the operation of the probe. The areas investigated were:

1. the interaction between the generator shock wave and the sidewall boundary layer. This test was performed for Case 1 alone, since this configuration was most susceptible to the resulting effects. Examination of both surface flow patterns and pressure distributions indicated that:

- a) As Goldberg had noted (32), the sidewall separation was much more extensive than in the strictly two-dimensional interaction of a reflecting shock.
- b) The wave system resulting from this separation placed a limit on the downstream extent of the surveys.

2. the effect of the probe on the interaction. With Tip 1 placed .127 cm. off the surface at various stream-wise positions and at yaw angles approximated from Oskam's study, further flow patterns and pressure distributions were taken. At all locations, the line of maximum upstream influence and the flow convergence line (based on flow patterns) and the pressure distribution remained unchanged - both locally and upstream of the probe's position - from the undisturbed case.

3. probe deflection. Horizontal and vertical deflections of the probe tip were measured with the probe upstream of the interaction region and at various distances from the test surface. A telescope and vernier indicated displacements from the 'no-flow' condition. Results obtained in this manner showed that the probe tip deflected horizontally approximately .13 cm. in the downstream direction, but negligibly in the vertical direction at all tested locations. This horizontal displacement was accounted for in all data reduction.
4. the probe's nulling ability in the presence of the shock. With the tip 2 cm. off the surface and at stations 3.18 cm. upstream and 11.56 cm. downstream⁸ of the generator's leading edge, the probe was manually rotated about its nulled position. The angular displacement and the output of the nulling transducer were concurrently plotted against each other on an XY plotter. The resulting curves were the same at both stations, indicating that the probe's nulling ability was not affected by the proximity of the shock.
5. the effect of pitch angle on measurement accuracy. Measurements obtained with a cobra probe which nulls in the XY-plane alone are subject to error when pitch angles are present. To determine the effect of pitch

⁸ Just upstream of the calculated shock location.

angle on probe readings, the probe was pitched in the freestream and the results compared with those obtained when it was not pitched. This test indicated that the yaw angle measurement was insensitive to pitch angle, but that, for a pitch angle of 10 degrees, the pitot pressure was in error by 3%. The experimental findings of Oskam and the computations made by Horstman and Hung (19) and by Knight (29) indicate that pitch angles in the region of the interaction to be surveyed in this study are not that severe, and, therefore, the readings obtained can be considered reliable.

6. the effect of tip changes. Surveys were taken at the same location in the X-Y plane with each tip. The results (Figs. 12 and 13) showed a good correlation for both pitot pressure and yaw angle.
7. whether or not the height of the fin was 'semi-infinite' from the standpoint of the current study. This question was resolved by removing 1.27 cm. from the top of the generator in Case 2. A survey was taken in the immediate vicinity of the calculated shock, and the results compared with a survey taken at the same location prior to the shortening of the generator. The results seen in Figs. 14 and 15 indicate that the generator was, indeed, 'semi-infinite' from the perspective of the survey location.

8. the effect of moving the generator over short streamwise distances. In order to minimize the number of times the probe had to be moved in Case 1 (which was, on the average, a 45 minute task), the generator was moved in the streamwise direction over a 2.54 cm. distance. Surface pressure distributions were taken and probe surveys were repeated at the extremes and center of this travel. The results, as indicated by the pressure distributions in Fig. 16, show no difference between the three positions forward of $X_S = 5$ cm. - the region in which all of the surveys were taken.

Chapter V
RESULTS AND DISCUSSION

5.1 SURFACE MEASUREMENTS

This section will present the data obtained from the surface flow visualizations and pressure distributions for both Cases. Similarities are drawn as they pertain to the basic structure and to the scaled features of the interaction.

5.1.1 Kerosene-Lampblack Patterns

The surface traces taken for Case 1 and Case 2 are presented in Figs. 17 and 18, respectively. The patterns are set in diagrams to indicated their proper location relative to the test configuration. It is observed that, though the size of the interaction varies with incoming boundary layer thickness, the patterns exhibit the same general characteristics. Most notable of these is the passage of the lampblack streaks from the downstream to the upstream side of the calculated shock. These streaks parallel those originating upstream of the interaction in a region which grows in width with distance along the shock and is centered about a line inclined 30 degrees to the incoming flow. The absence of a coalescence line is in agreement with the analy-

sis of Kubota (16), which would predict coalescence for the present conditions to occur when the center of the convergence region reaches an angle of 32 degrees. Instead, the flow patterns exhibit 'incomplete convergence' indicating, by Kubota's definition, that the flow is unseparated.

As observed by previous investigators, the 'footprint' of this interaction is conical in shape. By this, it is meant that surface features at a distance from the shock generator - whether flow patterns or isobars - seem to propagate along lines at angles to the calculated shock. These lines intersect the plane containing the shock at a point (the 'virtual origin') displaced some distance upstream of the fin's leading edge. Teng and Settles (33) have investigated the significance of similar surface flow patterns in the three-dimensional interaction generated by a sweptback compression corner in supersonic flow. Their findings indicate a definite division between the flow-fields which generate patterns that are cylindrically symmetric (surface features remaining constant along lines parallel to the corner) and those whose patterns are conically symmetric. The latter is hypothesized to result when the inviscid shock becomes detached from the corner. Although there is no physical obstruction such as the corner in this study, it is suggested that a similar feature - possibly a rapid thickening of the boundary layer - may be responsible for the appearance of conical symmetry here.

The presence of conical symmetry has most often been based upon the qualitative appearance of surface phenomena. In their study, however, Teng and Settles found such symmetry to be quantitative as well. By assuming conical symmetry about the corner line, it was possible to collapse streamwise pressure distributions at several spanwise locations onto one curve. Lu (34) had similar success in applying the assumption of symmetry about the calculated shock to surface pressure distributions through the sharp fin-generated shock wave/turbulent boundary layer interaction. Only in the 'inception region' near the fin's leading edge does the trend fail.

In a slightly different manner, an attempt was made to verify the quantitative presence of conical symmetry in the current study. Values for streak angles along a single streamwise cut through the interaction in the region of conical symmetry were obtained for use as a base profile. A virtual origin was located at the intersection of a line passing through the points of upstream influence (away from the shock generator) and an extension of the calculated shock (See inset of Fig. 19). The base profile was then propagated in the spanwise direction at .25 cm. intervals along rays emanating from the virtual origin. Finally, imaginary particles were introduced into the field and their paths traced. The end results are presented in Fig. 19 for Case 1 and Fig. 20 for Case 2. Comparisons with the ker-

sene-lampblack patterns seem to confirm conical symmetry in both Cases.

To further substantiate this procedure, the sequence was repeated for the stronger interaction generated by a 15 degree fin under the same incoming conditions. Surface pressure distributions taken by Lu (34) show that this interaction is conically symmetric away from the shock generator (Fig. 21). The generated particle paths are presented in Fig. 22, along with the kerosene-lampblack trace. The distinct surface characteristics of this flow-field, particularly the two convergence lines near the calculated shock position and the divergence line near the fin root, are accurately reproduced. This is felt to confirm the validity of the procedure used.

5.1.2 Surface Pressure Distributions

Surface pressure distributions taken for Case 1 are presented in normalized isobar form in Fig. 23. The results are typical of previous investigations and provide reinforcement for the conical symmetry observed in the surface flow patterns. When compared with this isobar map, the lampblack streaks converge within the pressure plateau.

The point of upstream influence is located along each streamwise pressure distribution at the intersection of a line tangent to the steepest portion of the distribution and

one representing the undisturbed pressure level. Values obtained in this manner are in good agreement with those obtained from the surface flow visualizations, where upstream influence is located at the point at which the lampblack streaks first deviate from the incoming flow direction.

5.1.3 Scaling of Surface Features

The result of scaling the upstream influence (as measured from the calculated shock position) by the method of Settles et al (6) and accounting for Mach number and generator angle differences by the method of Dolling and Bogdonoff (5) is presented in Fig. 24. The scaled values for several other investigations of this type of interaction are also presented, although the boundary layer thickness used to scale this data is that given as an incoming condition. Use of the incoming value (as opposed to that used in scaling the present data (see 'Experimental Program')) accounts for significant error in the plotted results of Oskam (1) only. All other data were obtained under conditions (either with large shock angles or not far from the spanwise location of the fin's leading edge) where the 'correct' boundary layer thickness should not have varied much from the incoming condition. As can be seen, this non-dimensionalizing technique collapses the data well, with the exception of those obtained by Kubota (16) at Mach 2.41. A possible explanation for this discrepancy will be provided at the end of this chapter.

From a different perspective, surface streak angles were measured along a single streamwise cut through each of the interactions of the current study. The spanwise position of these cuts was chosen such that they were at the same non-dimensional distance from the fin's leading edge (as measured along the shock). The distances from the shock were then scaled and plotted against their respective streak angles. Results are presented in Fig. 25, again indicating that the scaling procedure is correct. Repeating this procedure for a different non-dimensional spanwise position, however, shows that these curves are not very sensitive to changes in distance along the shock.

In a preliminary study, a series of tests were conducted to confirm the application of the scaling format of Dolling and Bogdonoff (5) to surface pressure distributions. A 9.5 degree sharp fin was mounted on and perpendicular to the test surface, on which one of two boundary layers - similar to those in the current study - was generated. Static pressures were measured along lines normal to the calculated shock, and lengths along and normal to the shock non-dimensionalized. Samples of pressure distributions along these lines at the same L_{SND} are shown in Fig. 26. Though the number of points obtained along each line when using the thinner boundary layer is small, the data that is present indicates that the scaling method properly accounts for variation in boundary layer thickness. It is thus concluded

that this approach can be applied equally well to pressure distributions and surface flow patterns - at least for the same Mach number, generator angle, and Reynolds number.

5.2 FLOW-FIELD SURVEYS

Cobra probe surveys were taken in one XZ plane in each interaction. The Y coordinate of both planes was chosen, as in the above analysis, such that it intersected the calculated shock at the same non-dimensional distance from the fin's leading edge. Further constraints were imposed by the physical dimensions of the wind tunnel and the probe. The values chosen for these locations were:

	Y (cm.)	L _S (cm.)	L _{SND}
CASE 1	12.1	26.9	1650
CASE 2	6.4	13.6	1640

Upstream influence along the lines of intersection between these planes and the test surfaces was examined and scaled. The dimensional values for these lengths were found to be 9.3 cm. for Case 1 and 4.8 cm. for Case 2. When

scaled, they become 590 and 580, respectively. The 2% difference is of the same order and direction as the difference in L_{SND} and the error induced by the choice of boundary layer thickness in the scaling procedure (see 'Experimental Program').

Measurements of yaw angle and pitot pressure were obtained simultaneously during each survey. Yaw angles at the test surface were found to be in agreement with those indicated by the surface flow patterns. Typical results of the data obtained from each survey are presented in Fig. 27. For further analysis, the results have been compiled in the form of contour maps.

As pointed out by Oskam (1), it is impossible to correctly derive velocities through most of the interaction from the measured pitot pressures and the corresponding surface pressures alone. This is due to the normal static pressure gradients created by the system of compression and expansion waves generated within the flow-field. In the region downstream of the calculated shock and beneath the height of the incoming boundary layer thickness, however, no such gradients are found (Oskam (1)). Mach numbers were derived for this region based on measured pitot pressures and accompanying surface static pressures, then plotted in Fig. 28 against the results of Oskam (1). As can be seen, the results are similar.

5.2.1 Yaw Angle Measurements

Contour plots of yaw angles in the surveyed planes are presented in Figs. 29 and 30. To avoid obscuring the data, only six contour values are plotted. The flow angle above the upper 10 degree contour is 10 degrees (the angle calculated by oblique shock theory), with the contour marking the highest value of Z at which the flow first deviates from this direction. As with the surface flow patterns, the physical length scale of Case 1 is larger than that of Case 2, but the general features are the same. It is necessary to point out that the 'deadband' (see Appendix A) used in the nulling routine contributes a certain amount of error to the placement of these contours. In regions of large angle gradients, this error is within the accuracy of the vertical measurement. In lower gradients, the error becomes slightly more significant. Fortunately, most of the contours do not fall in regions of the second type.

The three most significant and common features are:

1. the 2.5 degree contour. Though annotated with a specific value, this line actually represents a jump in flow angle of 3 to 4 degrees. The contour is quasi-linear, intersecting the test surface at the point of upstream influence (as indicated by the kerosene-lampblack patterns) with an included angle of 30 degrees. The varying discontinuity indicates that this

contour represents a coalescence of compression waves, though the lack of curvature and the direction of flow deflection suggest that these waves are not oriented solely in the XZ plane. These waves correspond to the lambda-foot observed by Zubin and Ostapenko (35). Yaw angle measurements made by Oskam (1) in the YZ plane also show this contour as quasi-linear, suggesting a coalescence plane stemming from the vicinity of the fin's leading edge. This gradual compression is felt to be responsible for the region downstream of the calculated shock in which the Mach numbers are higher than that calculated by oblique shock theory.

2. a region of sub-generator angle flow above the height of the incoming boundary layer and downstream of the calculated shock. The shape of this region is similar to that of the supersonic tongue found in transonic, two-dimensional shock wave/boundary layer interactions, and, indeed, the Mach numbers in this region have been shown to be higher than that obtained by oblique shock theory. As mentioned in the review section of this work, however, comparisons made by McCabe (8) and Oskam (1) seem to indicate that direct analogies between these two types of interactions cannot be drawn.

It is interesting to note that the angles at the center of this region are smaller than those measured by Oskam under similar conditions. As the surveys in the current study were obtained slightly farther outboard of the fin, the difference may be due to a weakening of a direct effect that the presence of the shock generator has on the interaction.

3. the presence of large yaw angles above the incoming boundary layer. Just upstream of the calculated shock, the 2.5 degree contour deviates from its linear trend, ending in a region in which the yaw angle approaches 16 degrees. A further investigation was undertaken to locate the origin of this anomaly and will be discussed later in this chapter.

In concluding this section, two final observations can be made regarding the findings of this study and those of Oskam. First, at $X_s = 12.2$ cm. in Case 2, the yaw angles vary by only 2 degrees through the interaction (Fig. 31). This supports Oskam's conclusion that it takes approximately 30 incoming boundary layer thicknesses for all transverse pressure gradients to disappear from this point in the interaction. Second, the 10 degree contour above the viscous layer downstream of the calculated shock (Case 1) is farther from the test surface than was previously observed. As in Point 2 above, this may be attributed to the differences in the proximity of the shock generator.

5.2.2 Pitot Pressure Measurements

The results of the pitot pressure measurements, normalized by stilling chamber (incoming stagnation) pressure, are presented in Figs. 32 and 33. Again for clarity, only four contours are plotted. The calculated downstream normalized value for these contours is .5. As with yaw angle, the plots of both Cases exhibit similar features. The contour labeled $\overline{PT} = .4$ shows the same linear trend as the 2.5 degree contour in the yaw angle plots. It too represents a varying discontinuity, supporting the idea that there is a coalescing compression fan at the base of the calculated shock. In neither Case does the pitot pressure profile of the boundary layer deviate much from its incoming shape as it passes beneath this system. Further downstream, however, the profiles fill out rapidly as the flow above it begins to orient itself with the shock generator. Oskam found this region to be characterized by negative pitch angles, leading to the conclusion that an attachment process was present.

5.2.3 Comparison with the Computation of Knight (29)

Before examining the results of scaling this interaction, it is worthwhile to compare the raw data obtained in Case 1 with that computed by Knight. The incoming conditions and generator angle used for this computation are those of Oskam et al (1,2,3). Their values differ from this study's in

that the current generator angle was .28 degrees larger and the incoming boundary layer was .1 cm. thinner. The calculated skin friction lines, presented in Fig. 34, are in good agreement with the kerosene-lampblack trace and the replicated surface pattern. Yaw angle and pitot pressure surveys for three different streamwise positions are compared in Figs. 35 and 36. The use of a logarithmic scale in these plots allows the entire height of the interaction to be presented, but tends to over-emphasize the lower portion of the boundary layer while de-emphasizing the upper regions. It can be seen that the computed flow first indicates a deviation in flow direction downstream of where it is measured. Further, it takes longer for the calculated boundary layer to recover from the effects of the shock than is observed experimentally. These differences are similar to those found by Oskam between the interactions generated by progressively smaller generator angles. It would seem that the numerical code predicts a weaker interaction than is actually present. The exact reason for this is unclear, though a more rigorous examination of the turbulence model may indicate a means of obtaining better results.

5.2.4 Scaling of Survey Results

In line with previous investigations, the data obtained during the surveys is first scaled by boundary layer thickness alone. The results of this procedure are presented in

Figs. 37 and 38. Neither the yaw angle plots nor the pitot pressures plots show adequate collapsing of the features.

As a second approach, the scaling method of Settles et al (6), which was found to work successfully on the test surface, was applied to both axes. As can be seen in Figs. 39 and 40, this procedure provides a vast improvement over the previous technique. Three of the above-mentioned features are collapsed in these plots. First, the point at which the 2.5 degree contour deviates from its linear trend is 230 units above the surface. Second, the sub-generator angle region downstream of the calculated shock is centered about a line 100 units above the test surface, with the 5 degree 'tongue' terminating between an X_{SND} of 270 and 300. Finally, the point at which the pitot pressure profile fills out occurs 285 units downstream of the calculated shock.

The 30 unit streamwise shift between the Case 1 and Case 2 is probably due to small errors in shock wave angle magnified over the spanwise distance from the fin. This difference is within the error-band of the experiment.

From this evidence, it is concluded that the Reynolds number 'residual' must be accounted for in scaling interactions of this type. In addition, the same transformation is applicable to lengths measured normal to the test surface as well as to those on the test surface - at least over the range of parameters examined. Thus, it may be possible to

experimentally obtain an extensive data set for a given set of conditions and, from it, generate a 'family' of interactions for different Reynolds numbers and boundary layer thicknesses.

5.2.5 Large Upstream Yaw Angles

As previously mentioned, the yaw angle profiles of both Case 1 and Case 2 display a large deviation from the streamwise direction in the flow above the incoming boundary layer and upstream of the calculated shock, peaking at a value close to 16 degrees. This was unexpected as no such feature was reported by Oskam (1). Peake (4) noted a similar phenomenon in his data, but attributed it to the vortex resulting from boundary layer separation. As the current interaction is considered unseparated, this explanation does not hold. Nor is the explanation thought to lie with Kubota's corner-vortex theory as the surveys were conducted relatively far from the fin.

Because of the larger dimensions in Case 1, surveys were made at two additional spanwise locations to observe the development of this anomaly with increasing Y . The Y values chosen for these surveys were 10.20 cm. and 8.33 cm. Five streamwise locations were surveyed at $Y = 10.20$ cm. to locate the point at which the large angles began to appear. One survey was then taken at $Y = 8.33$ cm., based on the

trend derived from the two previous spanwise locations, to located this point again. Results of these surveys indicate that this feature is present at all spanwise locations, though at a lower Z as the fin's leading edge is approached. This can be seen in Fig. 41. When a line is passed through the points at which the feature begins, it intersects the test surface at $X = -1.33$ cm. and $Y = -0.23$ cm. at an angle of 8.44 degrees.

The fact that the interaction seems to extend well above the test surface ($Z = 6.4$ cm. at $Y = 6.4$ cm. for Case 2) indicates that experiments must be conducted in relatively large facilities (in terms of boundary layer thickness) in order to avoid interference problems. Consideration must also be taken when working with shock generators that span the wind tunnel, as there is usually an identical interaction taking place on the wall opposite the test surface. This problem may explain the discrepancy found in scaling Kubota's (16) data at Mach 2.41, since they were obtained in a 6.35 cm. x 6.35 cm. facility with a boundary layer thickness on the order of .5 cm. A further investigation of this feature is needed.

Chapter VI

CONCLUSIONS

An experimental study of the scaling of the three-dimensional shock wave/turbulent boundary layer interaction generated by a fin with a sharp, unswept leading edge at a 10 degree angle-of-attack to the incoming flow has been reported in this thesis. The incoming freestream was at a Mach number of 2.95 and a Reynolds number of 63×10^6 /meter. The effect of variation in incoming boundary layer thickness was observed by using equilibrium turbulent boundary layers of 1.25 cm. and .50 cm. thickness. Fins were near adiabatic wall temperature.

Yaw angles and pitot pressures were obtained by a computer-controlled cobra probe in a streamwise plane normal to the test surface for each interaction. The spanwise position of these planes was such that they intersected the calculated shock wave at the same normalized distance from the fin's leading edge. Streamwise distance between surveys was less than .8 cm., with closer spacing in the vicinity of the shock. Vertical distance between data points was less than .1 cm. This resulted in a data set with a greater resolution in both directions than had previously been obtained.

From this data, the following observations and conclusions have been made:

1. The dimensions associated with the characteristics of this flow-field are a function of both freestream Reynolds number and local boundary layer thickness. The same normalizing method found to collapse upstream influence data is found to work equally well for lengths associated with non-surface features.
2. The interaction is found to extend further than 10 local boundary layer thicknesses above the test surface in the vicinity of the calculated shock, indicating that it is much larger than previously believed.
3. A region above the incoming boundary layer upstream of the calculated shock was found in which yaw angles of up to 1.5 times the shock generator angle were measured. This region was found to emanate from the vicinity of the junction between the fin leading edge and the test surface.
4. With the exception of the above feature, the results are in good agreement with the earlier findings of Oskam. The interaction is seen to be dominated by a series of compression waves upstream of the calculated shock. The present survey results support Oskam's proposal (based on surface flow patterns) that their effects are felt up to 30 incoming boundary layer thicknesses downstream of the calculated shock.

5. Comparisons with recent computational results of Knight for this flow-field indicate that the numerical approach seems to predict a weaker interaction than is actually present. The computed upstream influence is smaller and the length required for the boundary layer to recover - once it has passed beneath the calculated shock - longer. The numerical prediction is, however, adequate for many engineering applications.

6.1 RECOMMENDATIONS FOR FUTURE STUDY

While this study has added to the current understanding of the shock wave/turbulent boundary layer interaction, it has illuminated the need for further study of several areas. The areas recommended for subsequent investigations are:

1. An investigation into the cause of the high-yaw angle region upstream of the calculated shock. Though the origin of this feature was located in this study, its cause is still not understood.
2. An effort to locate the height at which the planar calculated shock is reached and how this height varies with distance along the shock.
3. A broader, but less detailed investigation to verify the scaling method over a wider range of Mach number, Reynolds number, and shock generator angle.

4. Finally, a study based on a preliminary computation to 'pre-locate' significant features. This would serve both to verify the numerical code and to economize the experimentalists efforts.

REFERENCES

1. Oskam, B. "Three Dimensional Flowfields Generated by the Interaction of a Swept Shock with a Turbulent Boundary Layer." Princeton University, Gas Dynamics Laboratory Report 1313, December 1976.
2. Oskam, B., Vas, I.E., and Bogdonoff, S.M. "Mach 3 Oblique Shock Wave/Turbulent Boundary Layer Interactions in Three Dimensions." AIAA Paper 76-336, July 1976.
3. Oskam, B., Bogdonoff, S.M., and Vas, I.E. "Study of Three Dimensional Flow Fields Generated by the Interaction of a Skewed Shock Wave with a Turbulent Boundary Layer." AFFDL TR 75-21, February 1975.
4. Peake, D.J. "The Three-Dimensional Interaction of a Swept Shock Wave with a Turbulent Boundary Layer and the Effects of Air Injection on Separation." Ph.D. Thesis, Carleton University, Ottawa, Canada, March 1975.
5. Dolling, D.S. and Bogdonoff, S.M. "Upstream Influence Scaling of Sharp Fin-Induced Shock Wave Turbulent Boundary Layer Interactions." AIAA Paper 81-336, January 1981.
6. Settles, G.S., Perkins, J.J., and Bogdonoff, S.M. "Upstream Influence Scaling of 2D and 3D Shock/Turbulent Boundary Layer Interaction at Compression Corners." AIAA Paper 81-334, January 1981.
7. Stanbrook, A. "An Experimental Study of the Glancing Interaction Between a Shock Wave and a Turbulent Boundary Layer." ARC-CP-No. 555, July 1960.
8. McCabe, A. "A Study of Three-Dimensional Interactions Between Shock Waves and Turbulent Boundary Layers." Ph.D. Thesis, University of Manchester, October 1963.
9. Lowrie, B.W. "Cross-Flows Produced by the Interaction of a Swept Shock Wave with a Turbulent Boundary Layer." Ph.D. Thesis, Cambridge University, December 1965.

10. Hammit, A.G. and Hight, S. "Scale Effects in Turbulent Shock Wave Boundary Layer Interactions." AFOSR TN 60-82, Proceeding of 6th Midwestern Conference on Fluid Mechanics, University of Texas, 1959.
11. Gadd, G.E. "Interactions Between Normal Shock Waves and Turbulent Boundary Layers." ARC R&M No. 3262, 1962.
12. Kooi, J.W. "Experiment on Transonic Shock-Wave Boundary Layer Interaction." AGARD-CP-168, Paper 30, 1975.
13. Johnston, J.P. "On the Three-Dimensional Turbulent Boundary Layer Generated by Secondary Flow." Journal of Basic Engineering, Series D, Trans. ASME, Vol. 82, 1960, pp. 233-248.
14. Dolling, D.S. and Bogdonoff, S.M. "An Experimental Investigation of the Unsteady Behavior of Blunt Fin-Induced Shock Wave Turbulent Boundary Layer Interactions." AIAA Paper 81-1287, June 1981.
15. Dolling, D.S. and Murphy, M. "Wall Pressure Fluctuations in a Supersonic Separated Compression Ramp Flowfield." AIAA Paper 82-986, June 1982.
16. Kubota, H. "Investigations of Three-Dimensional Shock Wave Boundary Layer Interactions." AFOSR-76-3006, January 1980.
17. Lighthill, M.J. "Attachment and Separation in Three-Dimensional Flow." Laminar Boundary Layers, Oxford University Press, 1963, pp. 72-82.
18. Hung, C.M. and MacCormack, R.W. "Numerical Solution of a Three-Dimensional Shock Wave and Turbulent Boundary-Layer Interaction." AIAA Paper 78-161, January 1978.
19. Horstman, C.C. and Hung, C.M. "Computation of Three-Dimensional Turbulent Separated Flows at Supersonic Speed." AIAA Paper 79-2, January 1979.
20. Escudier, M.P. "The Distribution of the Mixing Lengths in Turbulent Flows Near Walls." Rep. TWF/TN/1, Imperial College, London, 1965.
21. Law, C.H. "Three-Dimensional Shock Wave-Turbulent Boundary Layer Interactions at Mach 6." ARL TR 75-0191, June 1975.
22. Token, K.H. "Heat Transfer Due to Shock Wave Turbulent Boundary Layer Interactions on High Speed Weapon Systems." AFDDL-TR-74-77, April 1974.

23. Hayes, J.R. "Prediction Techniques for the Characteristics of Fin Generated Three Dimensional Shock Wave Turbulent Boundary Layer Interactions." AFFDL-TR-77-10, May 1977.
24. Neuman, R.D. and Hayes, J.R. "Prediction Techniques for Three-Dimensional Shock Wave/Turbulent Boundary Layer Interactions." AIAA Journal, Vol. 15, No. 10, October 1977, pp. 1469-1473.
25. Scuderi, L.F. "Expressions for Predicting 3-D Shock Wave-Turbulent Boundary Layer Interaction Pressure and Heating Rates." AIAA Paper 78-162, January 1978.
26. Green, J.E. "Interactions Between Shock Waves and Turbulent Boundary Layers." Progress in Aerospace Sciences. Vol.11, Pergammon Press 1970, pp. 235-340.
27. Lighthill, M.J. "On Boundary Layers and Upstream Influence, II. Supersonic Flow Without Separation." Proceedings of the Royal Society, A, Vol. 217, 1953, pp. 478-507.
28. Inger, G.R. "Upstream Influence and Skin Friction in Non-Separating Shock-Turbulent Boundary Layer Interactions." AIAA Paper 80-1411, July 1980..
29. Knight, D.D. "A Hybrid Explicit-Implicit Numerical Algorithm for the Three-Dimensional Compressible Navier-Stokes Equations." AIAA Paper 83-223, January 1983.
30. Settles, G.S. "An Experimental Study of Compressible Turbulent Boundary Layer Separation at High Reynolds Number." Ph.D. Thesis, Princeton University, September 1975.
31. Settles, G.S. and Teng, H.Y. "Flow Visualization of Separated 3-D Shock Wave/Turbulent Boundary Layer Interactions." AIAA Paper 82-229, January 1982.
32. Goldberg, T.J. "Three-Dimensional Separation for Interaction of Shock Waves with Turbulent Boundary Layers." AIAA Journal, Vol. 11, No. 11, 1973, pp. 1573-1575.
33. Teng, H.Y. and Settles, G.S. "Cylindrical and Conical Upstream Influence Regimes of 3D Shock/Turbulent Boundary Layer Interactions." AIAA Paper 82-987, June 1982.
34. Lu, F.K.P. "An Experimental Study of 3D Shock/Boundary Layer Interactions Generated by Swept Fins." MSE Thesis, Princeton University, January 1983.

35. Zubin, M.A. and Ostapenko, N.A. "Structure of Flow in the Separation Region Resulting from Interaction of a Normal Shock Wave with a Boundary Layer in a Corner." *Izvestiya Akademii Nauk SSSR, Mekhanika Zhidkosti i Gaza*, May-June 1979, pp. 51-58.

Appendix A

EXPLANATION OF PROBE NULLING OPERATION

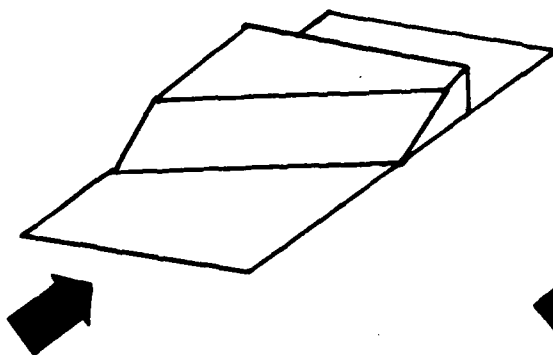
The following is a simplified explanation of the computer control over the nulling operation of the cobra probe. Reference to Fig. 42 will aid in understanding this procedure.

1. The computer reads the voltage form the nulling transducer.
2. This voltage is converted to a pressure (via calibration coefficients), then to an angular displacement from the null position through a second coefficient. Initially, the second coefficient is set at a value determined from previous work. Subsequent coefficients are computed if more than two nulling operations are required at any individual vertical position.
3. If this displacement falls within a pre-selected deadband, the computer reads the probe tip's vertical height above the test surface, angular displacement from the incoming flow direction, and the associated pitot pressure. Previous work with this system indicated that a deadband of .5 degrees was optimum for time and accuracy. The probe is then moved to the next vertical location and the process is repeated.

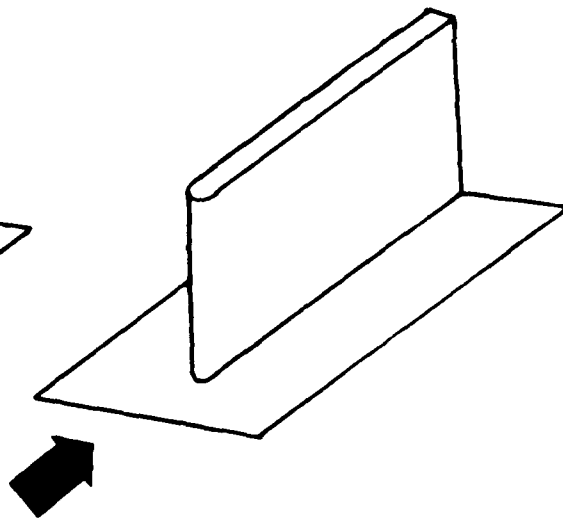
The distance between successive vertical positions is inversely proportional to the yaw angle gradient.

4. If the angular displacement from the null position exceeds the given deadband, the computer rotates the probe tip through the calculated angle to bring it to this position. The sequence then returns to step 1.

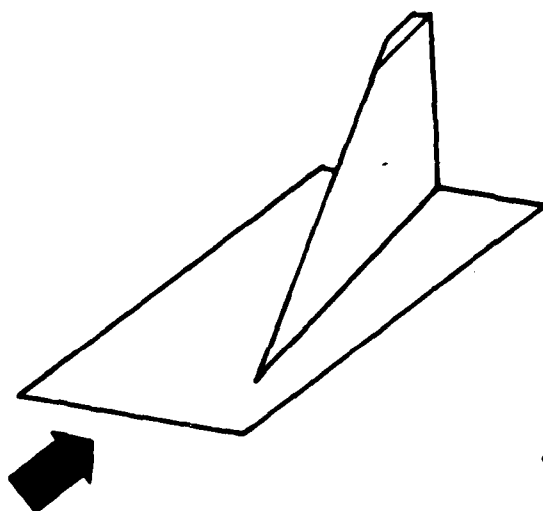
Swept Compression Corner



Unwept Blunt Fin



Swept Sharp Fin



Swept Blunt Fin

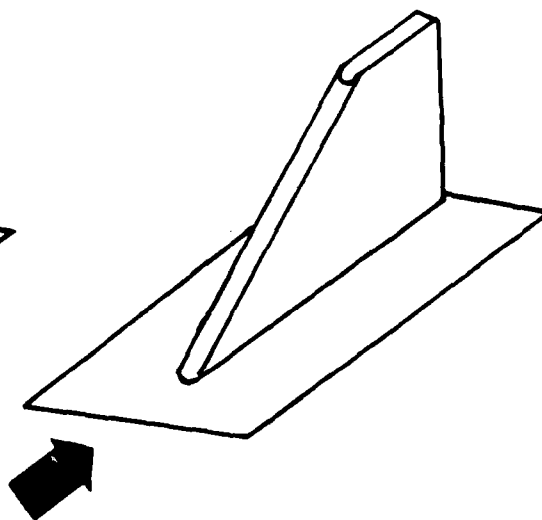


Fig. 1 Experimental geometries generating 3D shock wave/boundary layer interactions

Unswep Sharp Fin Interaction

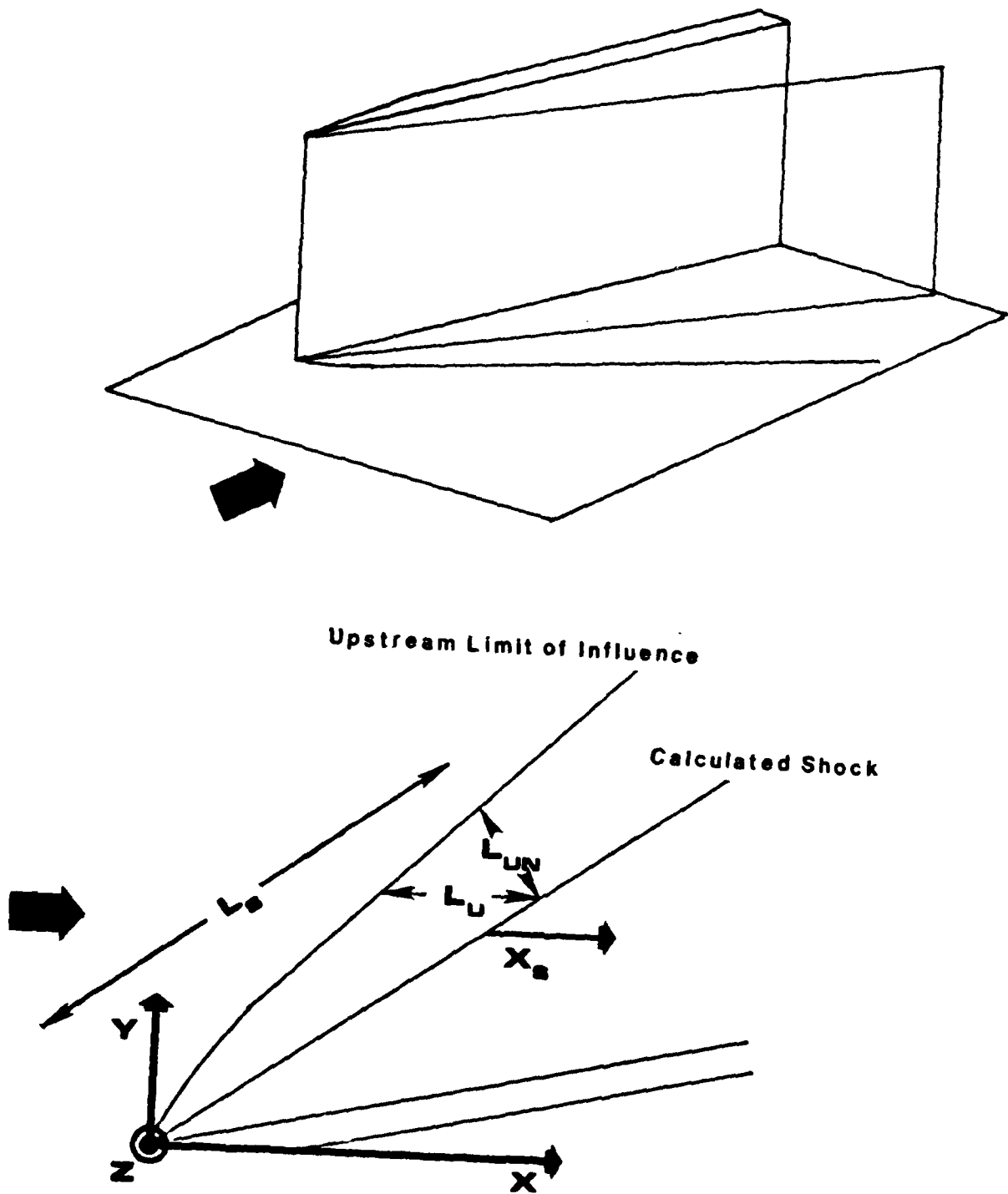


Fig. 2 Unswep sharp fin interaction and coordinate system

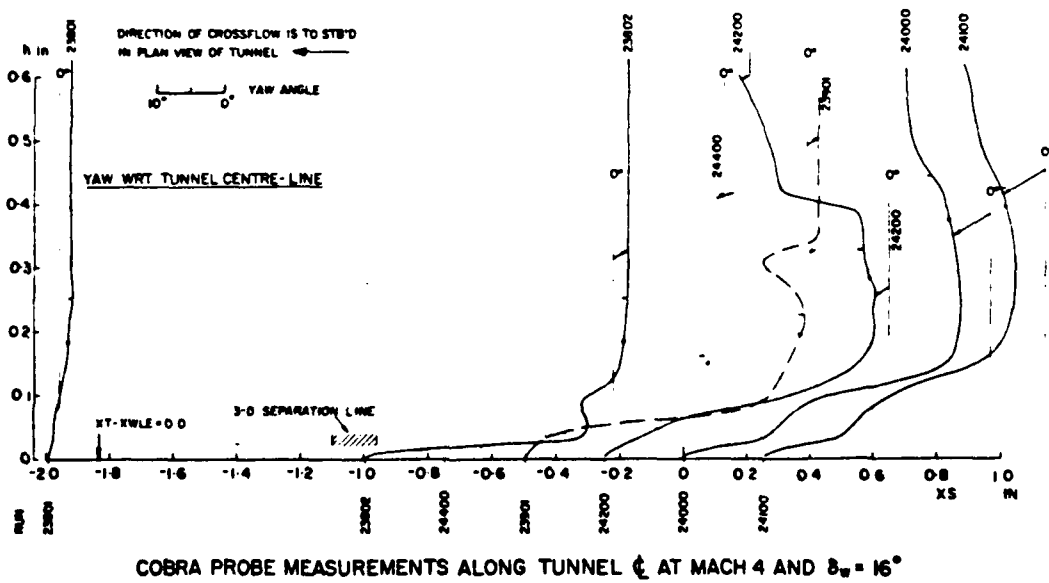
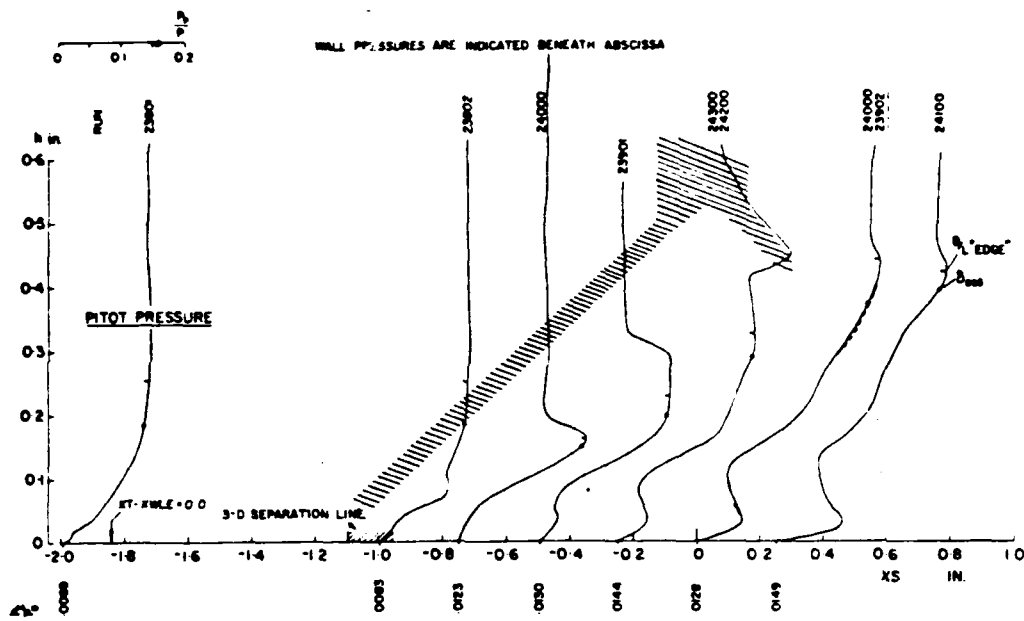
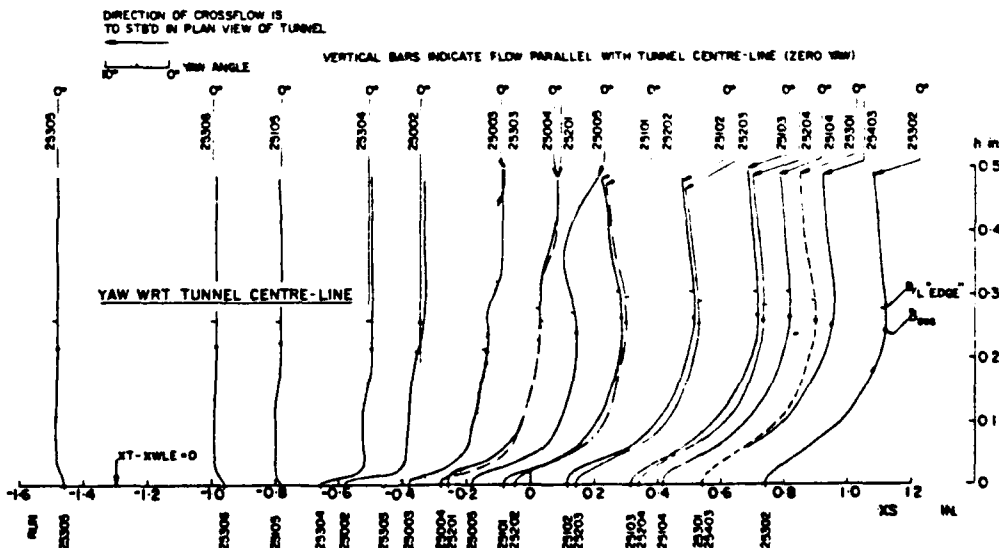
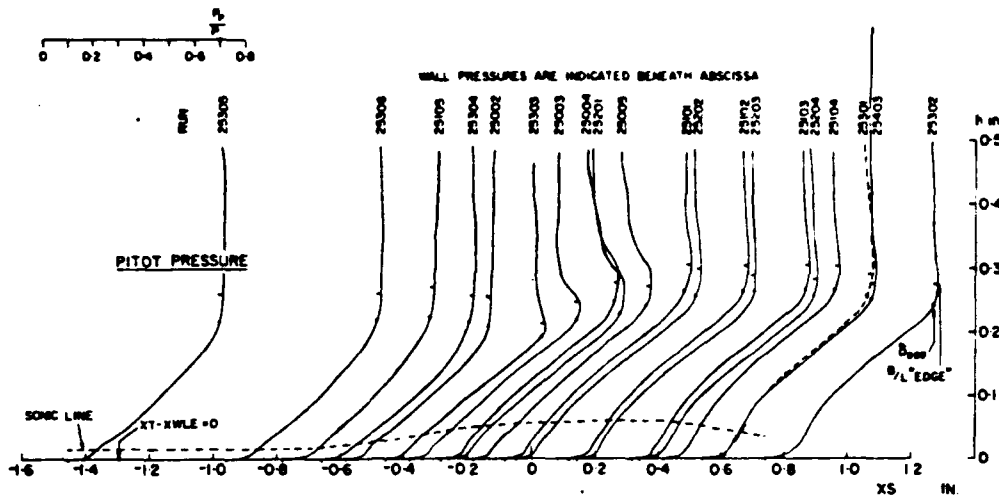


Fig. 3 Cobra probe measurements of Peake (4) at Mach 4 for a 16 degree fin



COBRA PROBE MEASUREMENTS ALONG TUNNEL ζ AT MACH 2 AND $\delta_w = 8^\circ$

Fig. 4 Cobra probe measurements of Peake (4) at Mach 2 for an 8 degree fin

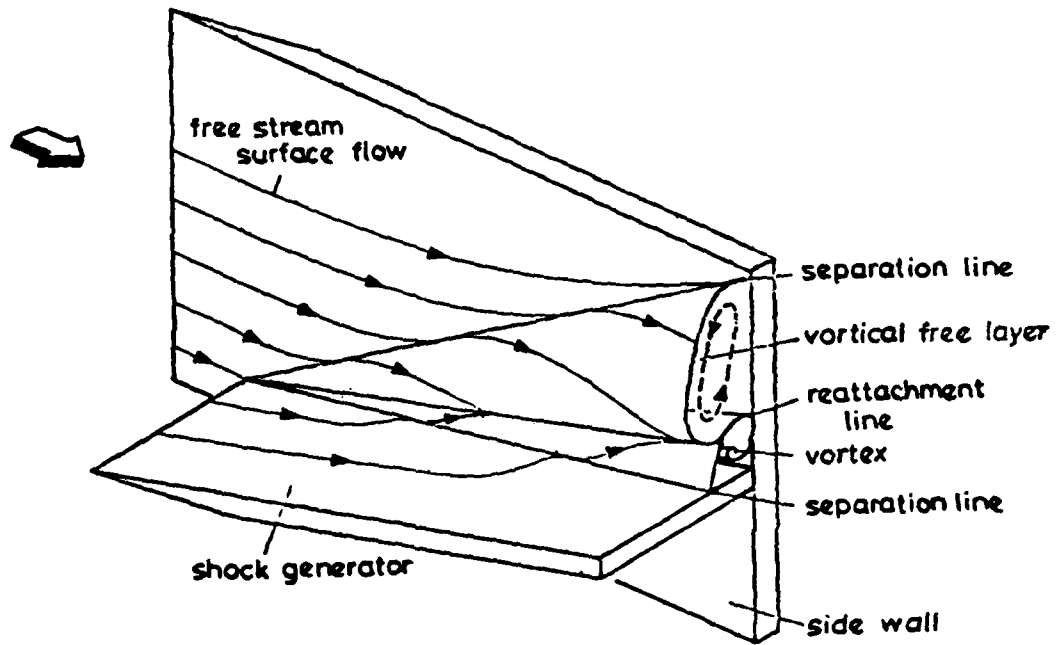
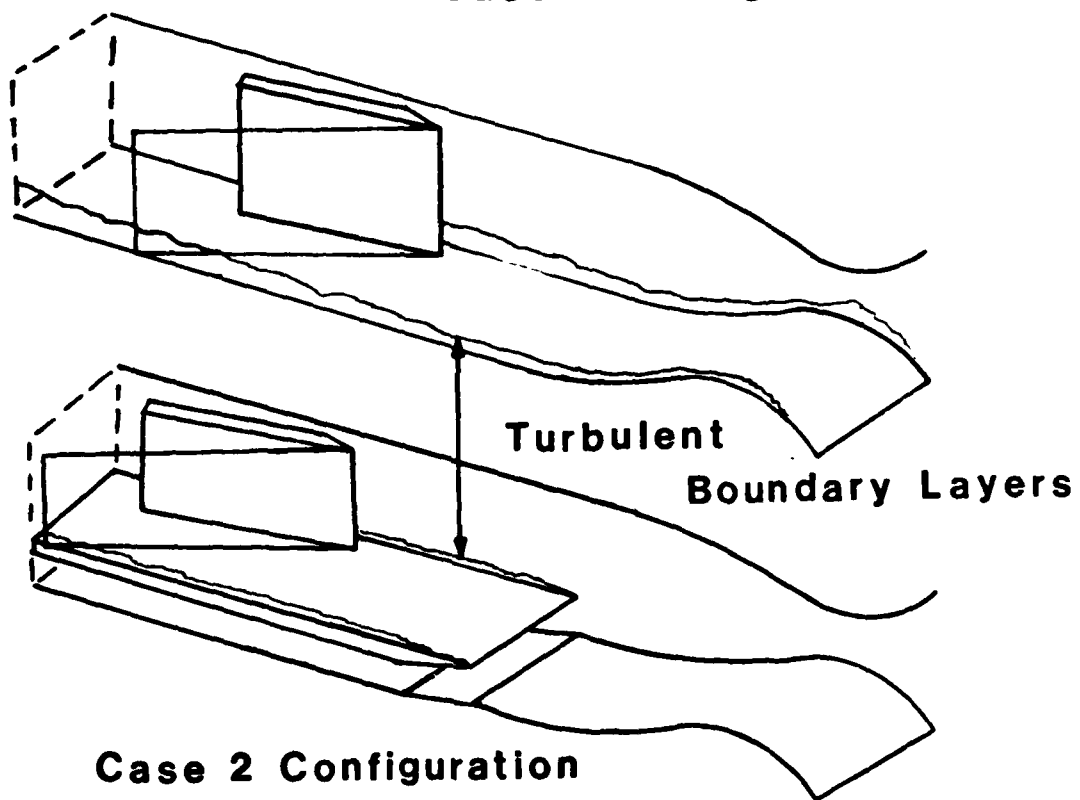


Fig. 5 'Double viscous layer' model of Kubota (16)

Case 1 Configuration



Case 2 Configuration

Fig. 6 Experimental configurations for Case 1 and Case 2

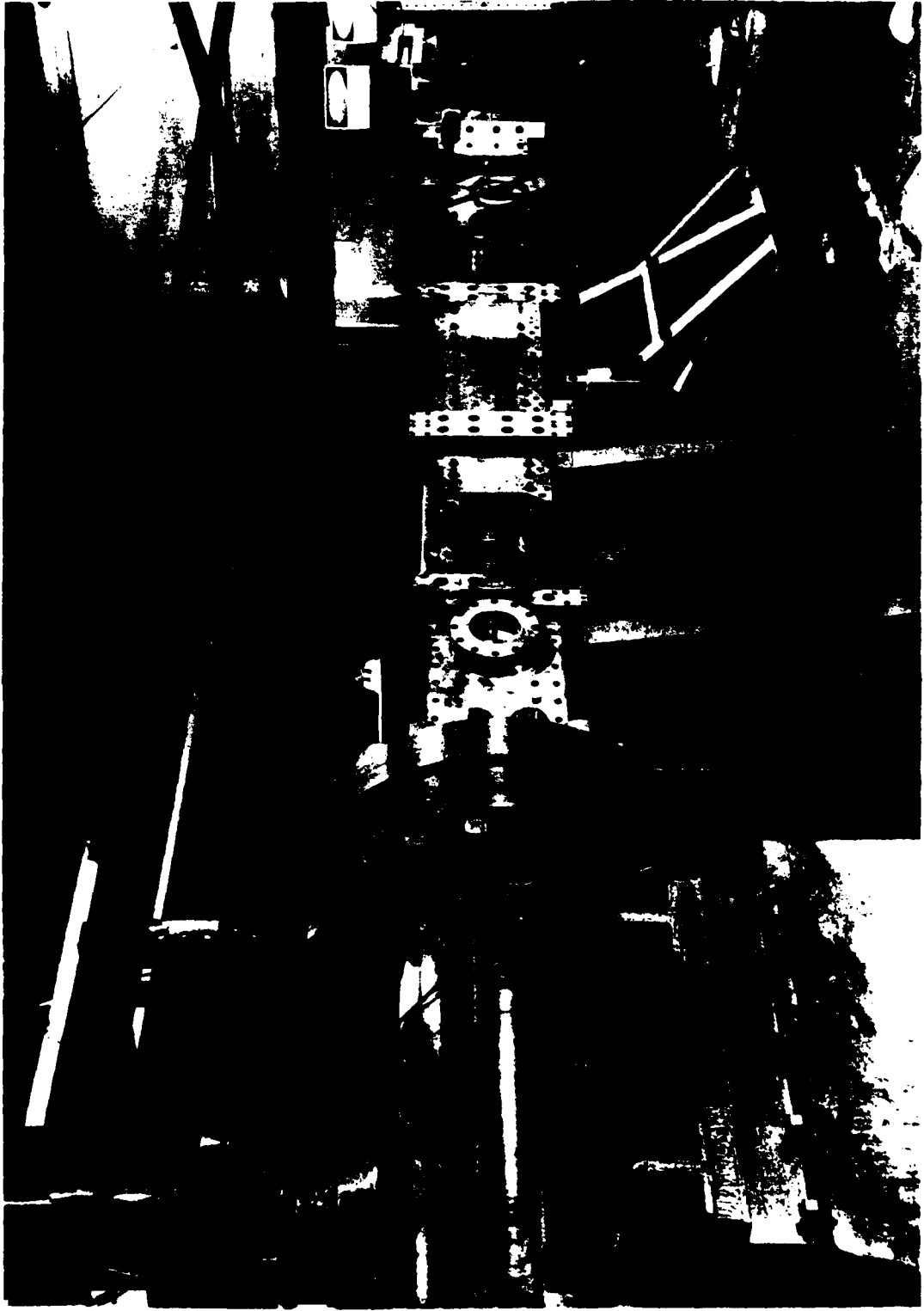
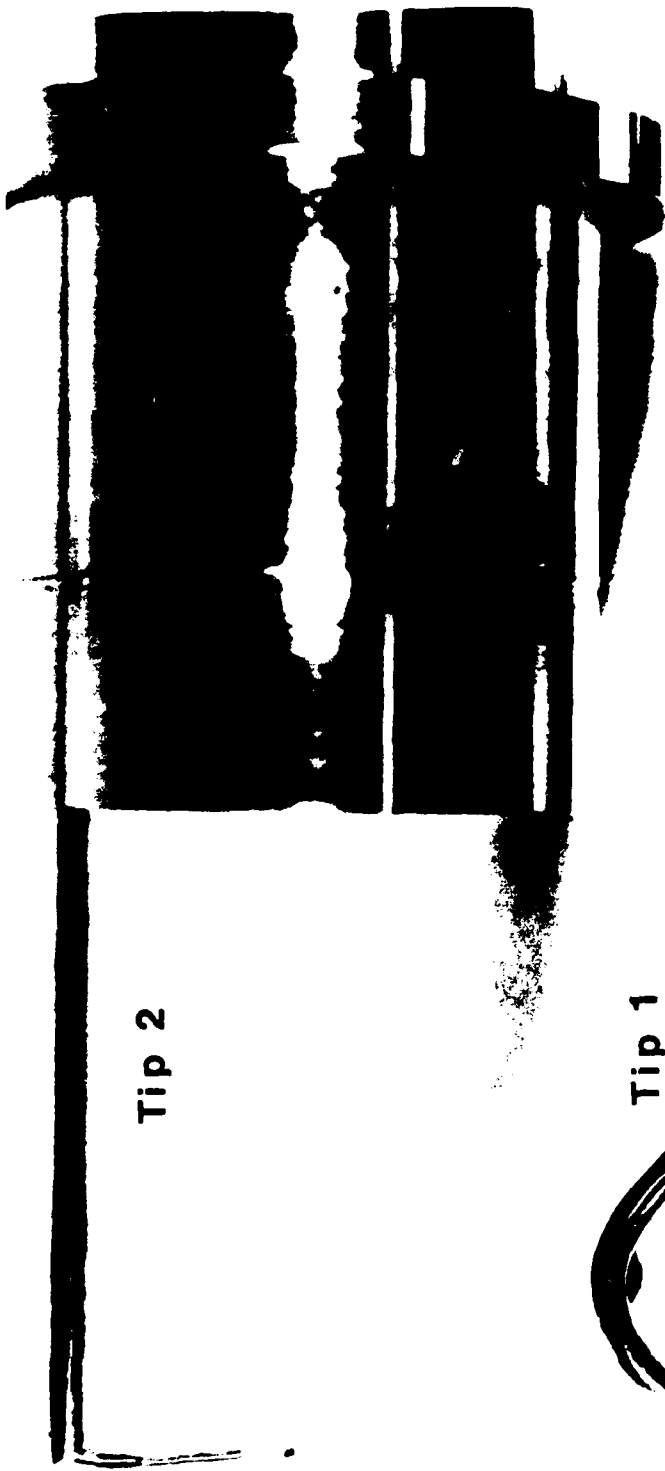


Fig. 7 Princeton University 20 cm. x 20 cm.
windtunnel



Fig. 8 Test models



Tip 2

Tip 1



Fig. 9 Probe tips

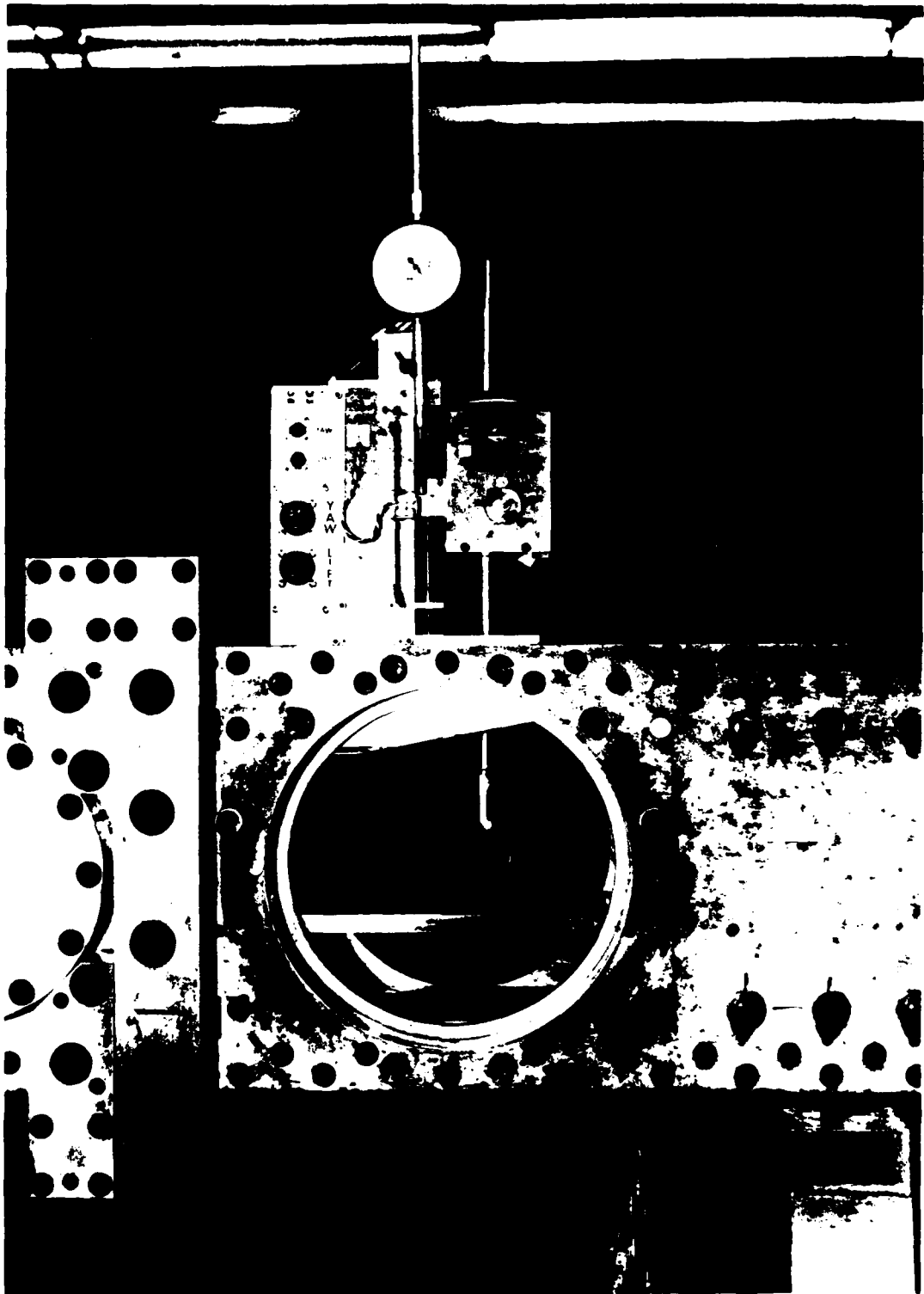


Fig. 10 Probe and drive configuration for
Case 2



Fig. 11 Eccentric window with Tip 2

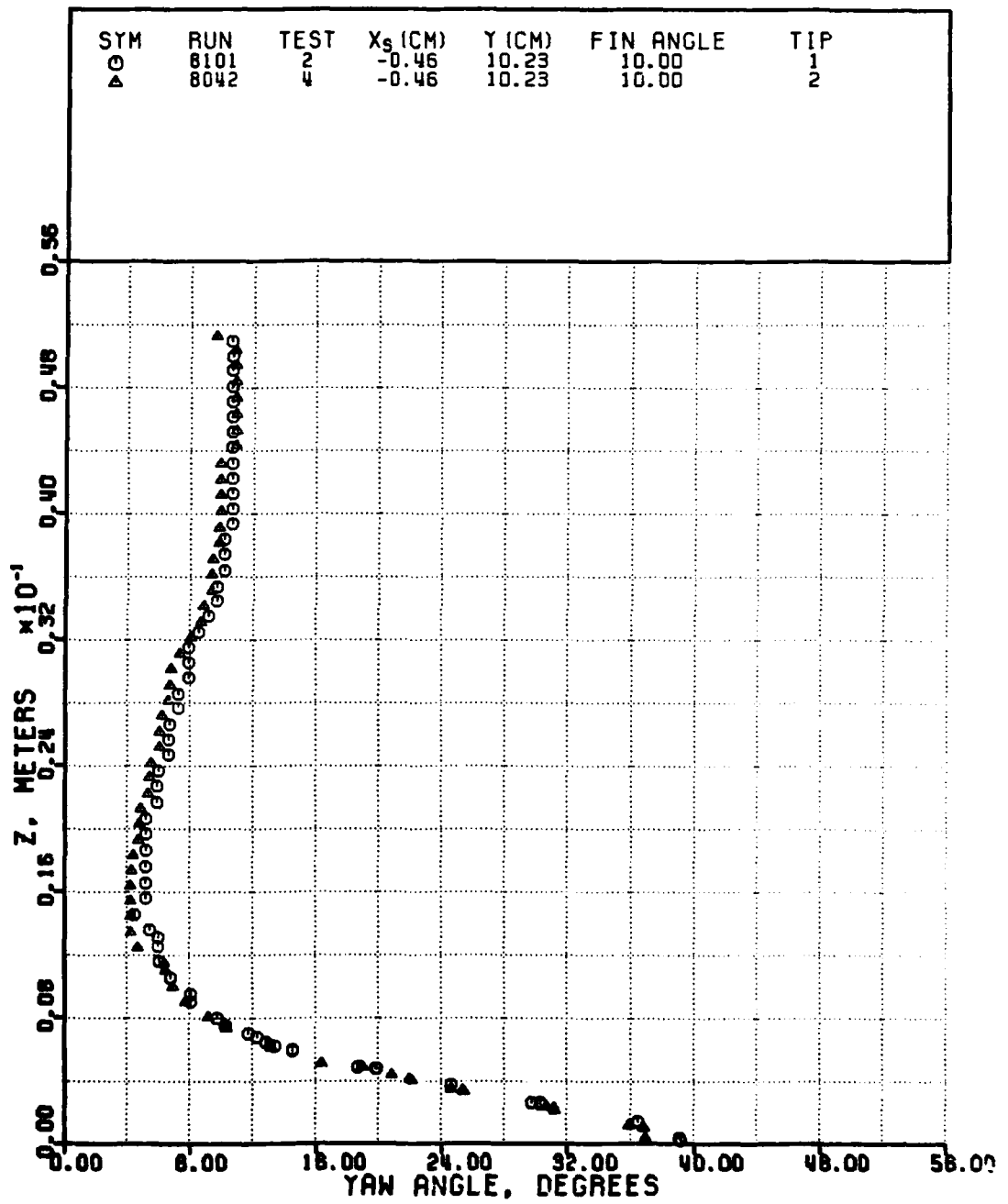


Fig. 12 Yaw angle results varying probe tips

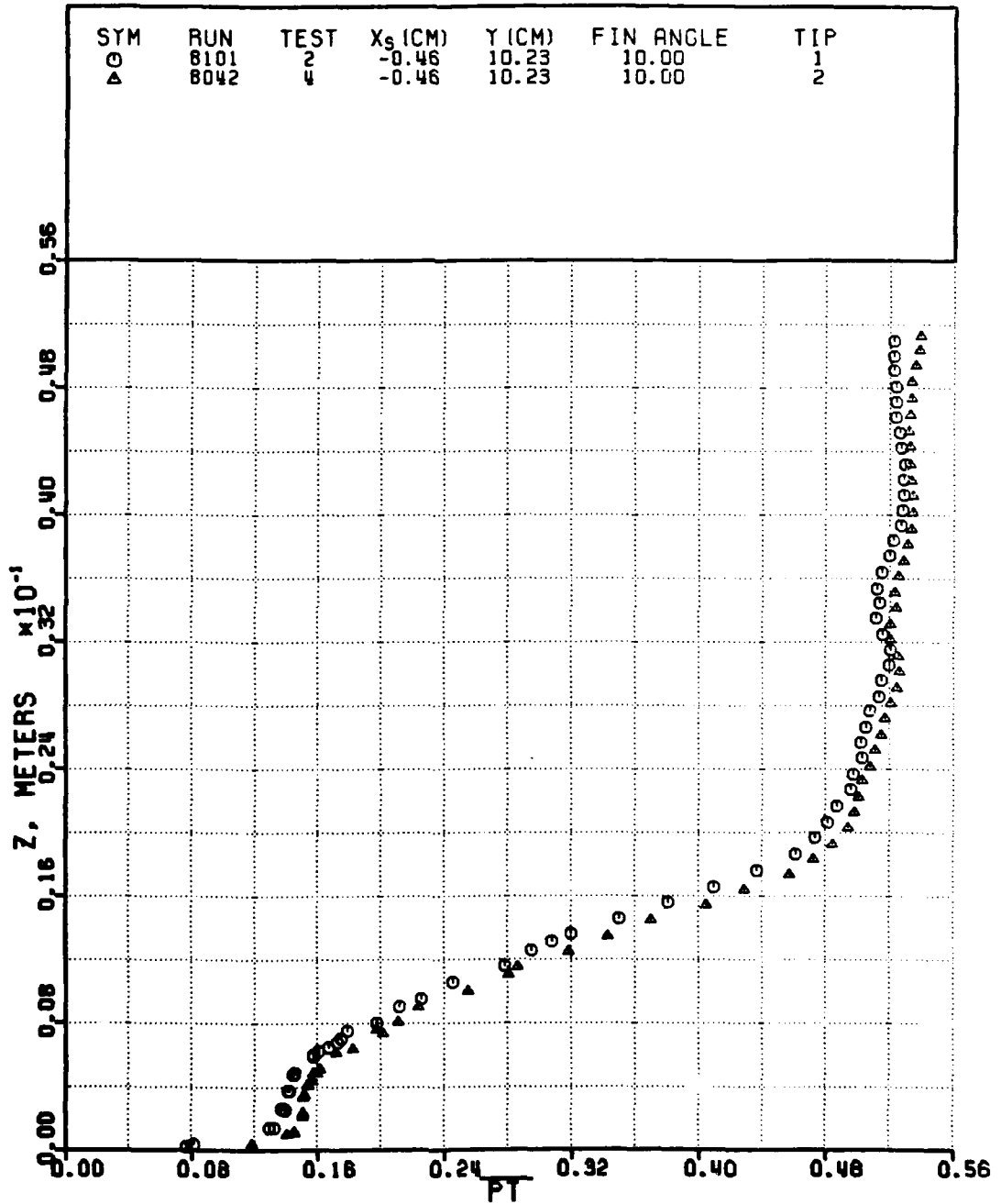


Fig. 13 Normalized pitot pressure results
varying probe tips

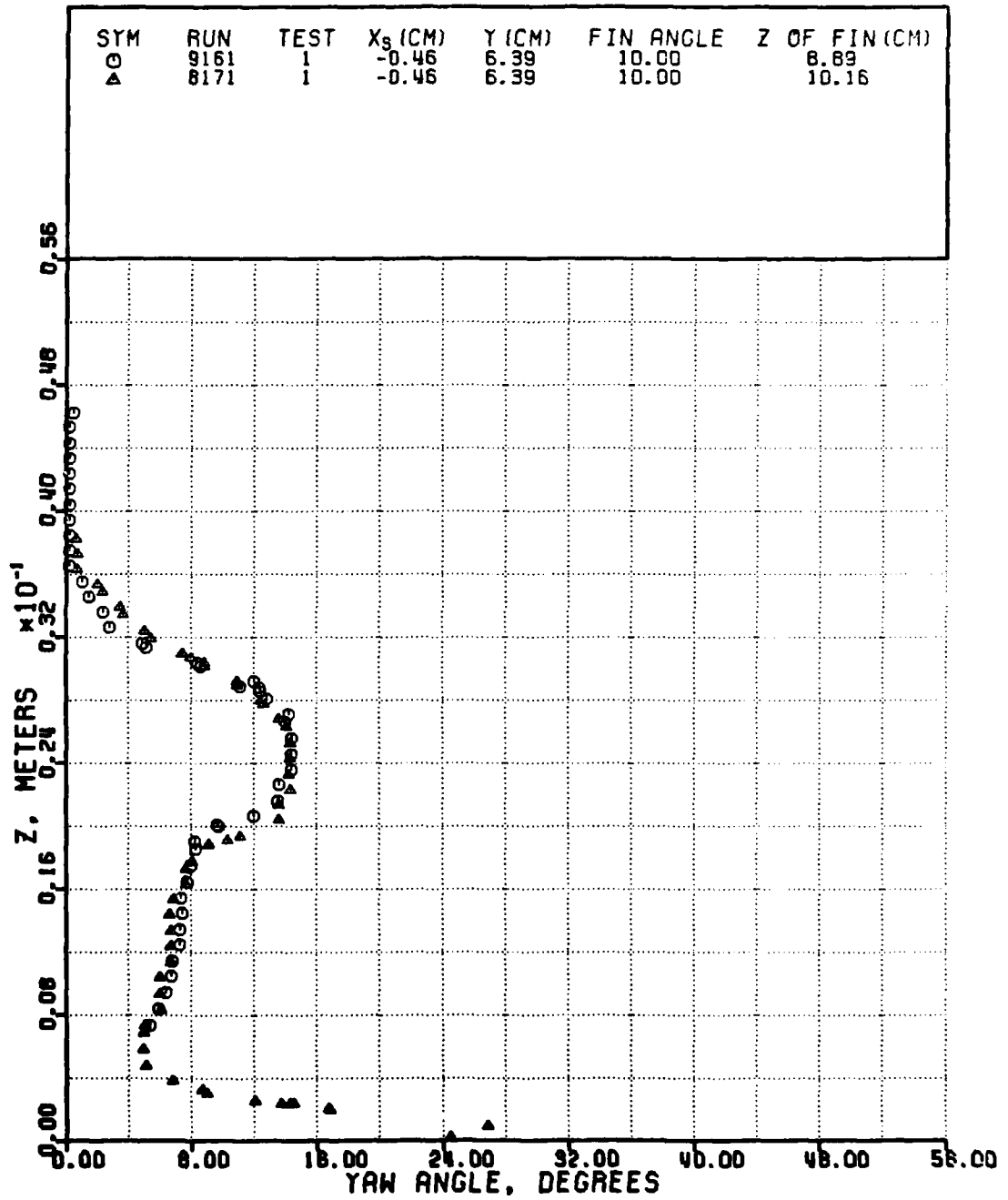


Fig. 14 Yaw angle results varying fin height

SYM	RUN	TEST	X _s (CM)	Y (CM)	FIN ANGLE	Z OF FIN (CM)
○	9161	1	-0.46	6.39	10.00	8.89
△	8171	1	-0.46	6.39	10.00	10.16

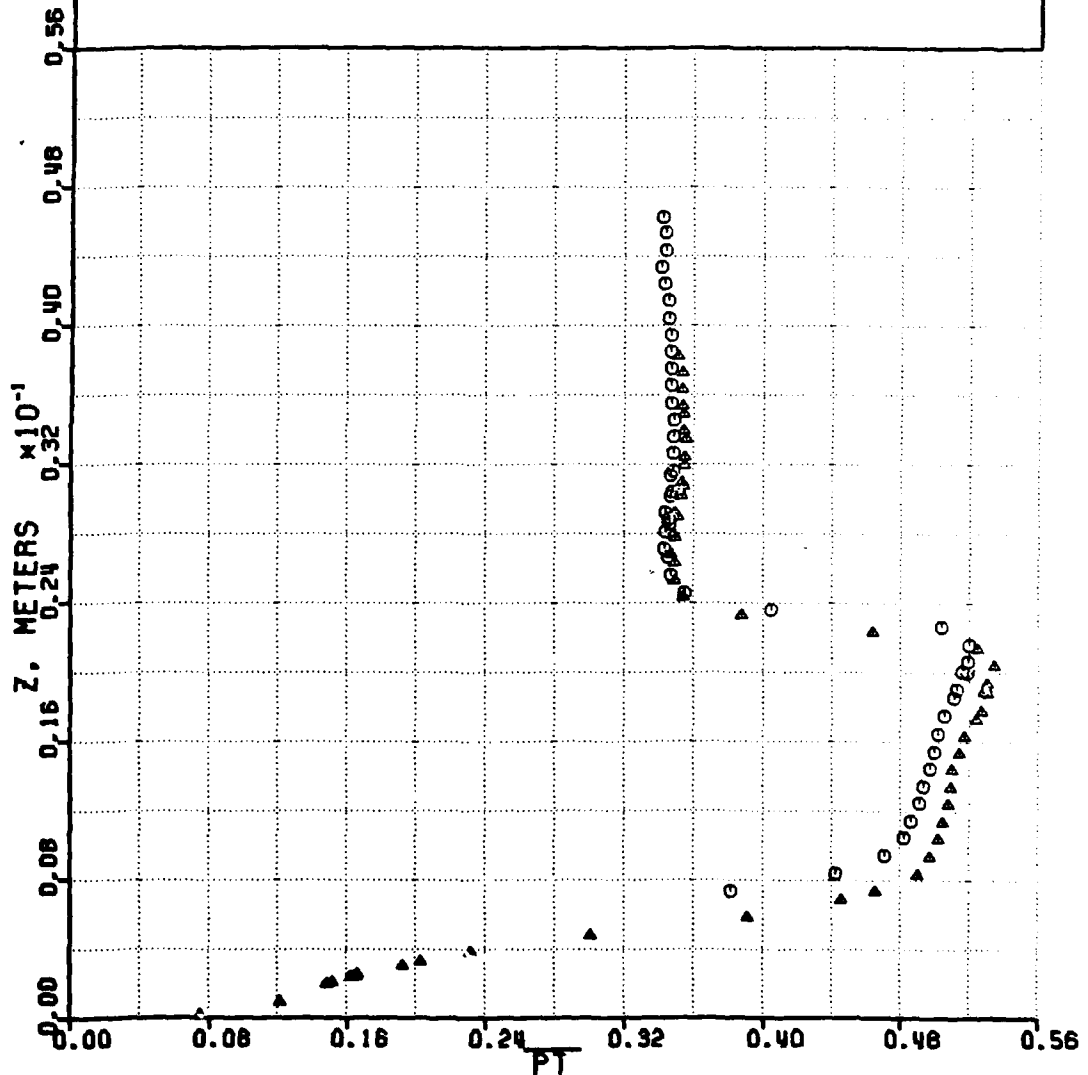


Fig. 15 Normalized pitot pressure results
varying fin height

	RUN	TEST	M1	Y (CM)	CM FROM BASE POSITION
□	8091	1	2.93	12.14	-1.27
▲	8091	2	2.93	12.14	0.00
+	8091	3	2.93	12.14	1.27

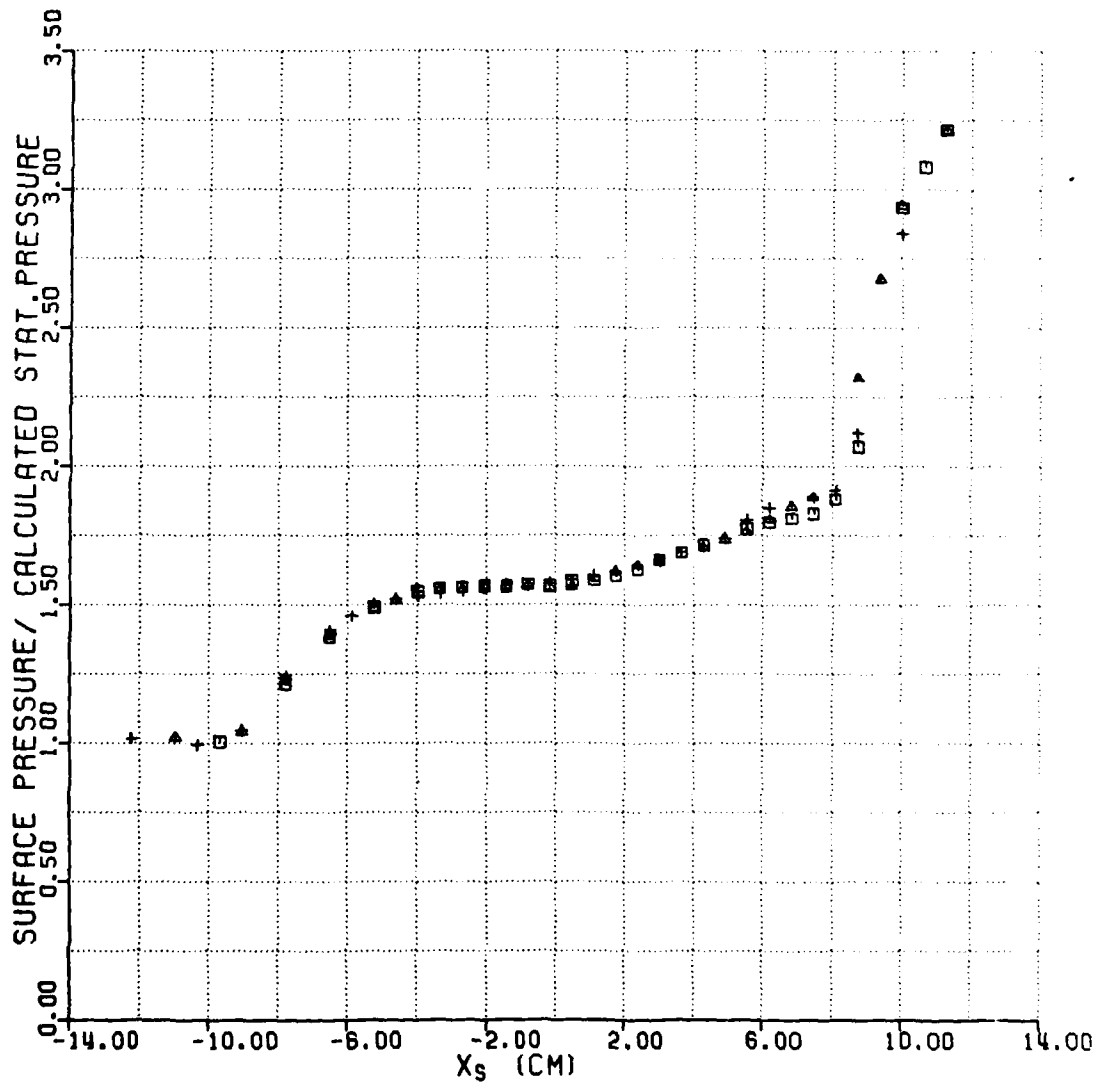


Fig. 16 Surface pressure distributions along a streamwise line varying fin position in Case 1

AD-A126 919

AN EXPERIMENTAL STUDY INTO THE SCALING OF AN
UNSWEPT-SHARP-FIN-GENERATED... (U) AIR FORCE INST OF TECH
WRIGHT-PATTERSON AFB OH W B MCCLURE JAN 83

2/2

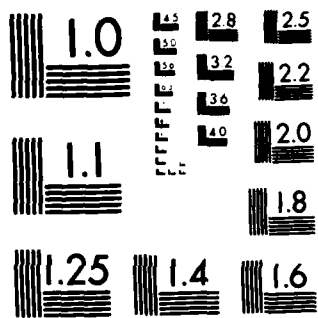
UNCLASSIFIED

AFIT/CI/NR-83-6T

F/G 20/A

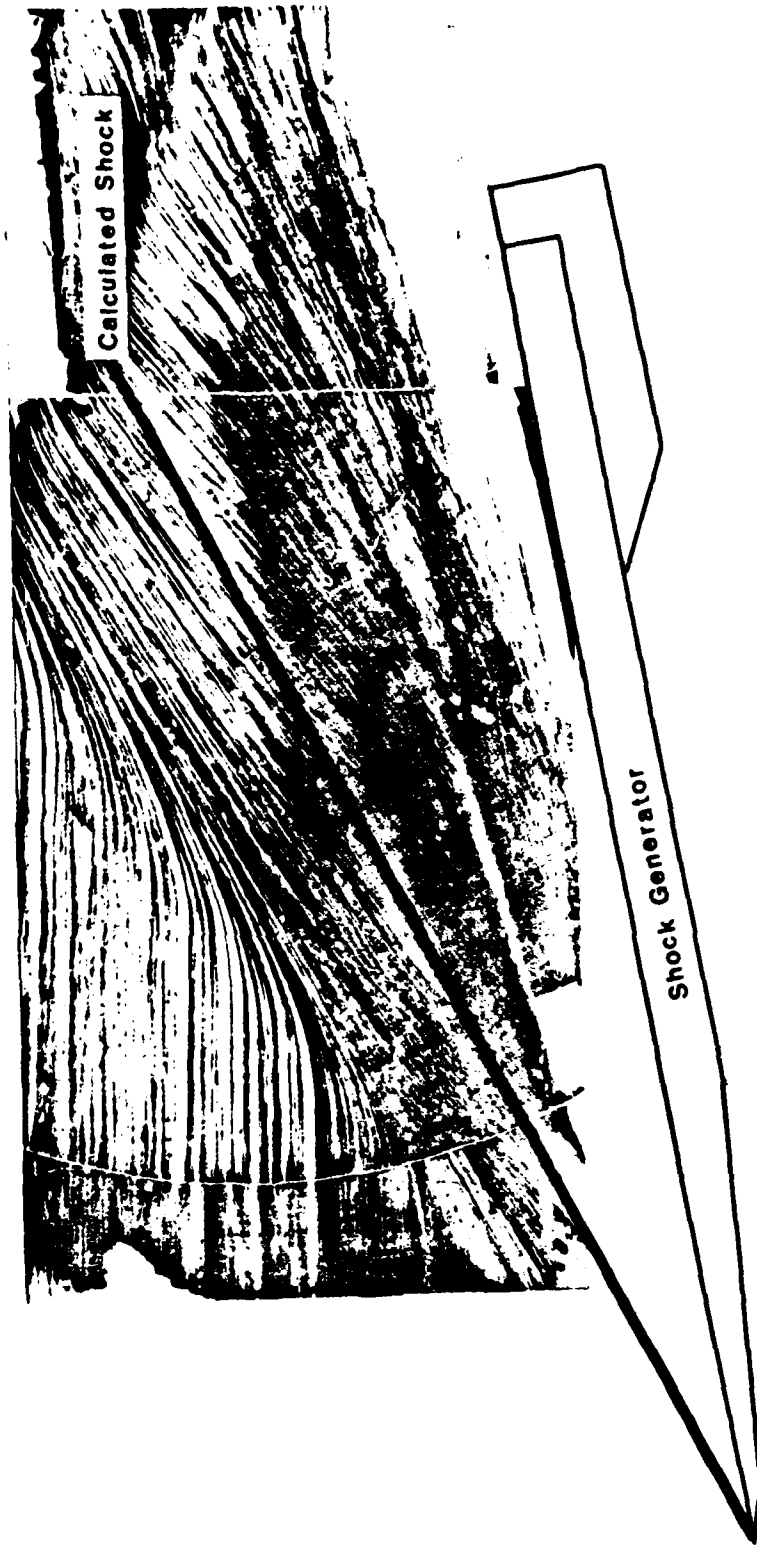
NL

END
DATE
FILMED
DTIC



MICROCOPY RESOLUTION TEST CHART
NATIONAL BUREAU OF STANDARDS-1963-A

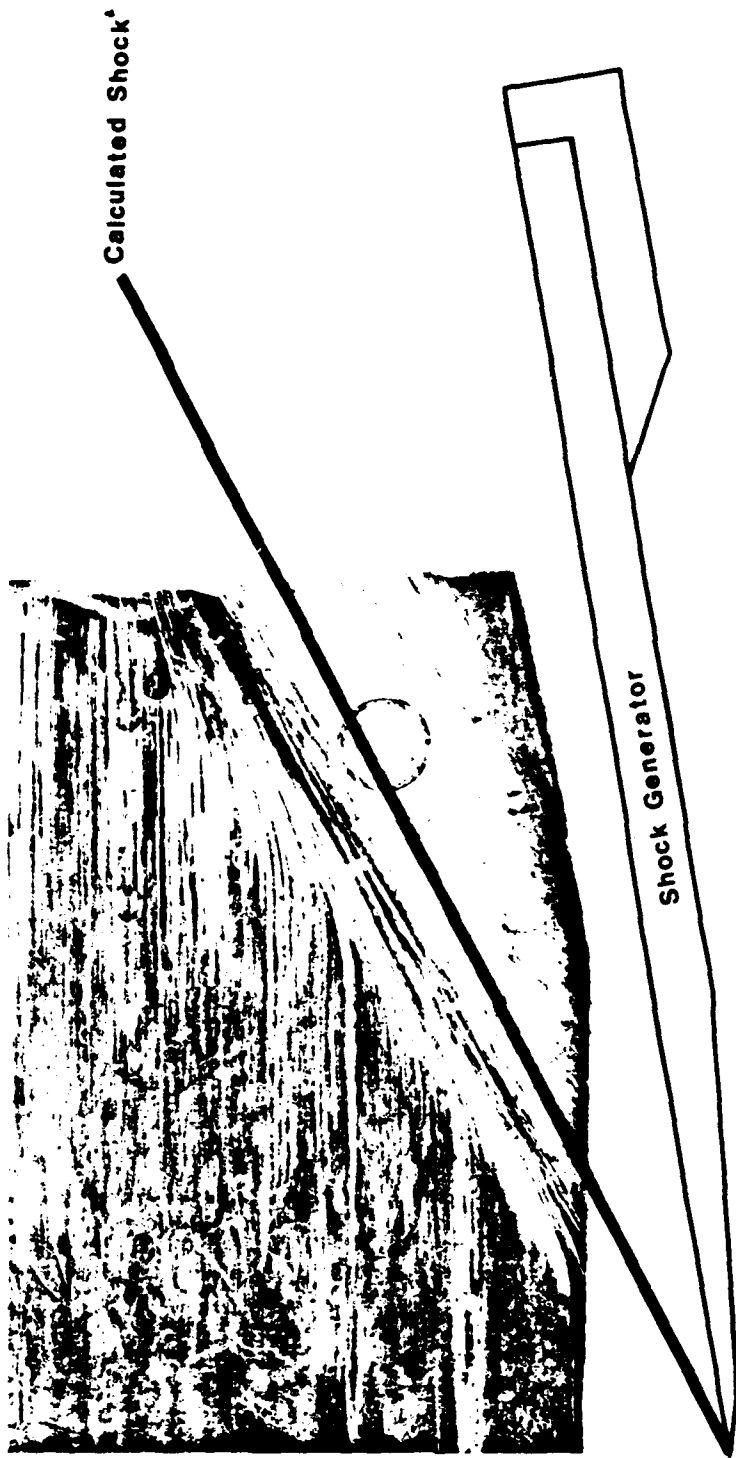
Tunnel Wall



Tunnel Wall

Fig. 17 Kerosene Graphite Trace for Case 1

Tunnel Wall



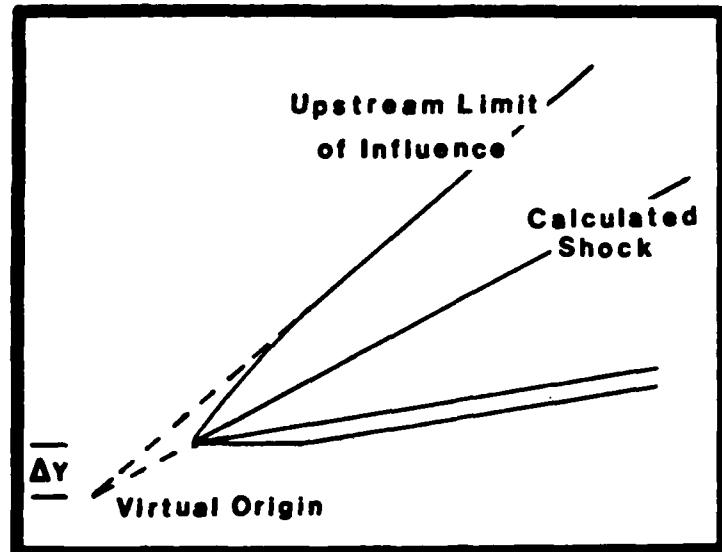
Tunnel Wall

Fig. 18 Kerosene Graphite Trace for Case 2

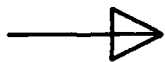
$Z = 0.000 \text{ CM.}$

CONICAL SYMMETRY

$\Delta Y = 3.924 \text{ CM.}$



FLOW
DIRECTION



CALCULATED
SHOCK

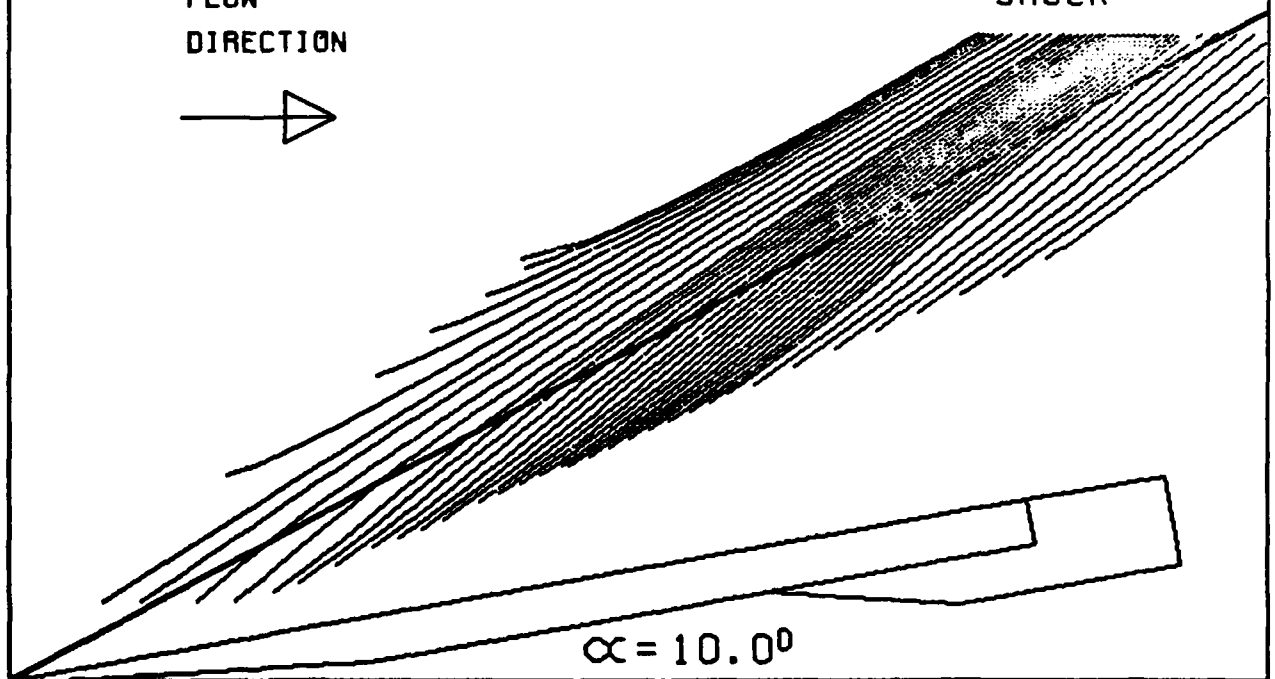


Fig. 19 Replicated surface pattern for Case 1
assuming conical symmetry

Z = 0.000 CM.

CONICAL SYMMETRY

$\Delta Y = 3.264$ CM.

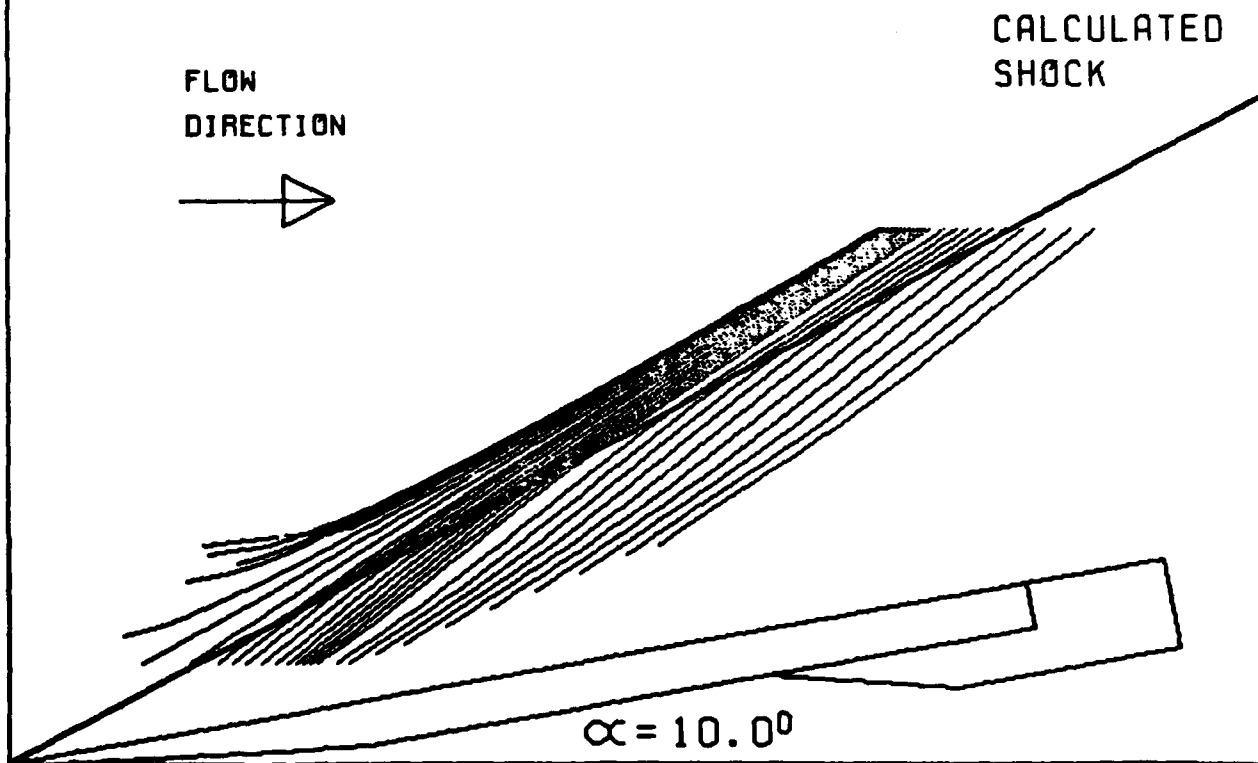


Fig. 20 Replicated surface pattern for Case 2 assuming conical symmetry

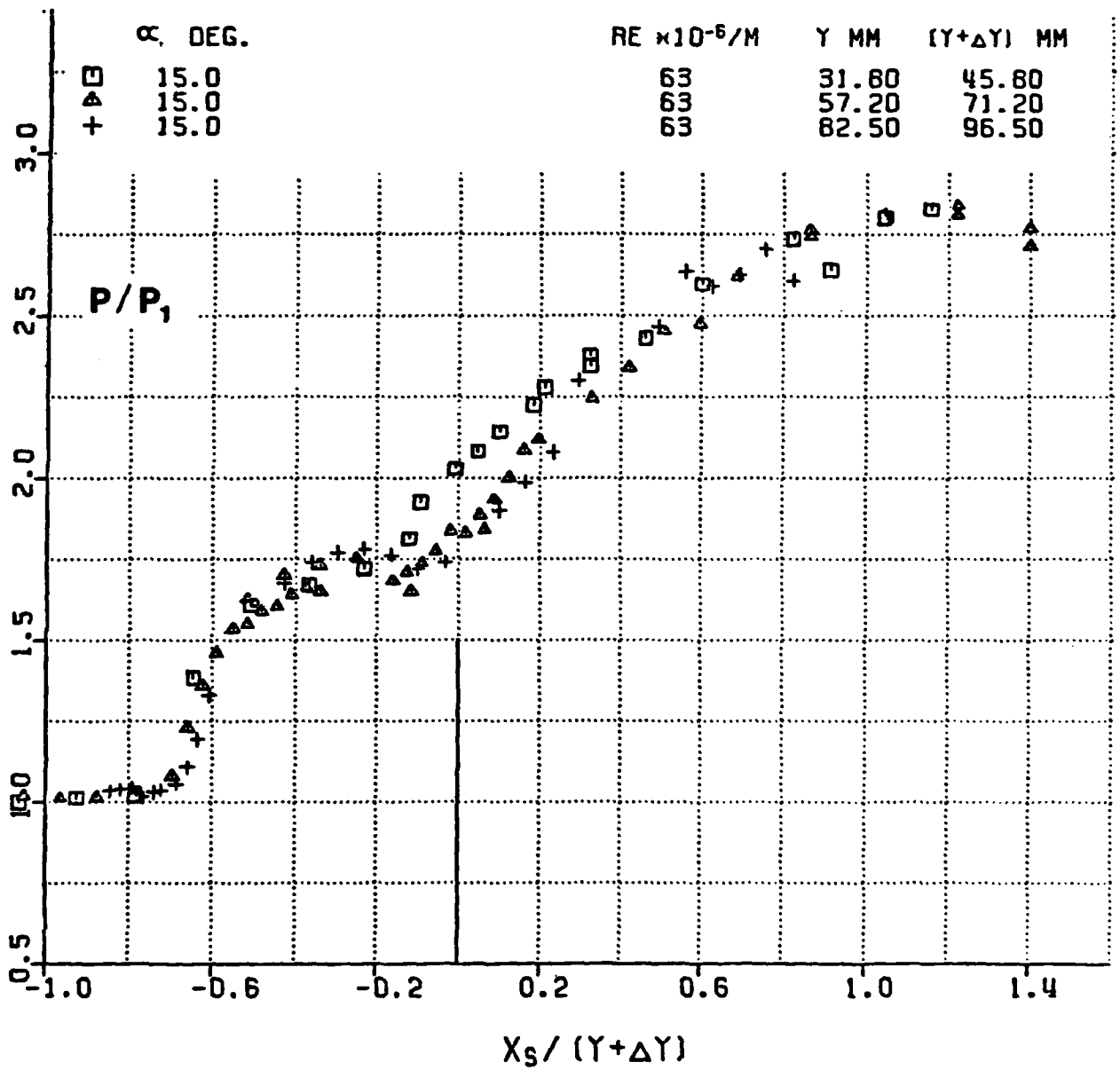


Fig. 21 Streamwise surface pressure distributions of Lu (34) for 15 degree fin interaction collapsed assuming conical symmetry

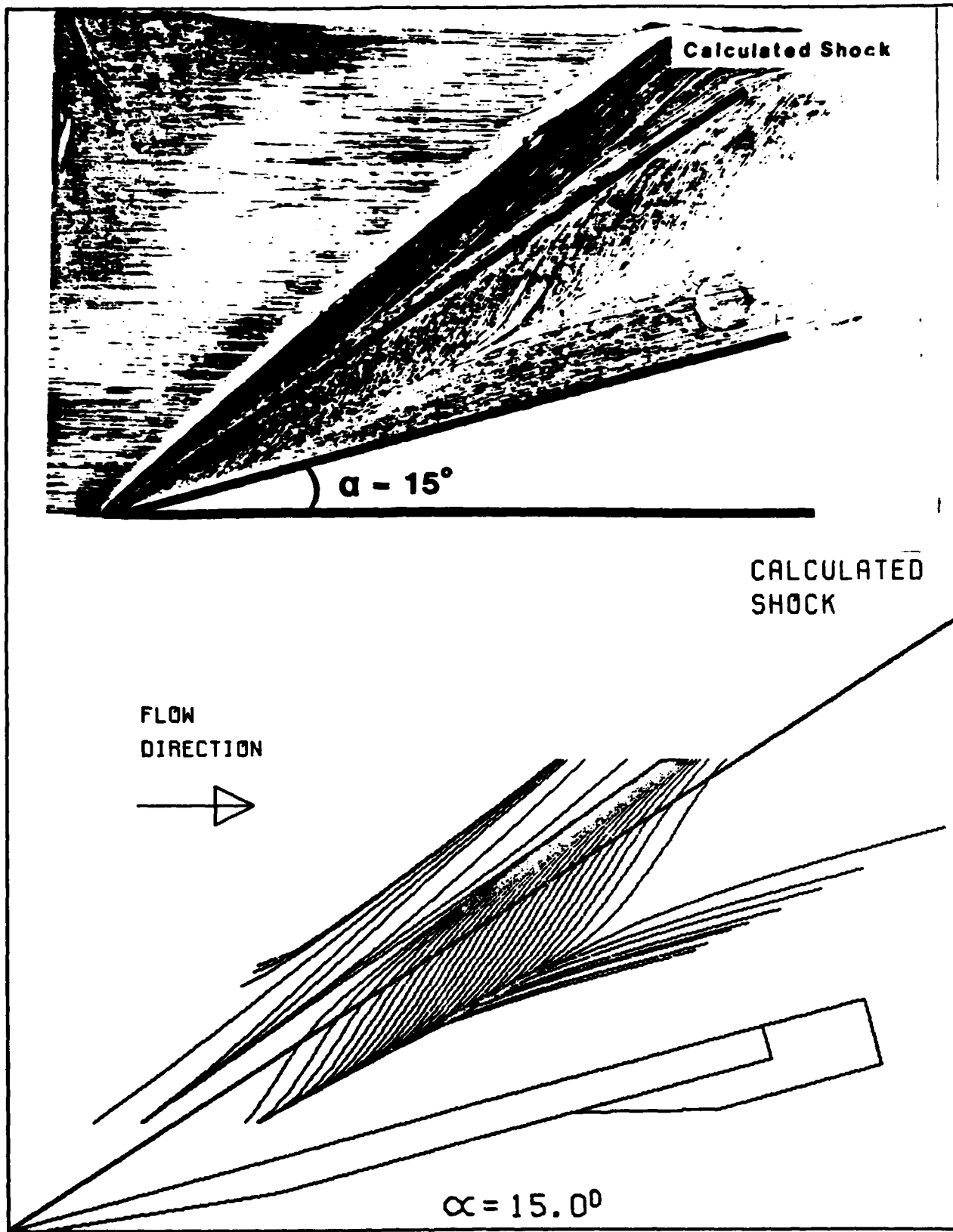


Fig. 22 Kerosene graphite trace and replicated surface pattern for 15 degree fin interaction

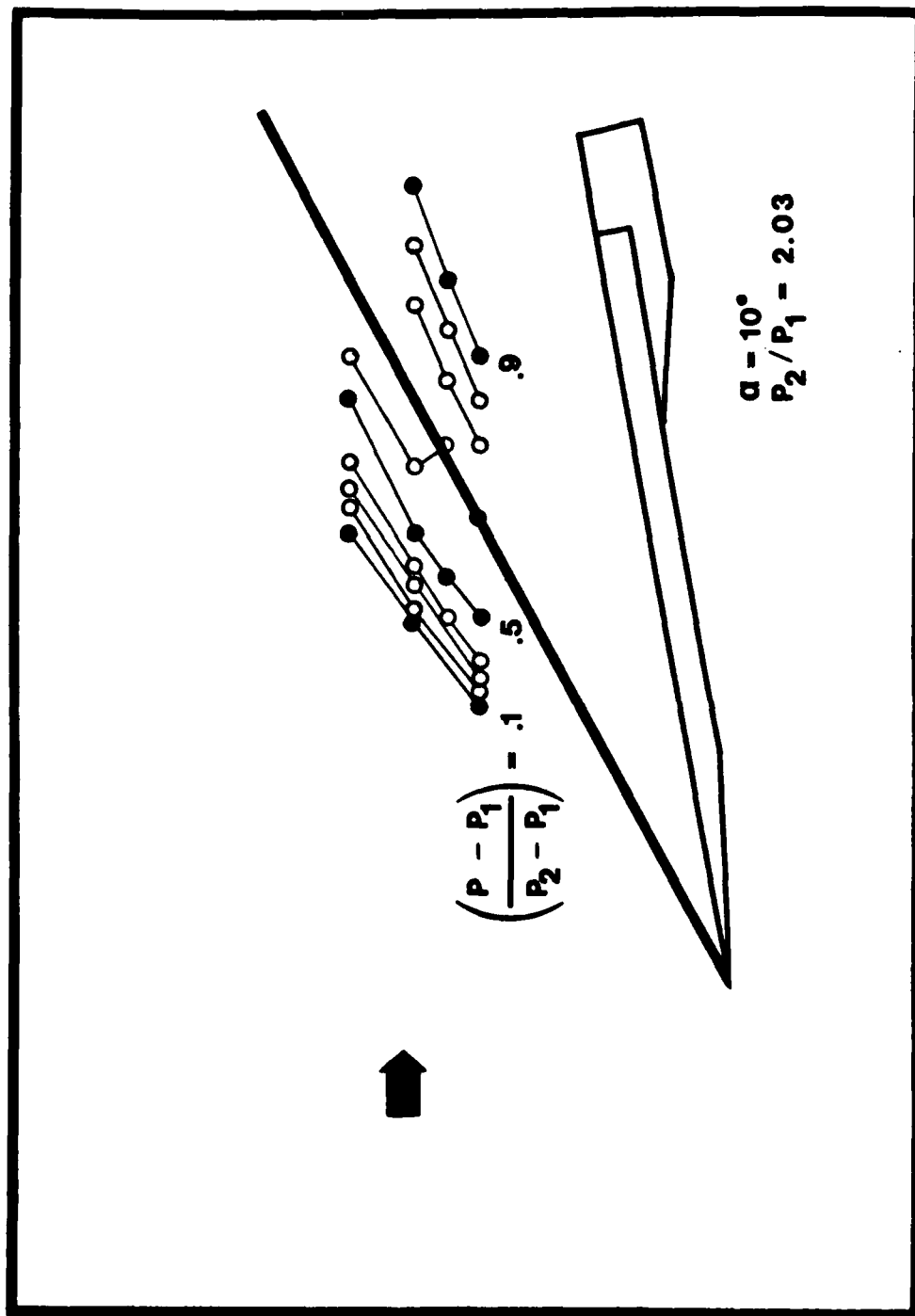


Fig. 23 Surface isobar pattern for Case 1

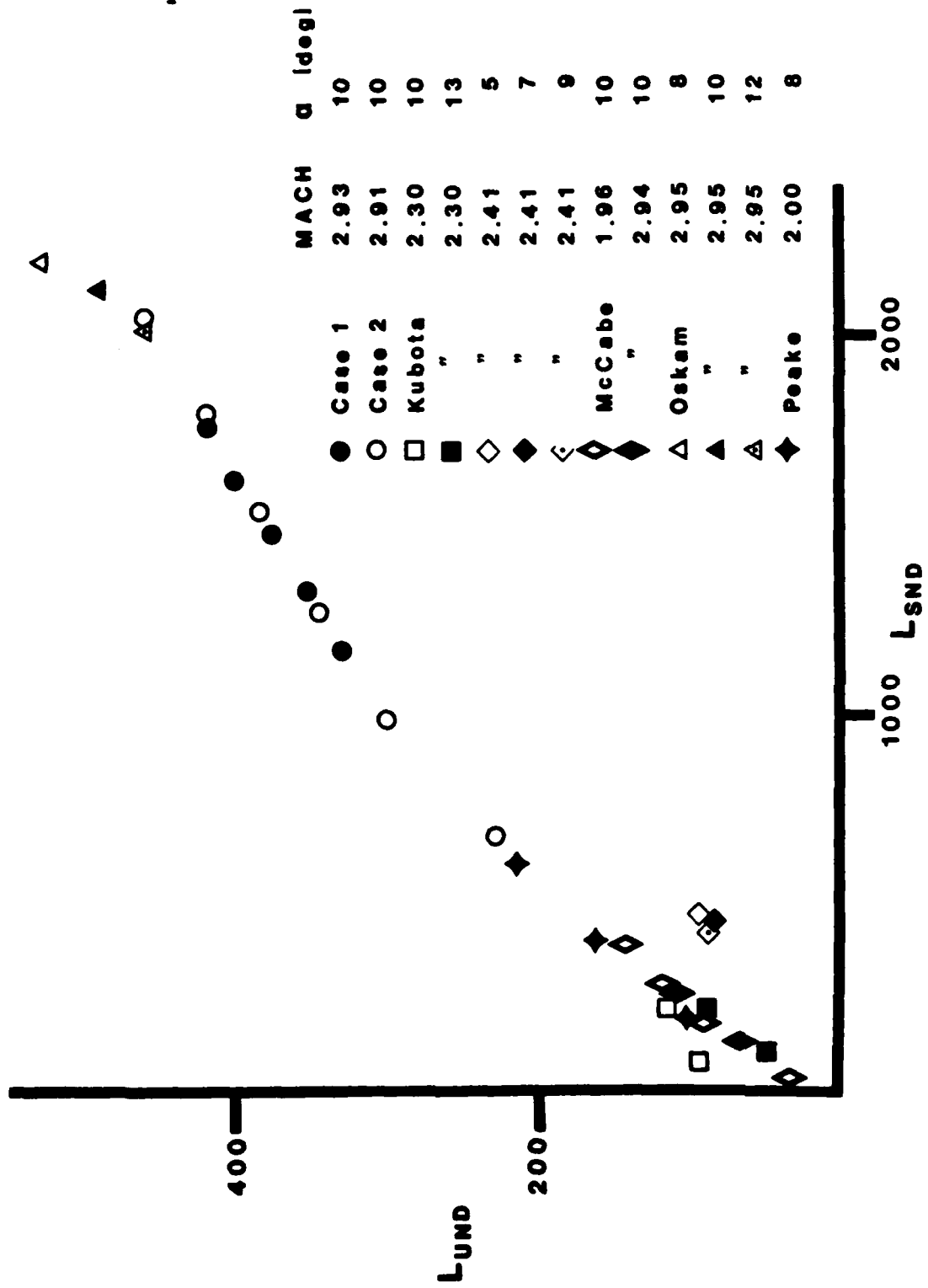


Fig. 24 Comparison of normalized upstream influence for several investigations

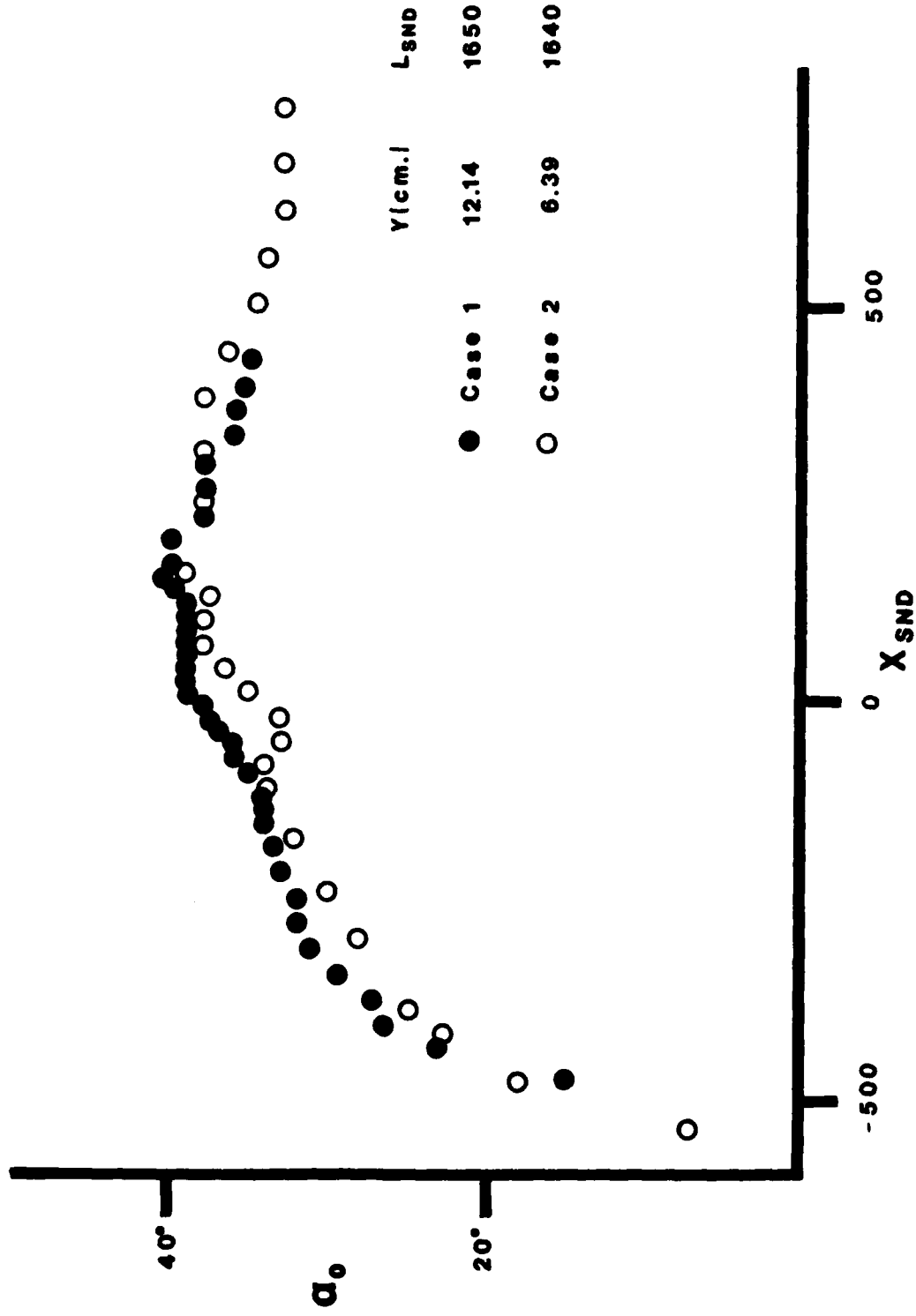


Fig. 25 Surface streak angles through interaction at the same normalized position

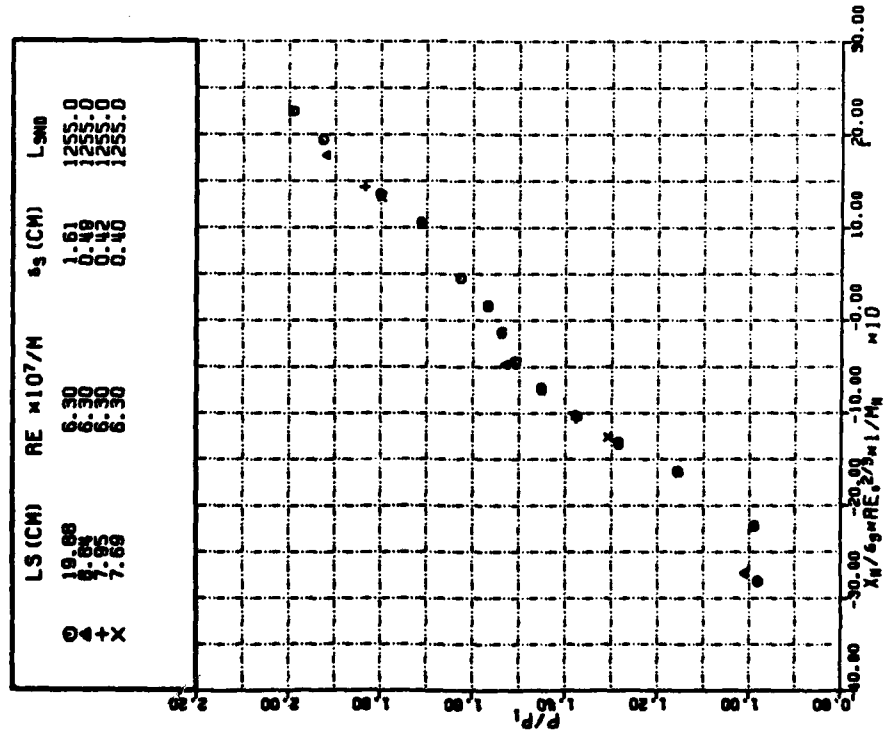
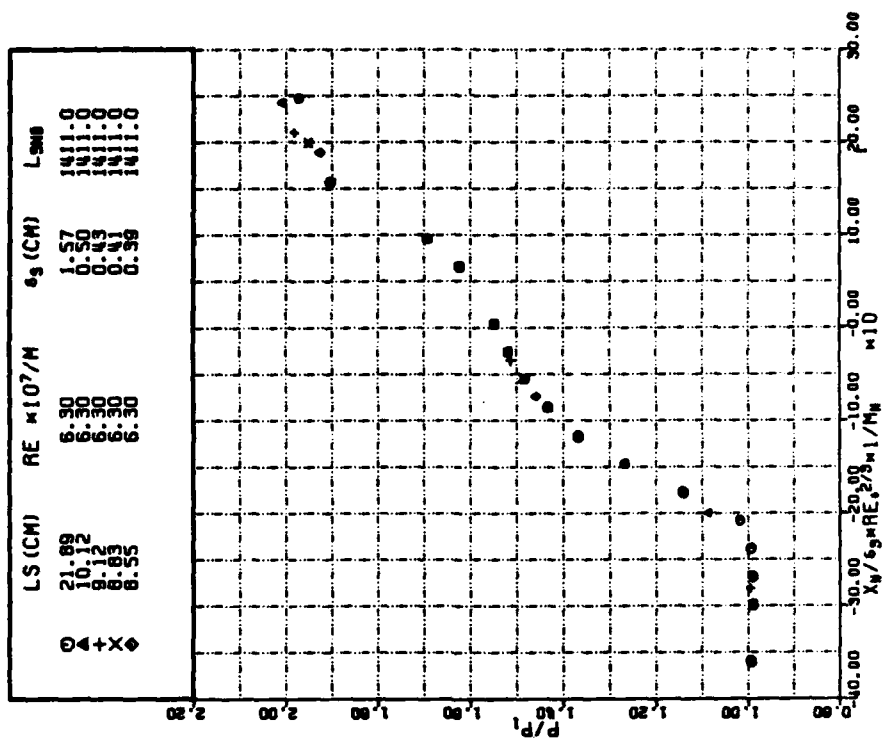


Fig. 26 Surface pressures along lines normal to the calculated shock at the same normalized position

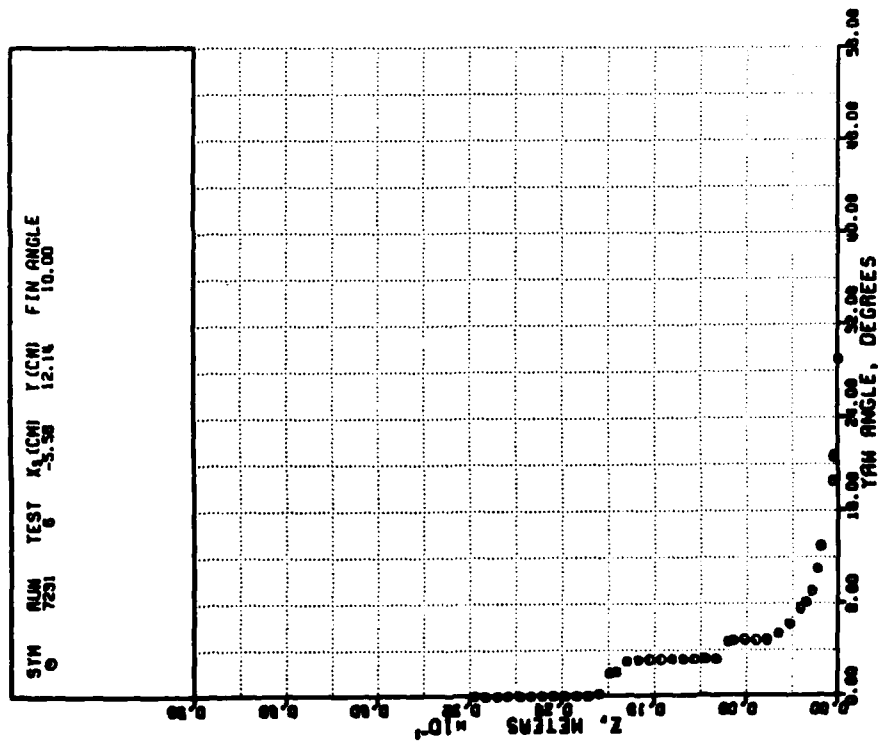
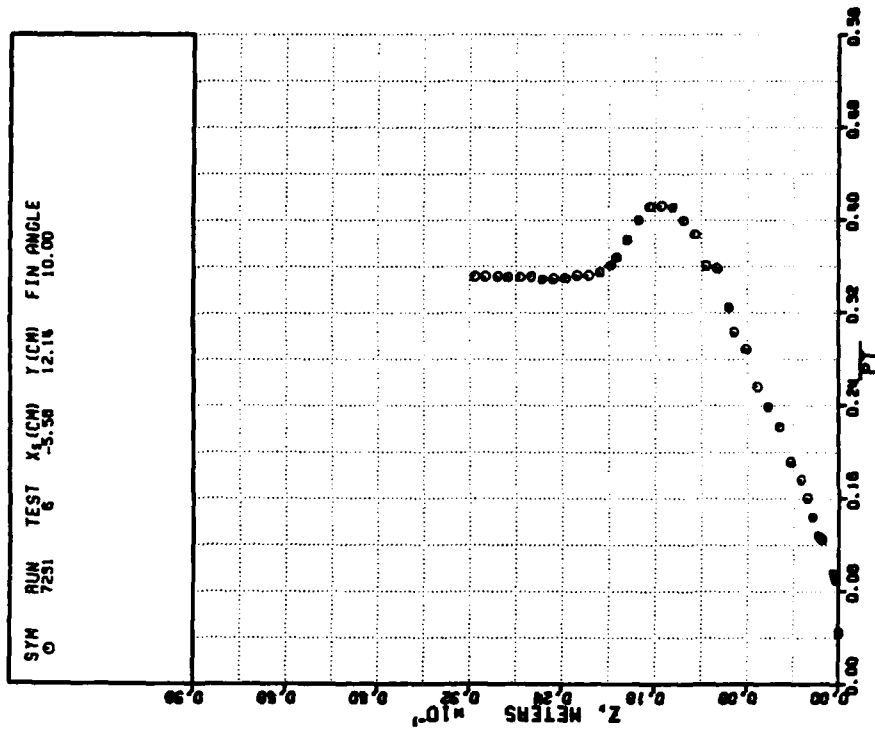


Fig. 27 Typical yaw angle and normalized pitot pressure results from a cobra probe survey

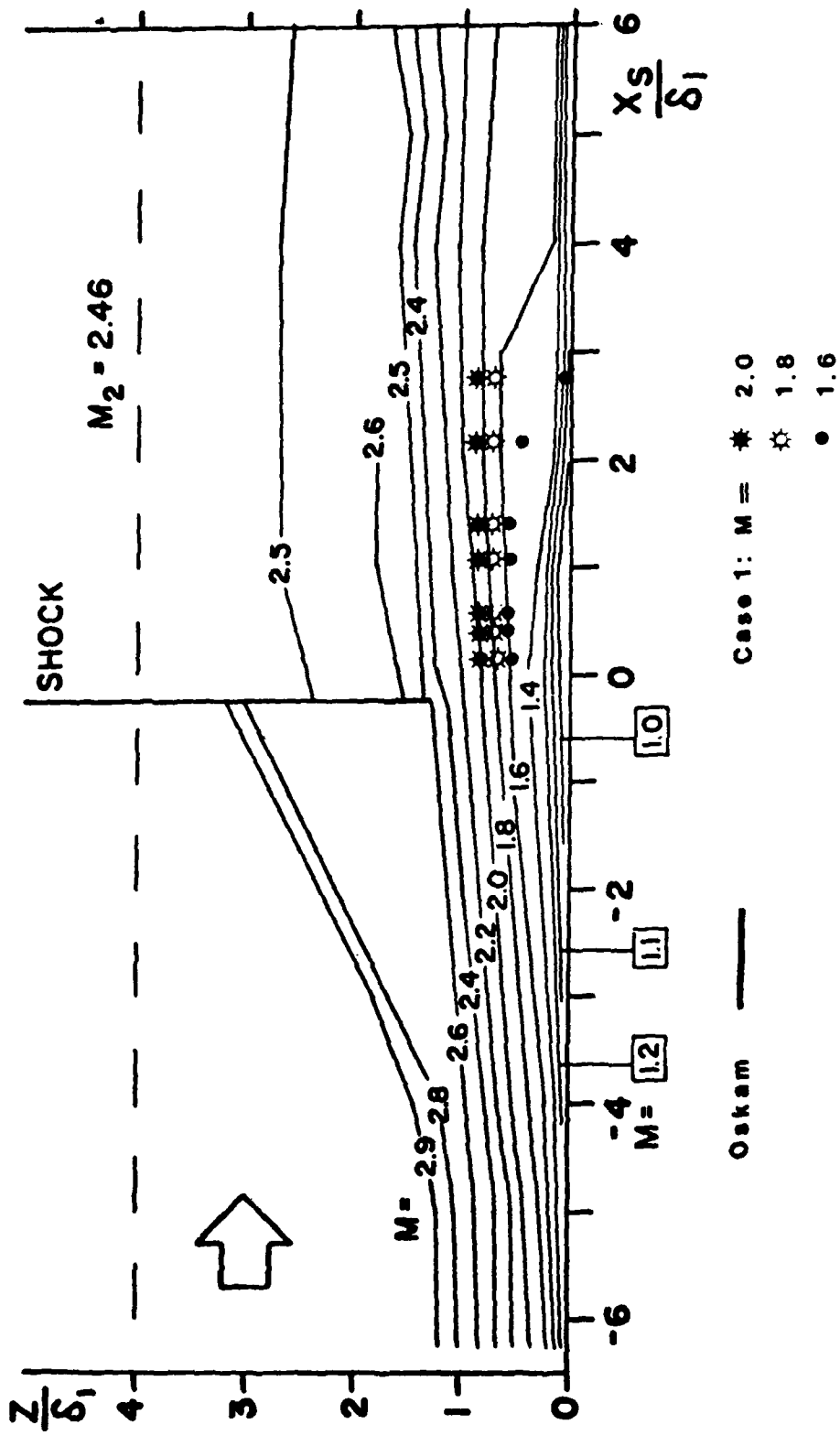


Fig. 28 Comparison of Mach numbers derived in Case 1 with the results of Oskam (1)

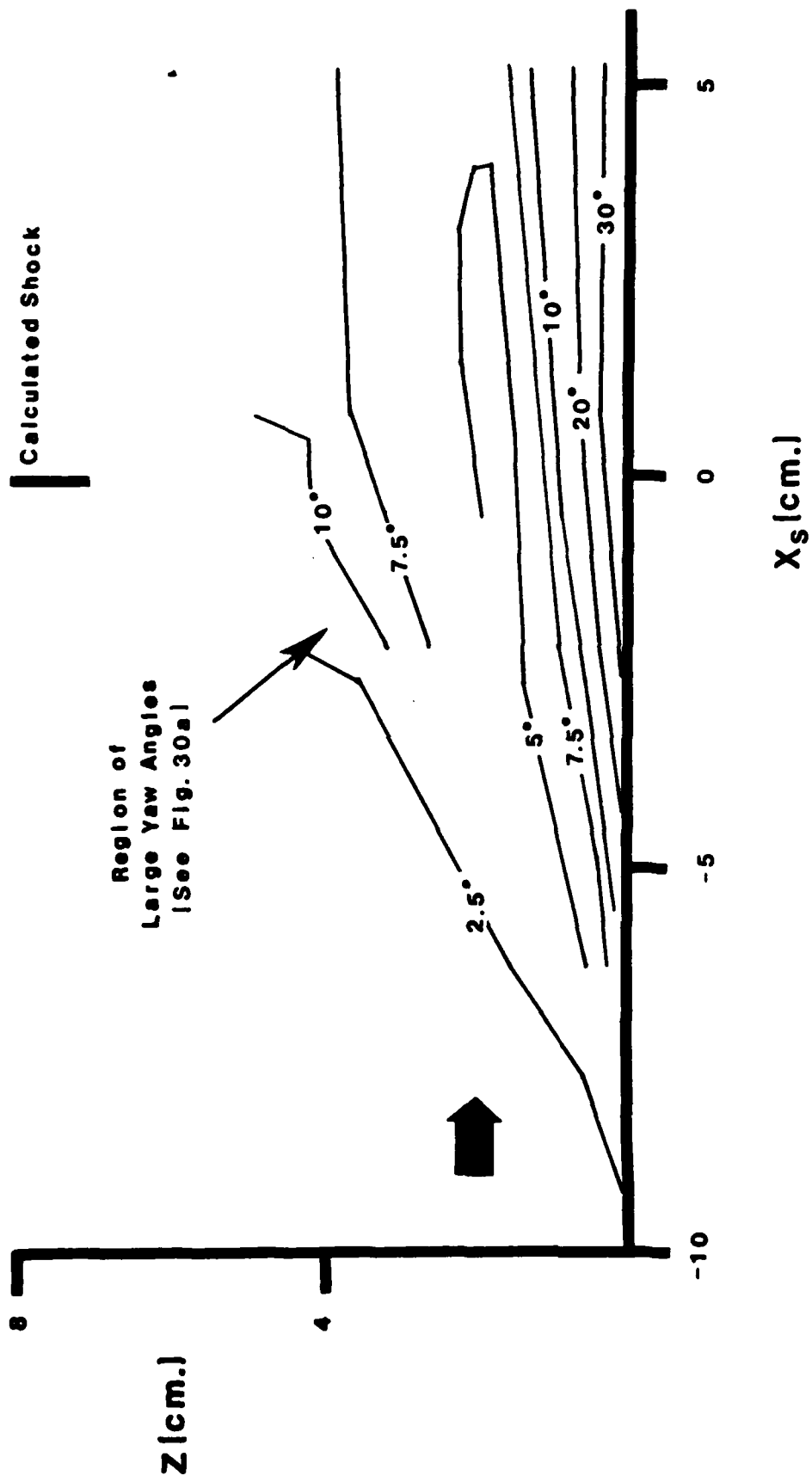


Fig. 29 Flow-field yaw angles for Case 1

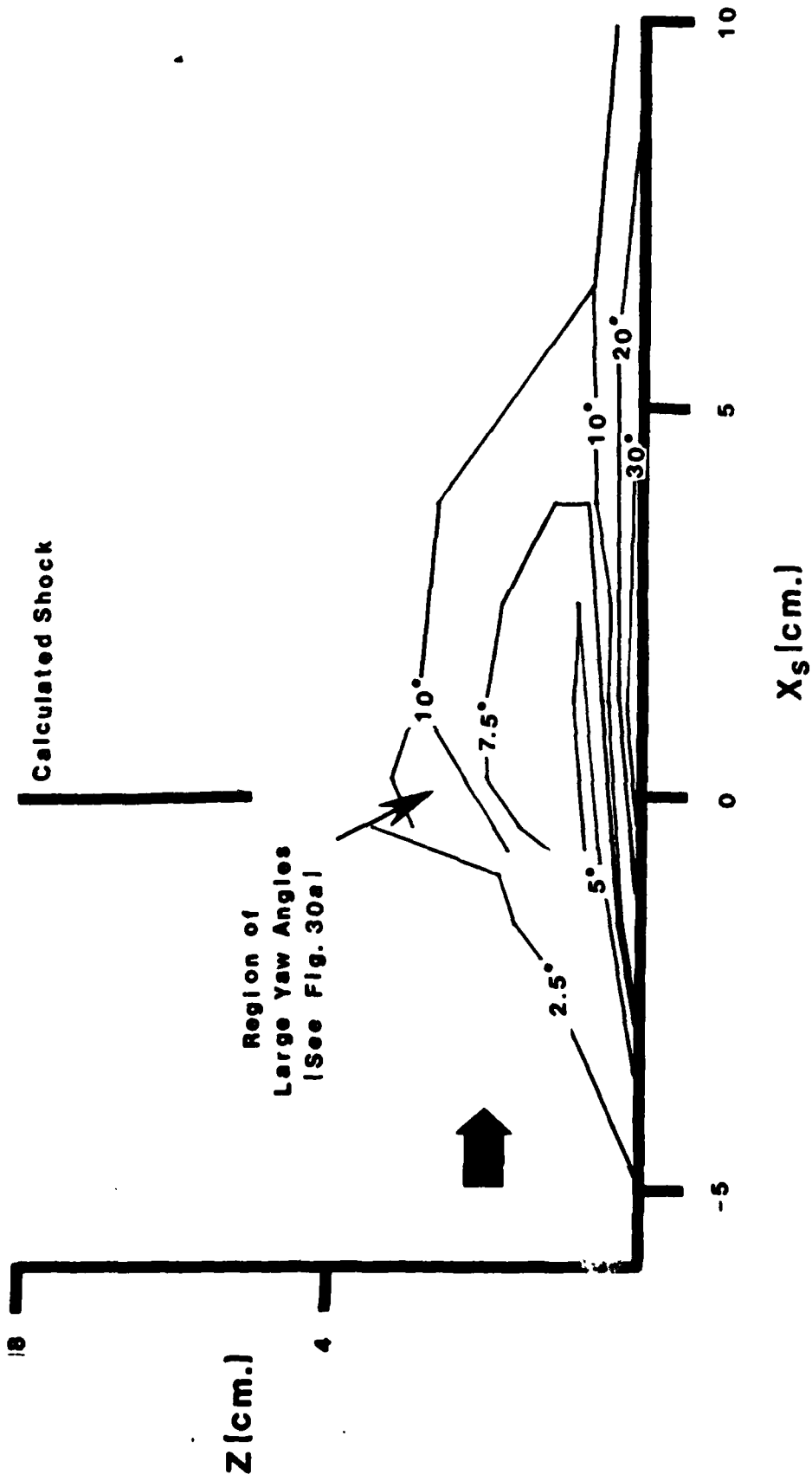


Fig. 30 Flow field yaw angles for Case 2

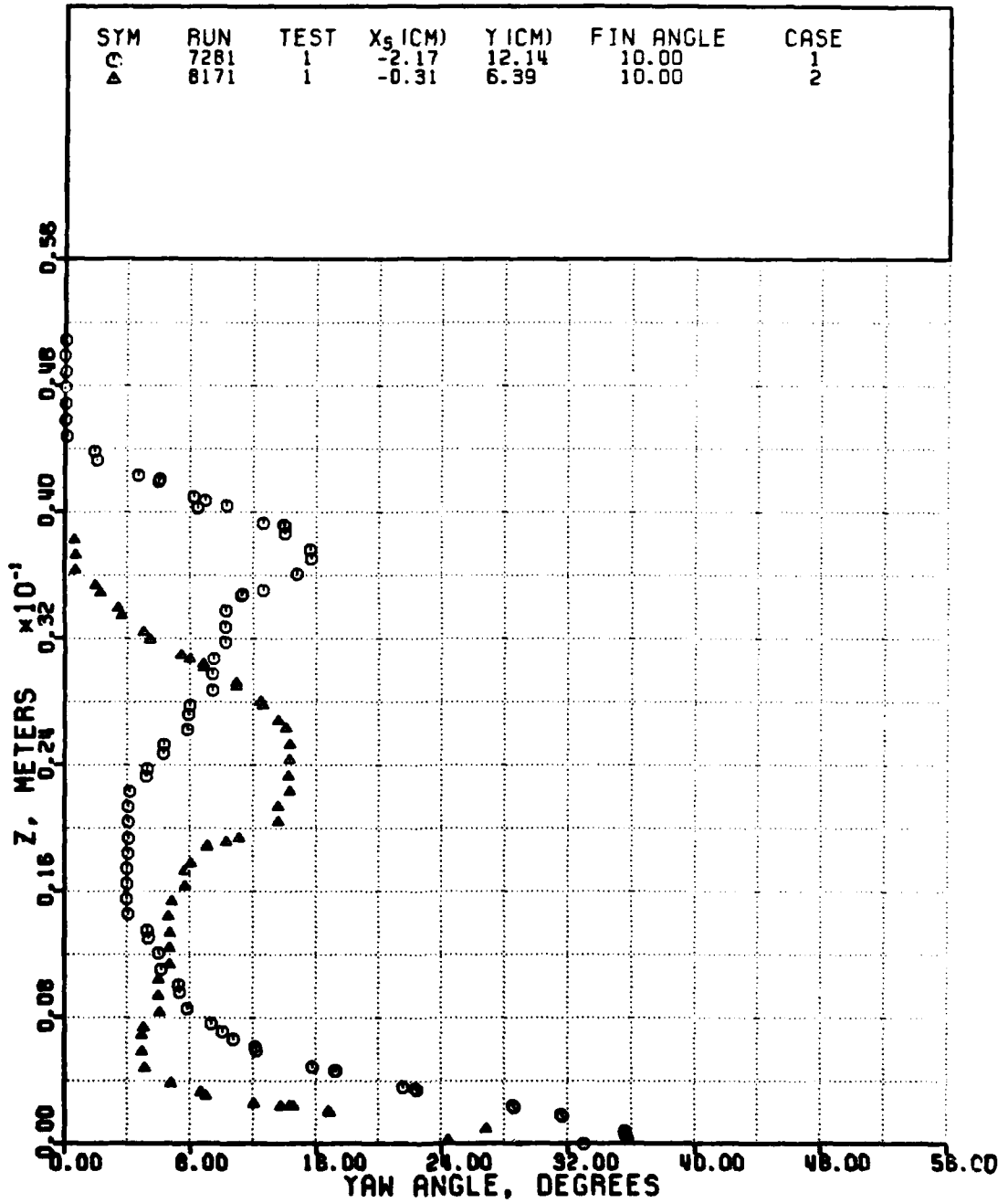


Fig. 30a Yaw angle results upstream of the calculated shock for both Cases

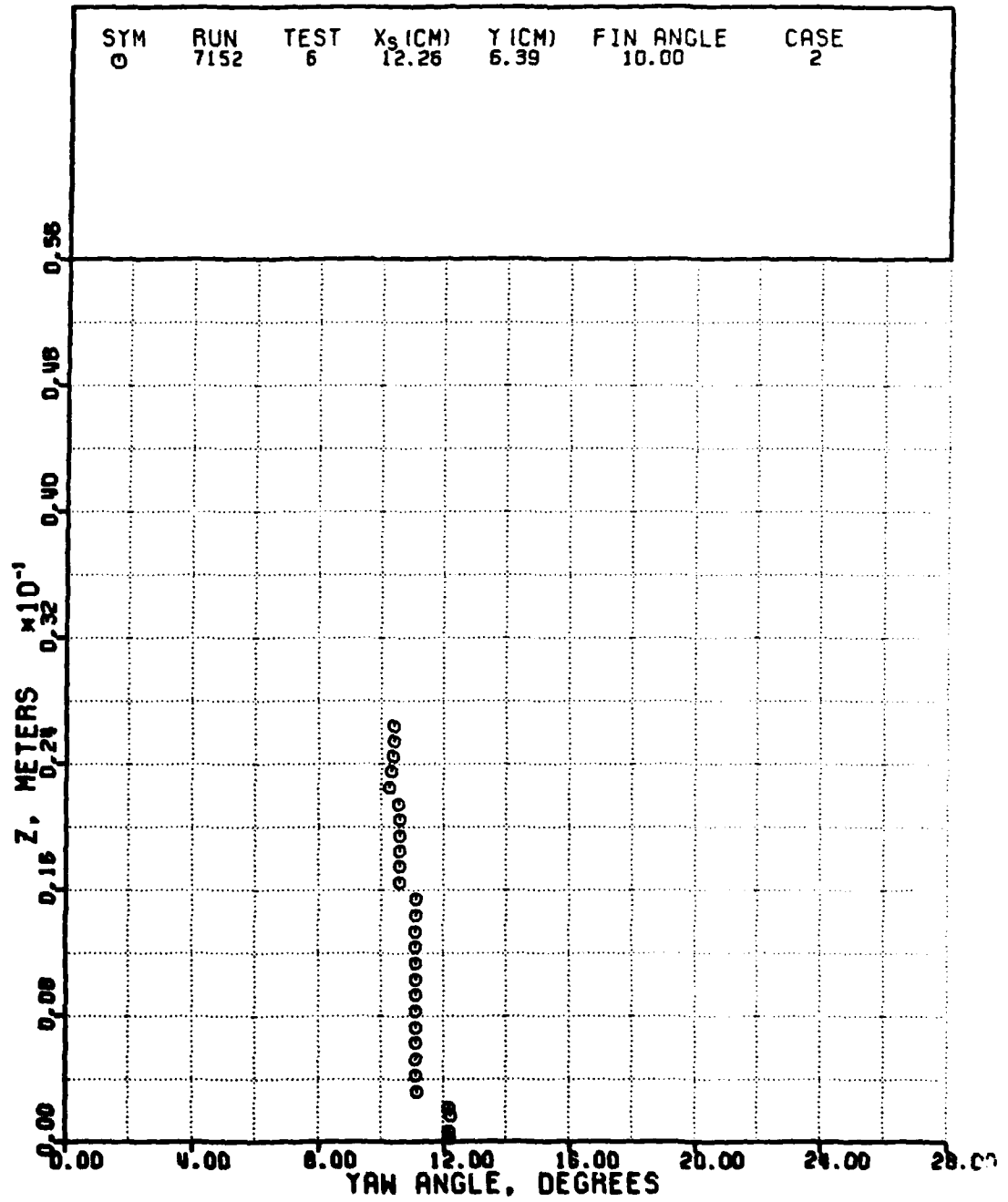


Fig. 31 Yaw angle results 20 incoming boundary layer thicknesses downstream of the calculated shock

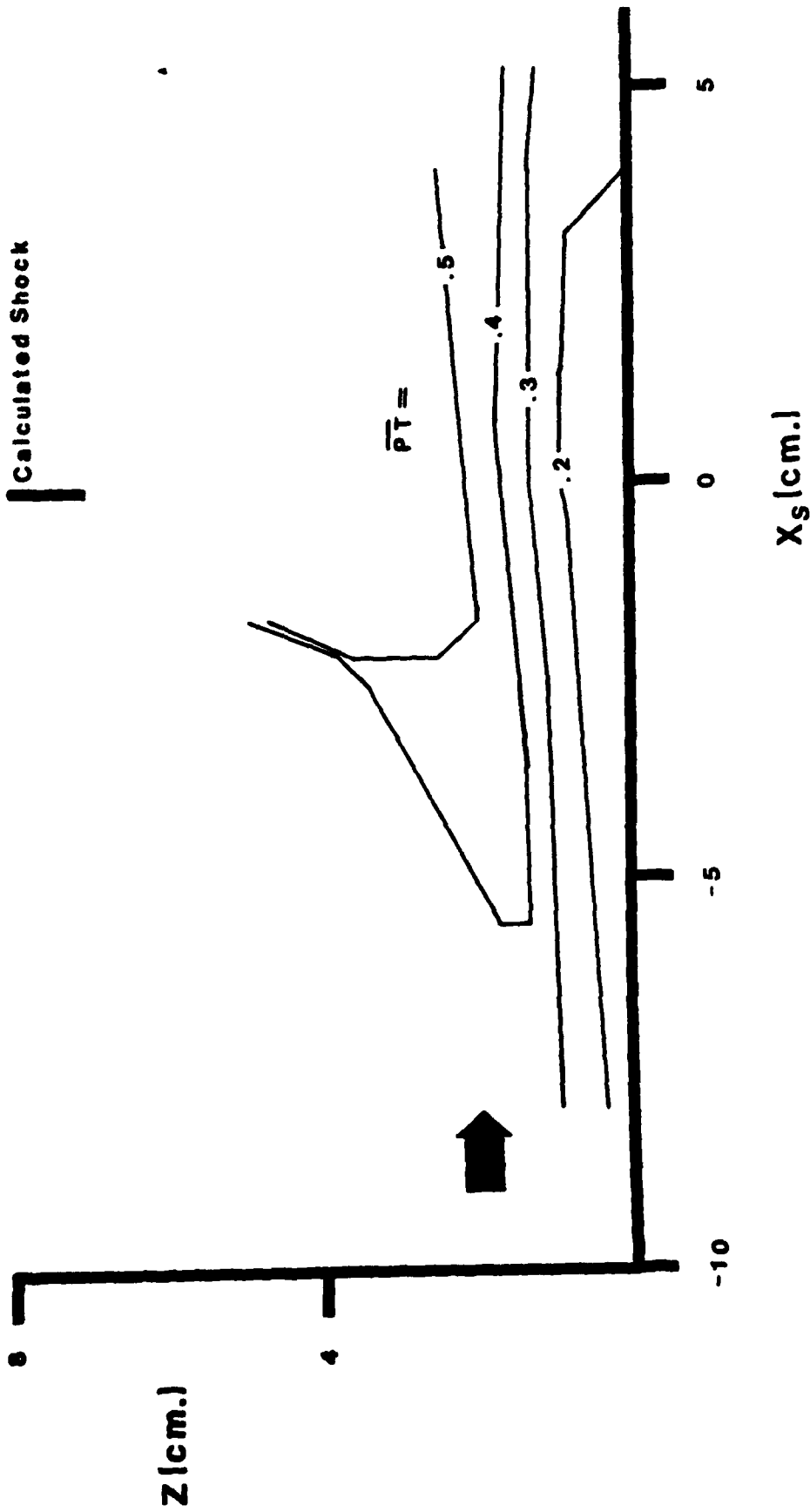


Fig. 32 Normalized flow-field pitot pressures for Case 1

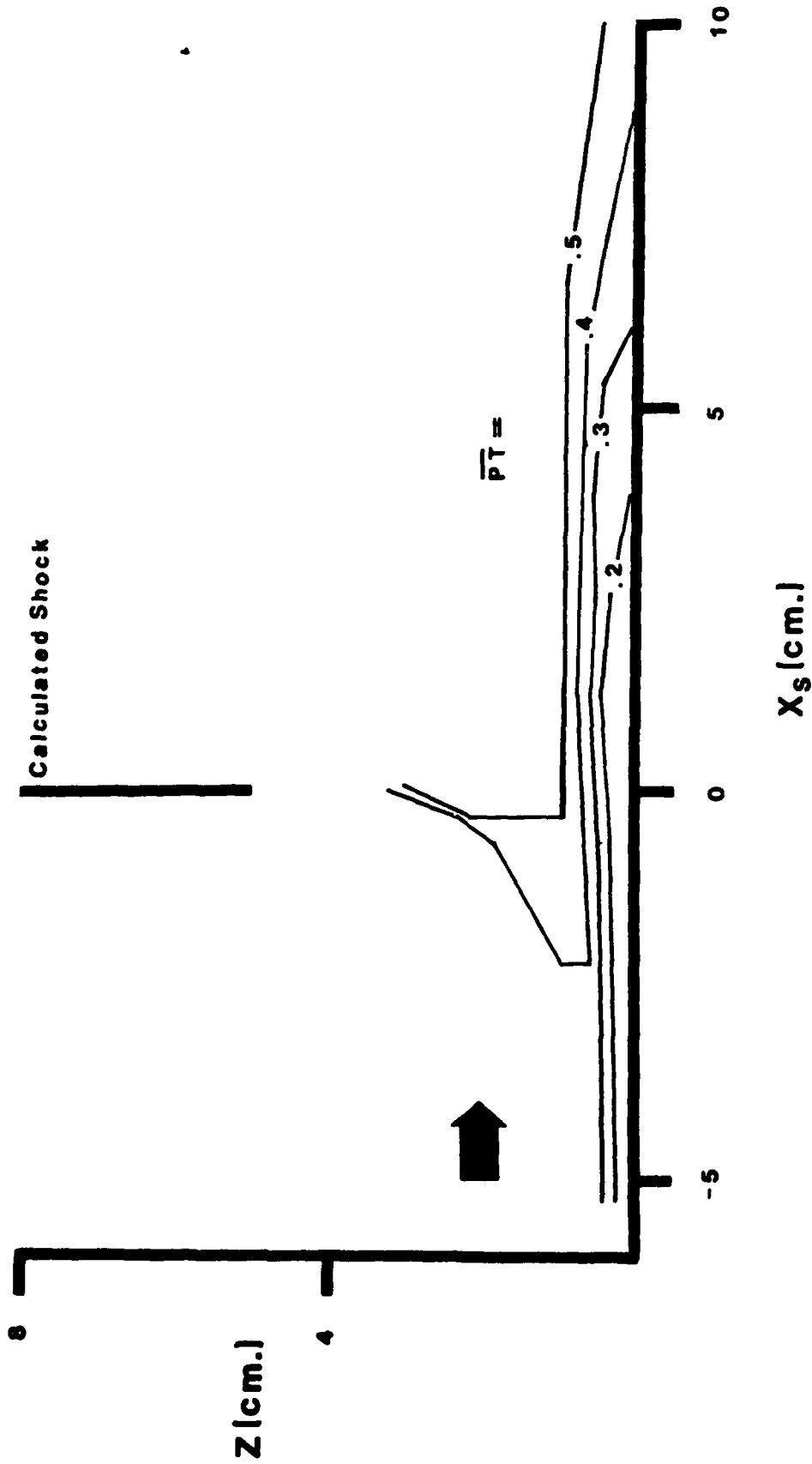


Fig. 33 Normalized flow-field pitot pressures for Case 2

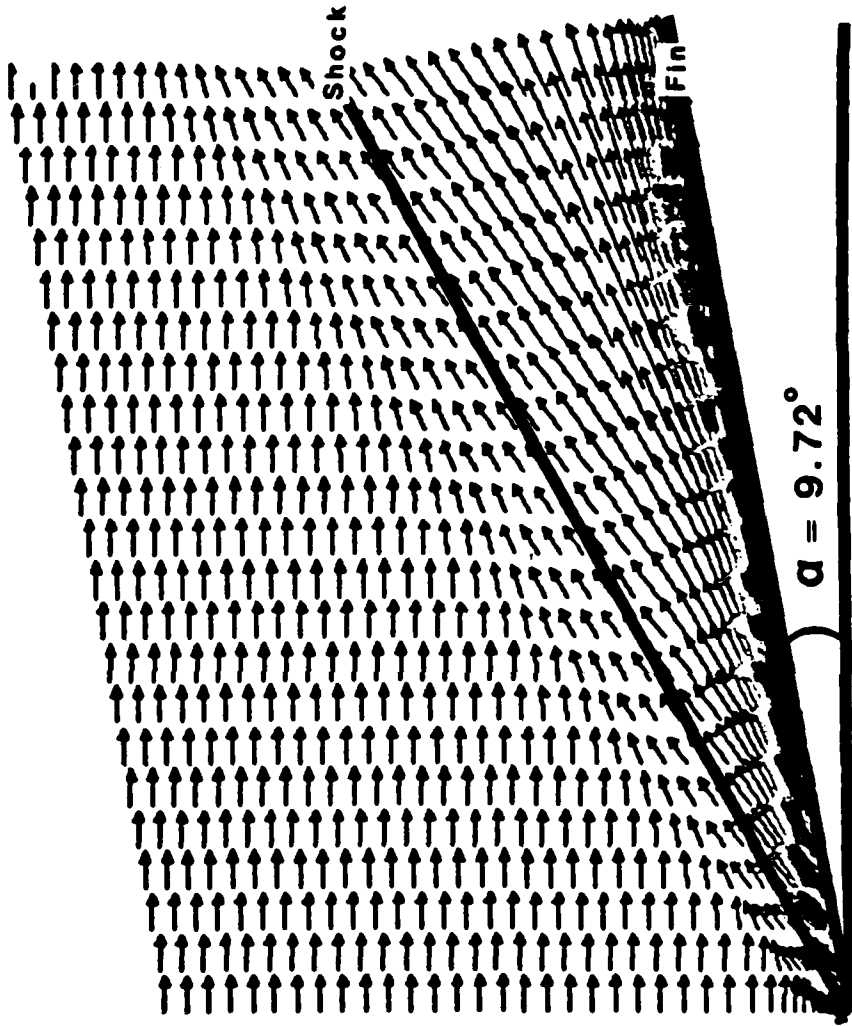


Fig. 34 Skin friction lines calculated by Knight (29)

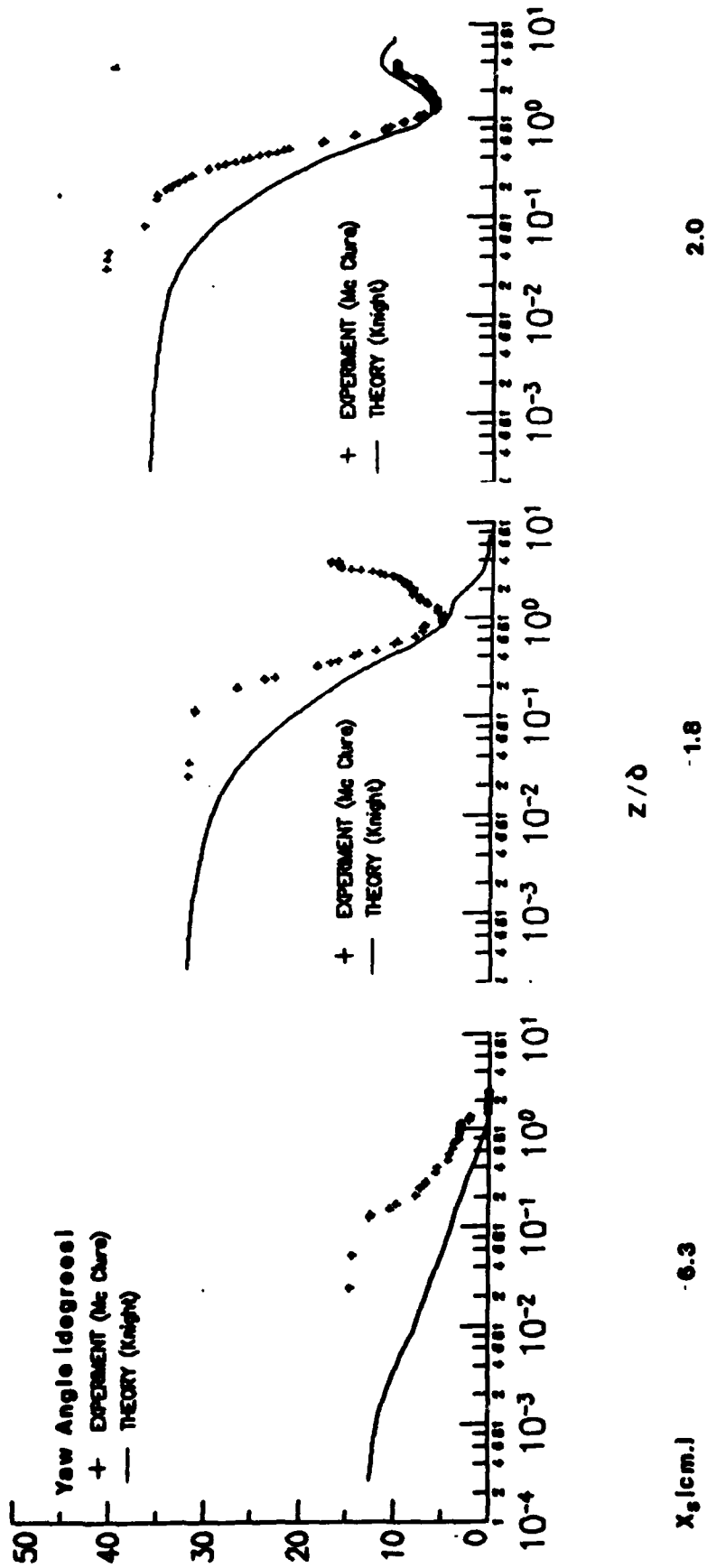


Fig. 35 Comparison of yaw angle results with computation of Knight (29)

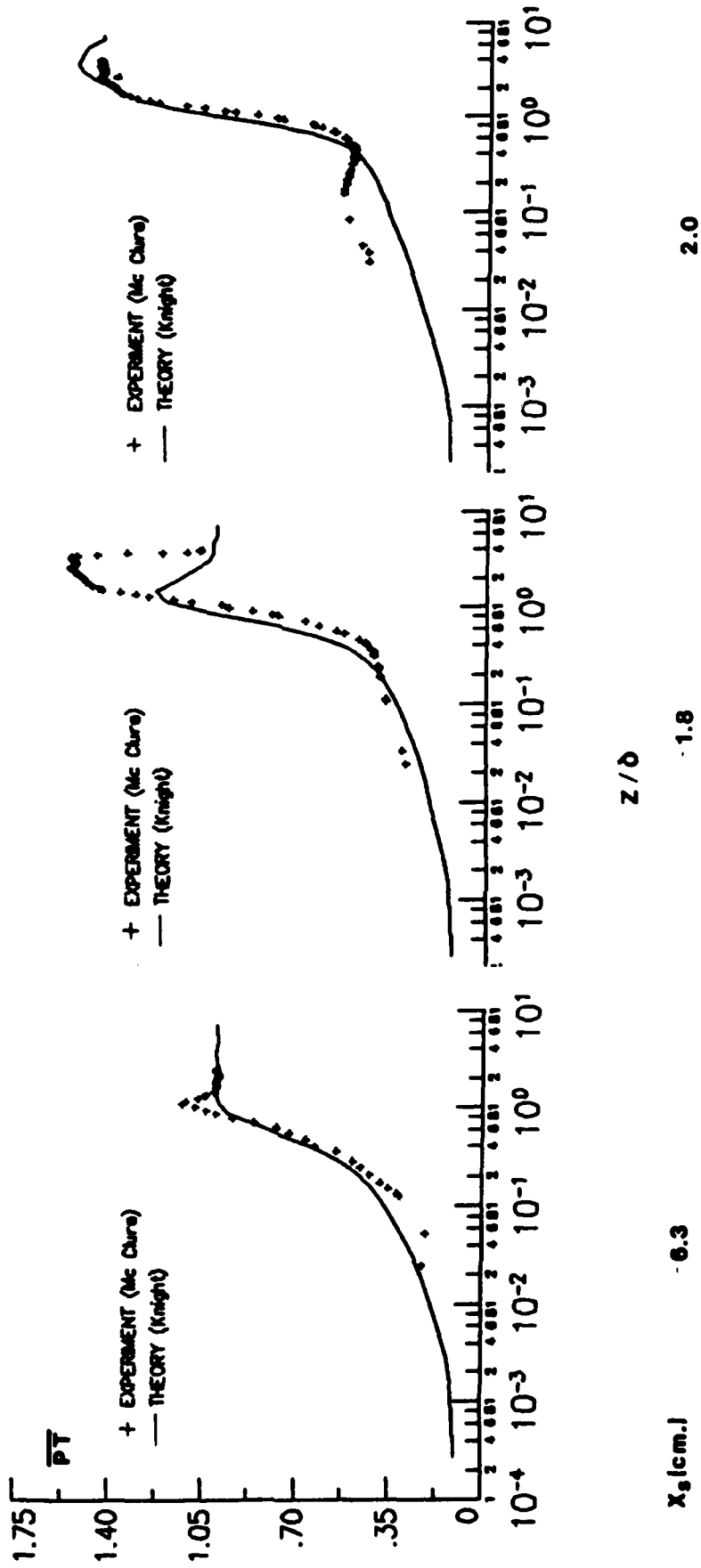


Fig. 36 Comparison of normalized pitot pressure results with computation of Knight (29)

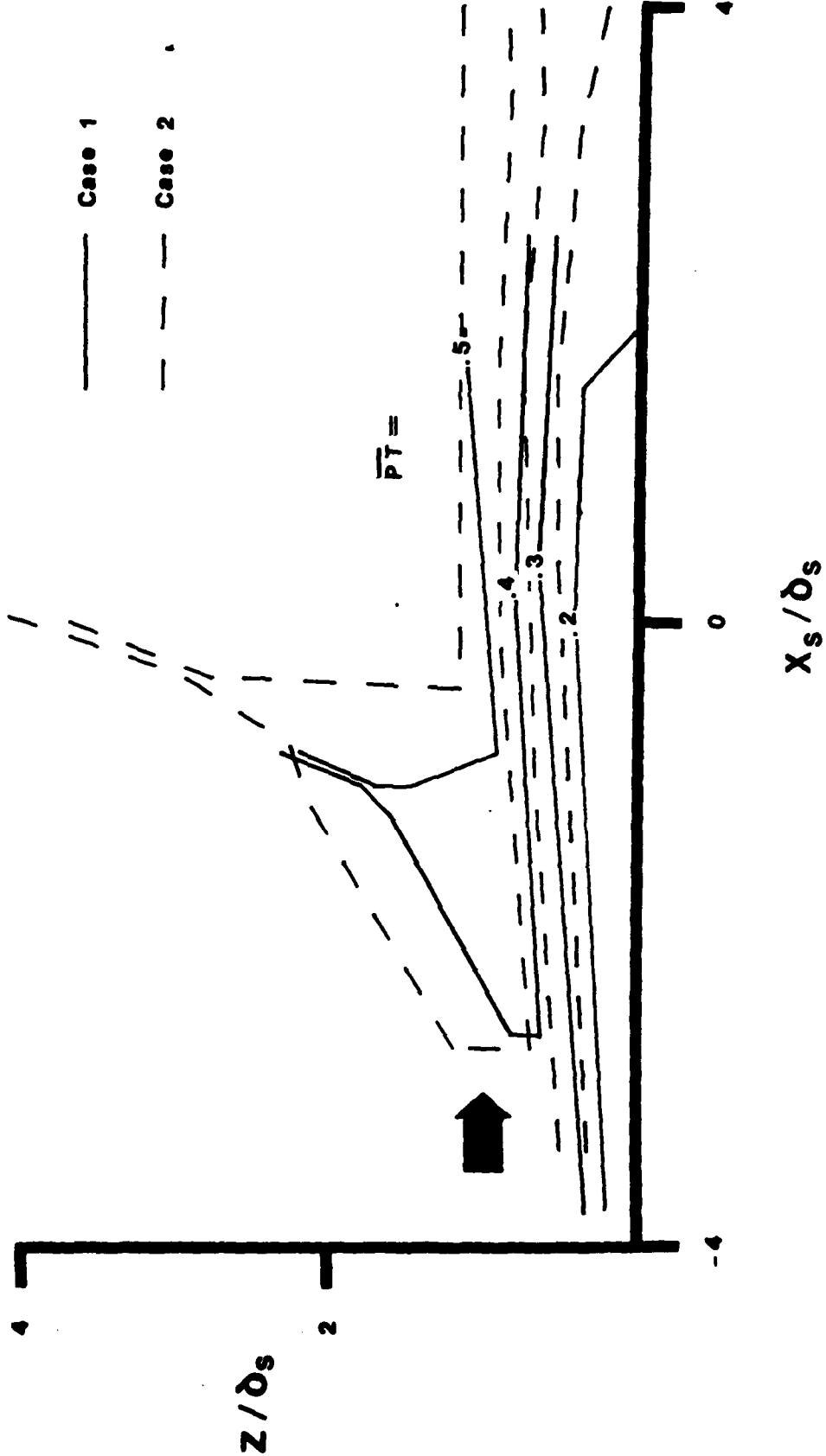


Fig. 37 Normalized pitot pressures in flow-field
 with dimensions normalized by boundary
 layer thickness

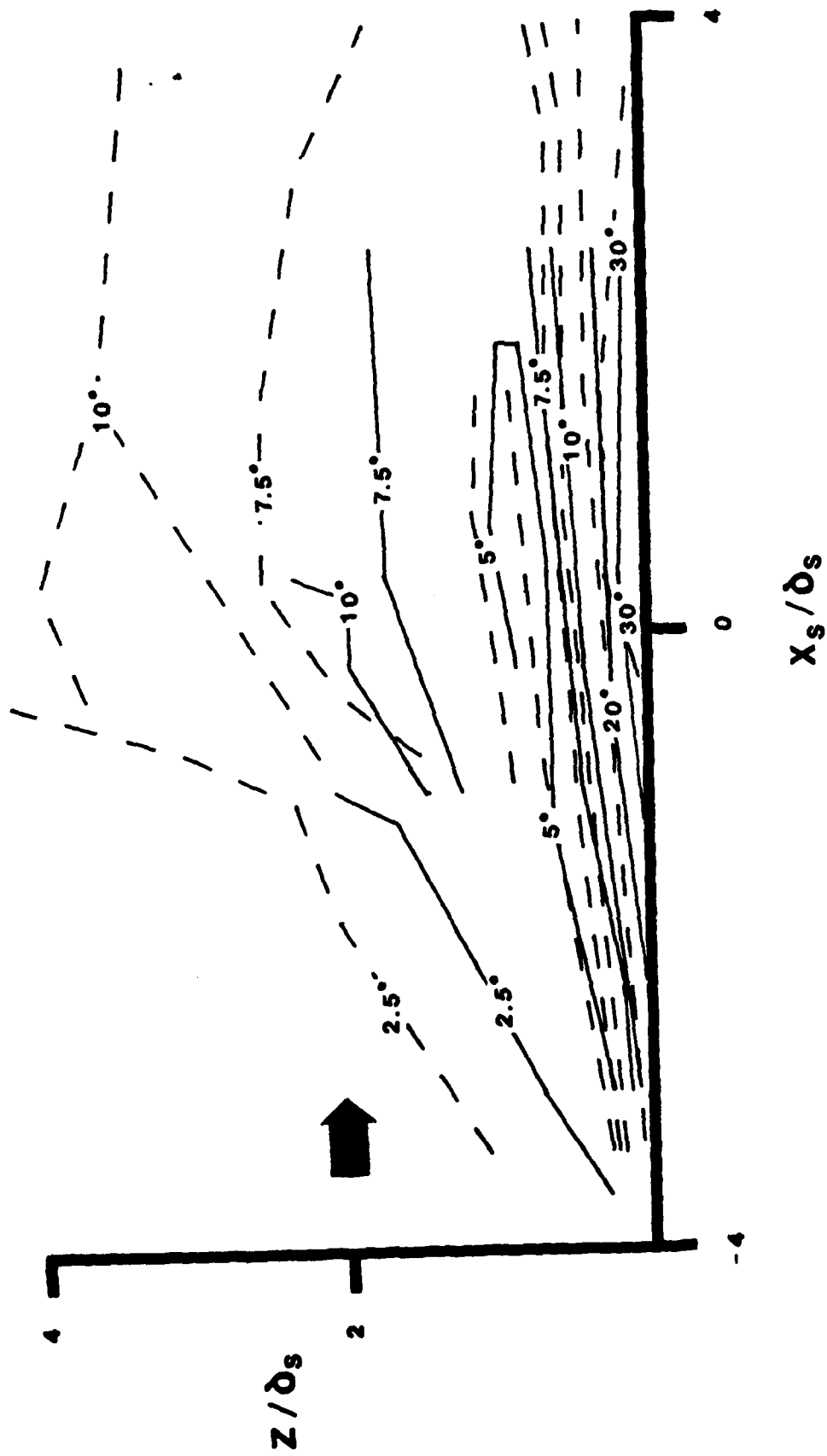


Fig. 38 Yaw angles in flow-field with dimensions normalized by boundary layer thickness (key of Fig. 37)

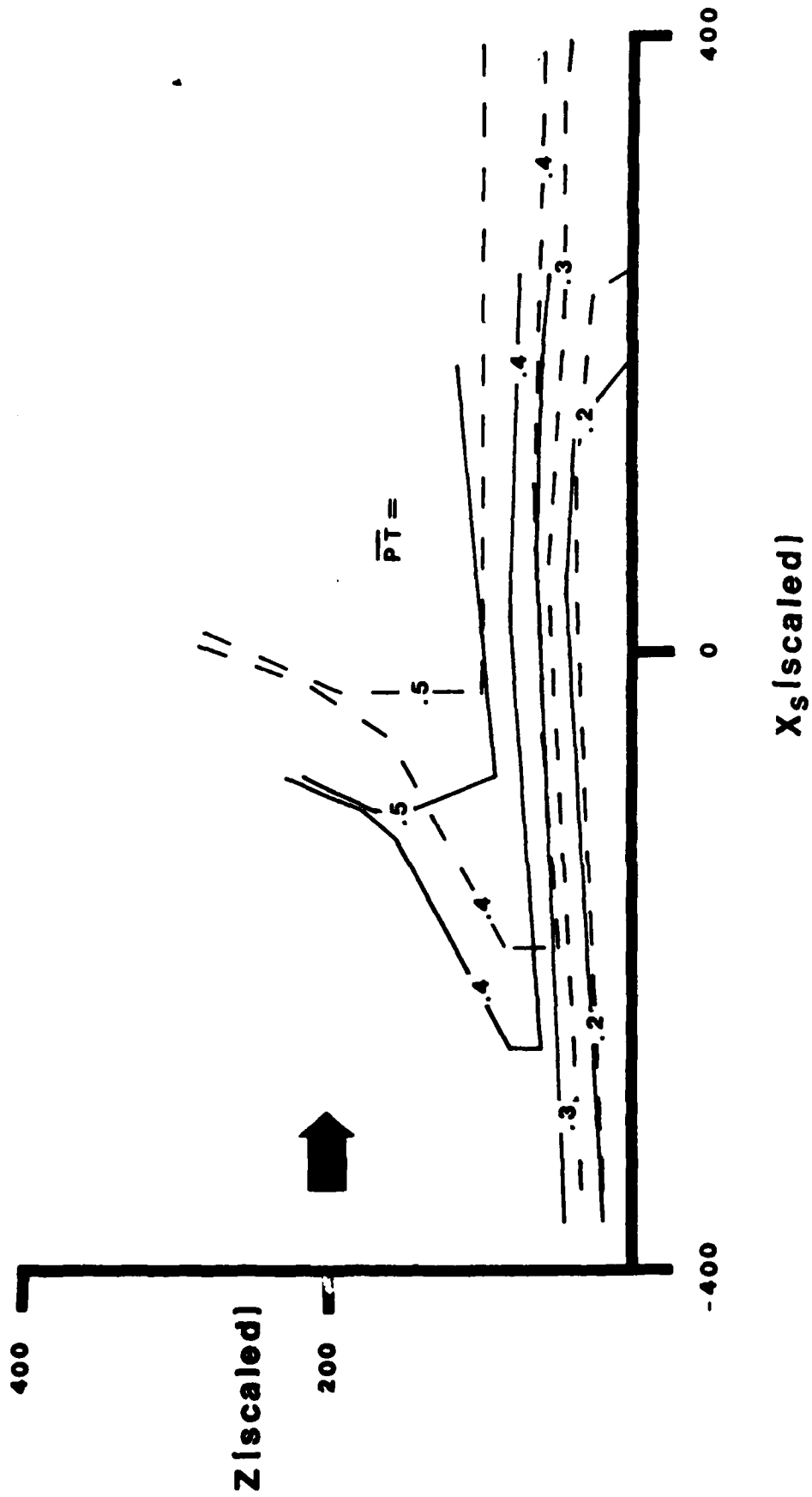


Fig. 39 Normalized pitot pressure in flow-field with dimensions normalized by method of Settles et al (6) (key of Fig. 37)

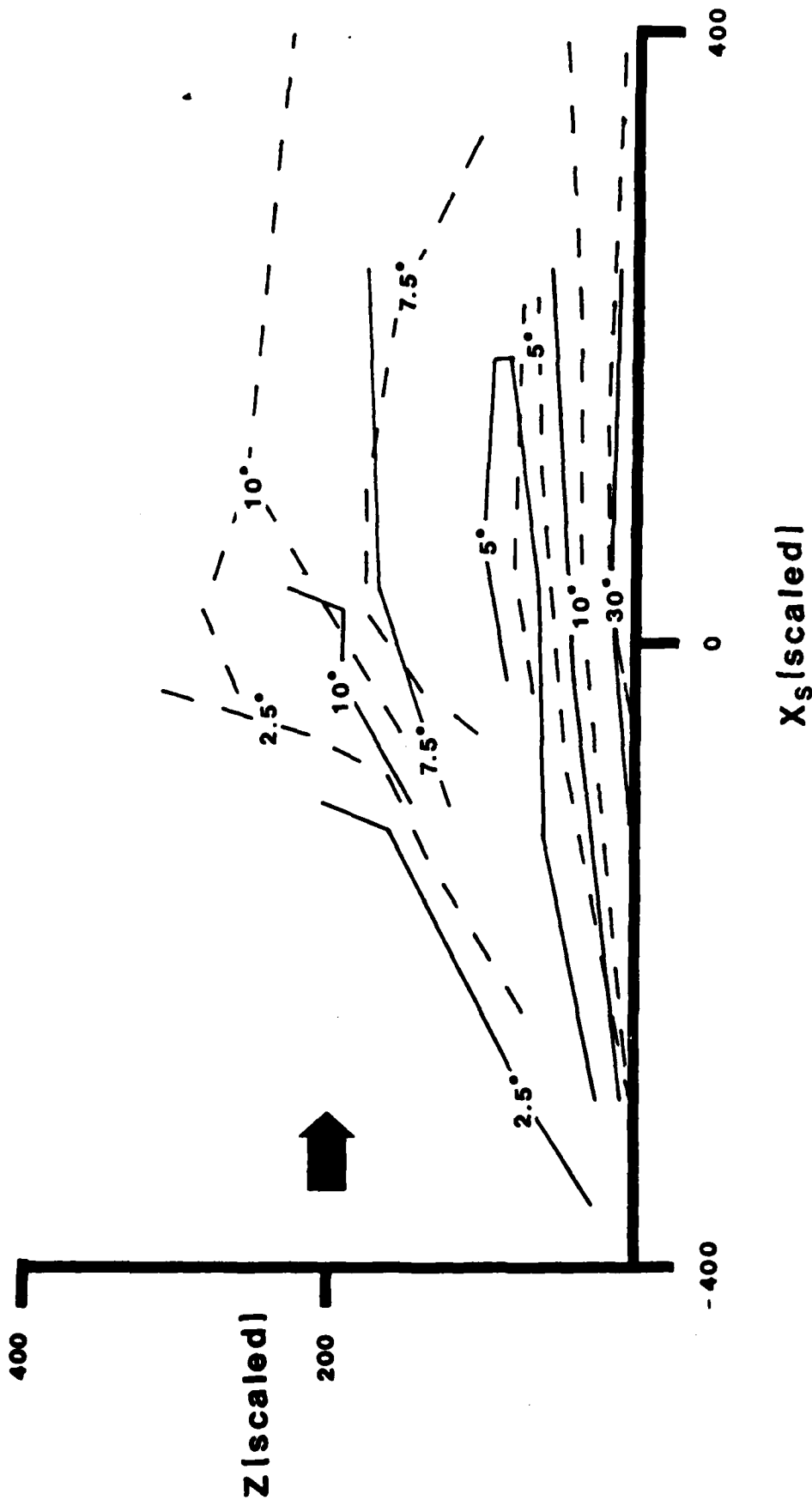


Fig. 40 Yaw angles in flow-field with dimensions normalized by method of Settles et al (6) (key of Fig. 37)

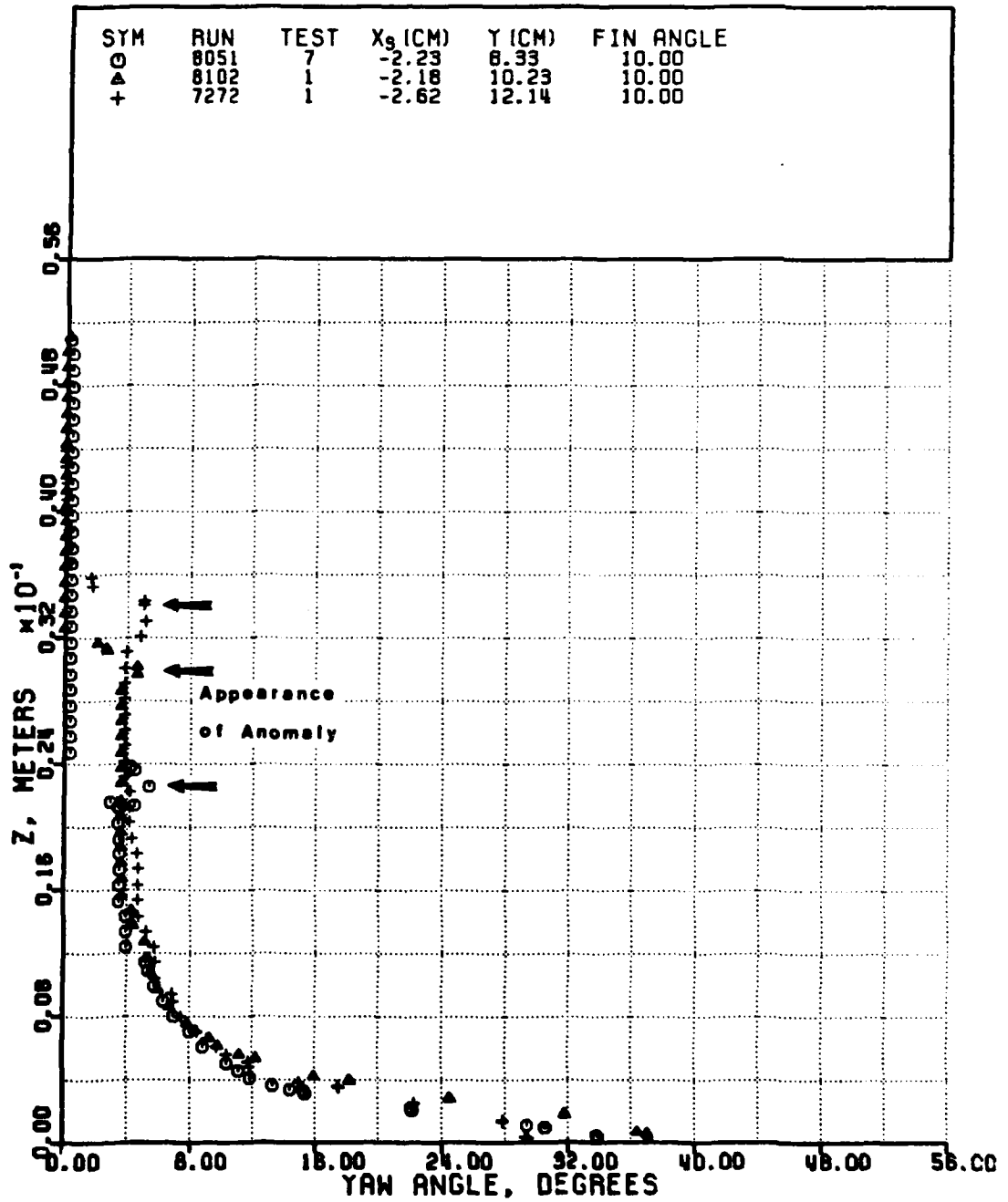


Fig. 41 First appearance of high-yaw angle anomaly at differing spanwise locations in Case 1

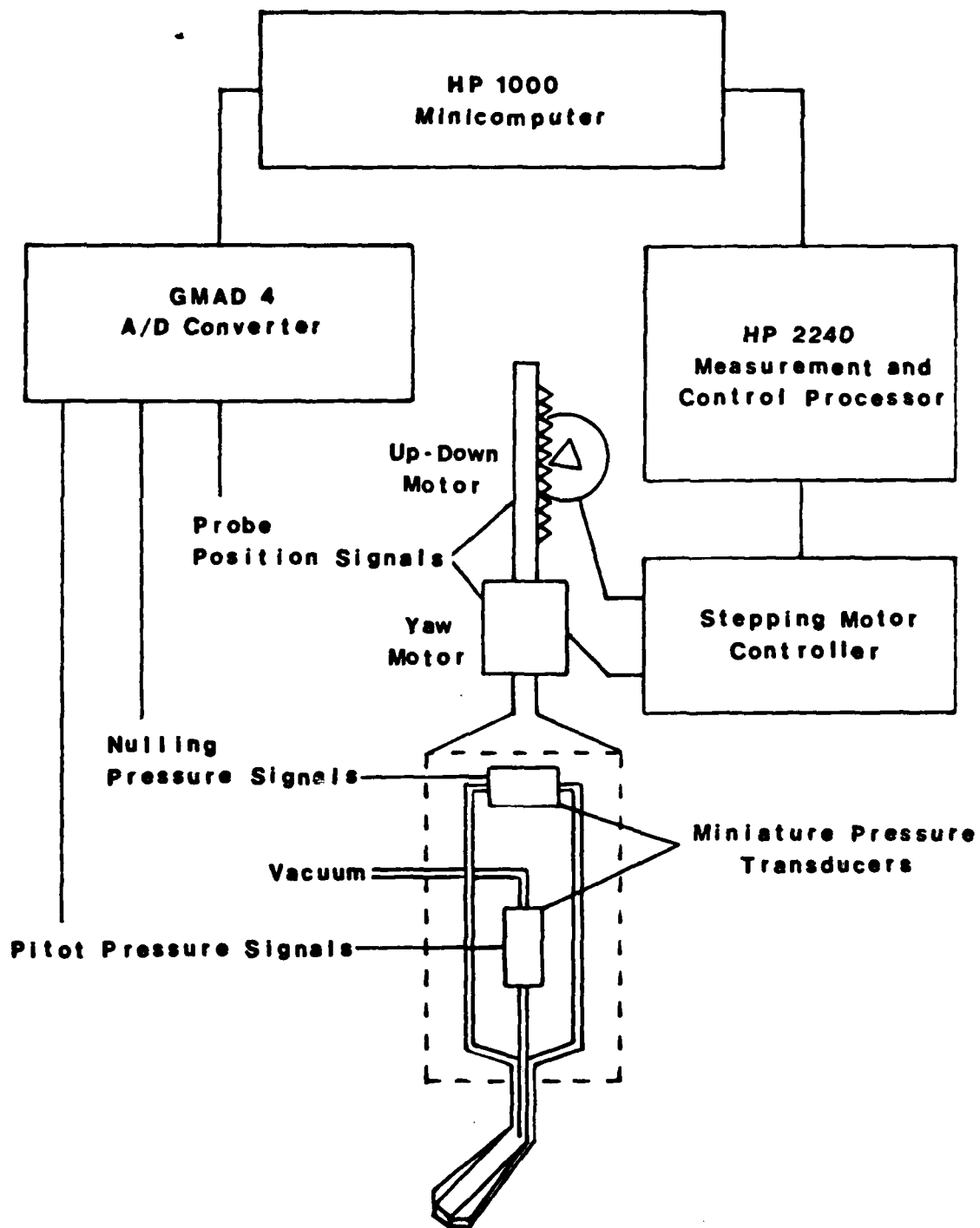


Fig. 42 Schematic of computer-controlled cobra probe

**DAT
ILMI**